Master Thesis

Comparison of Spin Manipulation with Spatially Oscillating Longitudinal or Transversal Magnetic Fields

vorgelegt der

Fakultät für Mathematik, Informatik und Naturwissenschaften
RWTH Aachen

angefertigt am

III. Physikalischen Institut B
Prof. Dr. Jörg Pretz

von

Jonas Salmann

Aachen, 29. Juli 2025

Erstgutachter
Prof. Dr. Jörg Pretz
III. Physikalisches Institut B
RWTH Aachen

Zweitgutachter
Prof. Dr. Andreas Lehrach
III. Physikalisches Institut B
RWTH Aachen

Abstract

Sona-transition units have been used since 1967 [1] to conduct non-adiabatic transitions between Zeeman states. Their energy levels depend on the external magnetic field. This means that spins and the external magnetic field have an opposite relative orientations after the particle beam passed through the Sona-transition region, which is an area of rapid inversion of the B-field. The Zeeman states will be changed as well, because they are equivalent to combinations of electron- and nuclear-spin orientations. In experiments [2][3] an unexpected effect had been observed though, that presented itself as oscillations of the measured intensities or polarizations when changing the magnetic field strength in the Sona-transition region. Only quite recent, this effect could be explained [4]: The spatially oscillating magnetic field of the Sona-transition unit acts on passing atoms as coherent photons. Here the magnets are aligned parallel to the beam line with a primary longitudinal magnetic field. The photon-like interaction between atoms and the B-field is mainly caused by the higher order radial component of the magnetic field. Therefore, a new setup with magnetic fields orthogonal to the beam line was developed. This new transversal Sona-transition unit consists of two coil pairs to produce opposing magnetic fields and was tested by varying several parameters like the distance from the beam axis to the coils or the position along the beam line. The corresponding results confirm simulations that are made in parallel for this new magnetic field configuration. Thereby, it was observed that just one coil pair and its transversal magnetic field is already enough to induce transitions within the hyperfine states.

Zusammenfassung

Sona-Transition-Units werden seit 1967 [1] genutzt um nicht-adiabatische Übergänge zwischen Zeemanzuständen durchzuführen. Deren Energielevel hängen von der relativen oriendierung von Elektronenspin, Kernspin und externem magnetischen Feld ab. Wenn also das Vorzeichen des externen Magnetfelds schnell um 180 ° gedreht wird, können so die Besetzungszahlen bestimmter Zuständ getauscht werden. Dieser Effekt kann z.B. genutzt werden um eine zuvor erzeugte Elektronenspin-Polarisation in eine Kernspinpolarisation umzuwandeln.In Versuchen [2][3] wurde allerdings ein unerwarteter Effekt beobachtet, der sich als Oszillation der gemessenen Besetzungszahlen bzw. Polarisationen zeigt, wenn das Magnetfeld in der Sona-Transition-Region geändert wird. Erst vor kurzem konnte dieser Effekt erklärt werden [4]: Die räumlich oszillierenden magnetischen Felder der Sona-Transition-Unit wirken wie kohärente Photonen auf hindurchfliegende Atome. In diesem Fall sind die Magnete parallel zum Strahlrohr ausgerichtet, was ein primär longitudinales Magnetfeld erzeugt. Die photonenähnliche Interaktion zwischen Atomen und dem Magnetfeld wird hauptsächlich durch die radiale Komponente höherer Ordnung des Magnetfelds erzeugt. Daher wurde ein neuer Aufbau mit Magnetfeldern orthogonal zum Strahlrohr entwickelt. Diese neue transversale Sona-Transition-Unit besteht aus zwei Spulenpaaren, die entgegengesetzte Magnetfelder erzeugen. Durch die Variation mehrerer Parameter, wie dem Abstand zwischen der Strahlachse und den Spulen oder der Positon entlang des Strahlrohrs, kann deren Einfluss auf die Besetzungszahlen der Zeeman-Zustände gemessen werden. Die entsprechenden Ergebnisse bestätigen Simulationen, die parallel für diese neue Magnetfeldkonfiguration durchgeführt wurden. Dabei wurde bemerkt, dass ein einzelnes Spulenpaar und sein transversales Magnetfeld bereits ausreichen um Übergänge innerhalb der Hyperfeinzustände anzuregen.

Table of contents

1 Introduction

Spin is a quantum mechanical property of most objects in atomic and subatomic physics. In experiments it usually shows up as an angular momentum, a magnetic dipole moment or due to the Pauli principle it is determining the configuration of electron shells and the stability of nuclear isotopes or the cross section of many nuclear reactions. It already found its way into everyday technology, such as NMR imaging, where a small surplus of about 10^{-6} of the nuclei are spin polarized. Therefore it is important to be able to measure and produce spin polarization for many research purposes but also for possible future industrial applications like energy production with nuclear fusion.

In nuclear fusion reactors the cross section of the reaction $\mathrm{t}(\mathrm{d},\mathrm{n})\alpha$ at the exact same temperature and density conditions can theoretically be increased by 50 %, when the fuel is polarized. The reason is that out of six possible nuclear spin combinations of a colliding deuteron and triton only four can fuse, because antiparallel spins cannot form the intermediate product ^{5}He with a nuclear spin of $^3/_2$. Such an increase of the reaction cross section and power density also increases the plasma temperature which corresponds to a higher number of collisions with larger collision energies, increasing the power output even more.

In research spin is relevant in various fields. For example spin orientations are important for energy levels in atomic physics. The weak interaction prefers reactions with one helicity of neutrinos, i.e. the relative orientation of spin and movement direction. **E**lectric **d**ipole **m**oments (EDM) are a proposed property of elementary and subatomic particles, that is tied to their spin. To do research about concepts related to spin, usually polarized sources are required and often experiments are conducted using particle accelerators.

There are several options to create spin polarization. One type of polarized source is an atomic beam source (ABS) with a subsequent region of inhomogeneous magnetic field, that use the Stern-Gerlach effect to separate atoms of different spin orientation by their magnetic dipole moment. A second type of polarization method is to pump states optically. Thereby, the particles in the lower energy spin state are excited with light or other electromagnetic radiation to a state, that decays mainly into the higher energy spin state. This method can only be used to polarize the electron spin of an atom or ion, because states, that differ only by nuclear spin have too small energy differences. Lamb-shift sources are a third type of polarized source. They polarize the electron spin of atoms or ions in the metastable $2S_{1/2}$-state by coupling atoms with one electron spin orientation to the short lived $2P_{1/2}$-state. This atoms decay to the ground state and only atoms with the other electron spin orientation remain in the $2S_{1/2}$-state. With more advanced methods, the nuclear spin can be polarized as well (see section 2.2).

These technologies can also be used to measure polarization. Additionally

nuclear polarization can be measured by colliding nuclei with specific targets, so that the products have different solid angle distributions depending on the nuclear spin polarization. By observing the precession of spins and measuring inductive effects or the transfer of angular momentum, spins can be detected as well.

Pumping optically can only produce electron spin polarization and current Lamb-shift methods can only measure nuclear spin polarization if the regarded atoms have a specific electron spin configuration. To overcome such limitations a Sona-transition unit has already been proposed in 1967 [1]. Here the non-adiabatic transitions are conducted by rapidly inverting the magnetic field polarity. In case of hydrogen-like atoms or ions with nuclear and electron spin $1/2$, the states of parallel electron and nuclear spin are interchanged while the states with antiparallel electron and nuclear spin are not transitioned. This means that a beam of electron spin polarized particles can be turned into a nuclear spin polarized beam or vice versa.

This principle has already been used in experiments. For example, electron spin polarized atomic hydrogen beams got successfully turned into nuclear spin polarized atomic beams in 1977 for atoms in the metastable $2S_{1/2}$-state [2] and in 2007 for atoms in the $1S_{1/2}$ ground state [3]. Thereby, Lamb-shift methods or optical pumping are used to produce electron spin polarization in the first place.

The conducted experiments did not only find the expected non-adiabatic transitions, but also found unexpected oscillations of the occupation numbers of the hyperfine substates depending on the magnetic field strength near the Sona-transition region. This behavior is now recognized as the Okorokov effect [5][6]. The particles experience an oscillating magnetic field, when passing through a Sona-transition unit, which is equivalent to what they experience when interacting with photons. Therefore, the oscillations can be interpreted as resonances of multi-photon transitions between the Zeeman states [4]. Such transitions can only be conducted if the angular momentum is conserved. In such a multi-photon transition the spin angular momentum of the photons, which is ± 1 in $\hbar$-units for each photon, have to add up to the difference between the total angular momenta m_F of the initial and final Zeeman state. For Zeeman states, that are energetically close to each other in hydrogen atoms, this difference is ± 1. To fulfill this condition, only an odd number of photons is able to induce´ transitions [7]. By calculating the energy of a single photon and multiplying it with the number of photons, the energy difference between two Zeeman states can be measured at a resonance point, which opens the possibility to conduct spectroscopy of the Zeeman states with this method.

A possible future application of a Sona-transition unit is the **bo**und **b**eta decay experiment (BOB), that shall measure the Zeeman states of metastable hydrogen atoms that are produced by the reaction $\mathrm{n} \rightarrow {}^1\mathrm{H} + \bar{\nu}_e$ and verify predictions of the occupation numbers. One specific Zeeman state, the creation of which is

prohibited by parity rules, is not easily to singled out with current Lamb-shift methods (see section 2.2) but may be measured by using a Sona transition. For this experiment to be successful understanding the atomic behavior in a Sona-transition unit is crucial.

In this thesis a Lamb-shift method is utilized, that uses a modified Lamb-shift polarimeter. Such a Lamb-shift polarimeter takes a potentially nuclear spin polarized beam of atoms, molecules or ions into a partially metastable atomic beam by ionizing it, if necessary, and neutralizing it again in a cesium cell (see section 3.4). By deexciting all atoms, that do not have a specific nuclear spin state (see section 2.2), measuring the amount of remaining metastable atoms and repeating this measurement for each possible nuclear spin state, the relative amount of particles in each nuclear spin state, i.e. the polarization, can be calculated.

To measure the behavior of spin systems in a Sona-transition unit, a beam of polarized metastable atoms is produced and send into a Sona-transition unit. After passing it, the metastable atoms are filtered by spin state and measured like in an unmodified Lamb-shift polarimeter.

Simulations without a radial B-field component suggest that the transversal component is responsible for the Okorokov effect, because these simulations show no oscillations. In longitudinal Sona-transition units that consist of magnets aligned parallel and antiparallel to the beam to create a rapid inversion of the magnetic field direction the radial component is just a higher order effect, that is primarily proportional to the distance from the beam-pipe center. This inhomogeneity of a B-field component, crucial for the observed effect, might cause unclear results because in the end the average is taken over the entire beam. To avoid this potential problem, a new kind of Sona-transition unit is proposed. Instead of having mainly longitudinal magnetic fields, this transversal Sona-transition unit uses magnets that are aligned orthogonal to the beam line. These explicitly created transversal field is more uniform throughout the beam cross section, which means, it has a more similar effect on all atoms within the beam, making it easier to produce better fitting simulations. The aim of this thesis is to simulate the induced Sona transitions for the new field configuration and do conduct the corresponding measurements to validate the predictions.

2 Theory

2.1 Energy levels of the hydrogen atom

2.1.1 Bohr and orbitals

The energy levels creating the spectral lines of hydrogen-like atoms and ions were first described by Niels Bohr with the equation

$$E_n = -\frac{1}{n^2} \cdot \left(\frac{e^2 \cdot Z}{4\pi\varepsilon_0} \right)^2 \cdot \frac{m_e}{2\hbar^2}, \tag{1}$$

using the electron mass m_e and the nuclear charge number Z. These energy levels E_n define the possible electron shells, that exist in a system consisting of a nucleus and an electron, a so called hydrogen-like atom. In atoms or ions with more electrons the same shells exist but have different energies, due to the charge of further electrons changing the effective potential of the first electron.

Later these energy levels could be explained with orbitals. These also predict the existence of a number of possible azimuthal quantum numbers l and corresponding magnetic quantum number m_l for each principal quantum number n. In the n-th shell exist n possible $l < n$ with $l \in \mathbb{N}_0$ and for each l exist $2\,l+1$ possible values for $m_l \in \mathbb{Z}$ in the range $-l \leq m_l \leq l$.

These quantum numbers define the number of possible orbitals in each shell. As the electrons have a spin of $s = 1/2$, the additional spin quantum number m_s is $\pm 1/2$ and the exclusion rules of the Pauli principle allow two electrons with opposing m_s in one orbital. As the number of electrons in the most outer shell of a ground state atom shapes the chemical properties of the corresponding element, elements with increasing atomic numbers Z periodically have similar properties. Arranging the known elements by their properties, that are influenced by the number of electrons allowed in each electron shell, gives the periodic table of elements.

2.1.2 Fine structure

If one takes into account, that the orbital angular momentum $\vec{L}$ and the spin $\vec{S}$ combine to a total angular momentum of the electron $\vec{J}$, one realizes, that there exist multiple possible values for $|L-S| \leq J \leq L+S$. Each of these states has a slightly different energy level, due to the magnetic dipoles

$$\vec{\mu}_s = -g_s \mu_B \frac{\vec{S}}{\hbar}, \; (\vec{\mu}_s)_z = -g_s \mu_B m_s \tag{2}$$

and

$$\vec{\mu}_L = -g_l \mu_B \frac{\vec{L}}{\hbar}, \; (\vec{\mu}_L)_z = -g_s \mu_B m_l, \tag{3}$$

created by the electron charge and the angular momenta interacting with each other. This splitting of the Bohr energy into multiple states is called fine structure.

Apart from this spin-orbit interaction, relativistic corrections of the solutions to the classical Schrödinger equation are also part of the fine structure, as well as the Darwin term that includes the influence of quantum fluctuations on the energy levels.

2.1.3 Lamb shift

A closer inspection of the fine structure states reveals, that there can be multiple ways to achieve a specific J by adding l and m_s. For example, the $J = 1/2$ state of hydrogen atoms with their electron in the second shell ($n = 2$) can be achieved by combining the angular momentum quantum number $l = 0$ and the spin quantum number $m_s = 1/2$ but also by combining $l = 1$ and $m_s = -1/2$.

This means, that in this case $J = 1/2$ can be realized with s-orbitals ($l = 0$) or with p-orbitals ($l = 1$), which have different probability density distribution around the nucleus (see fig. 1). There are three reasons, why these energies of these sub states differ.

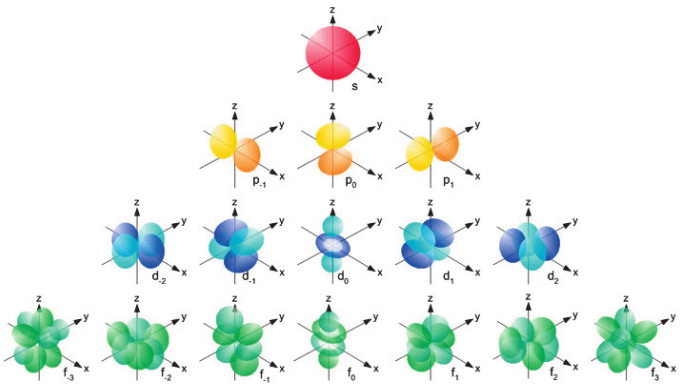

Figure 1: s-, p-, d- and f- orbitals (top to bottom) of hydrogen atoms (source: [8, p. 128]).

First the electron has different self energies, because the potential is not a perfect coulomb potential in the nucleus, where orbitals with $l \neq 0$ have a negligible probability density while the s-orbital with $l = 0$ has a higher density in this region. A second effect is, that the probability densities of different orbitals change the vacuum polarization. Therefore, the energy levels of electrons with different orbital angular momenta l shift differently. Third the anomalous magnetic

moment of the electron contributes to this energy difference ΔE_{Lamb}. It is called Lamb shift. For example, difference between the s- and p-orbital in the $n = 2$-shell of hydrogen atoms is 4.4 μeV between $2S_{1/2}$ and $2P_{1/2}$ (source: [9, p. 22]).

2.1.4 Hyperfine structure

When including the nuclear spin $\vec{I}$ in addition to the angular momentum of the electron $\vec{J}$, these combine to a total angular momentum $\vec{F}$ analogue to the combination of $\vec{L}$ and $\vec{S}$ (see section 2.1.2). As a result F can obtain one of $|J-I|+(J+I)+1$ values in the range $|J-I| \leq F \leq J+I$ with different energies, caused by the interaction of the magnetic dipoles of the electron and the nucleus. The energy difference is proportional to the hyperfine constant A.

For $J = 1/2$, which is the only J relevant in this thesis, and the proton spin $I_{\text{proton}} = 1/2$ the possible total angular momenta are $F = 0$ and $F = 1$ (see fig. 2) with the magnetic moment of the proton spin

$$\vec{\mu}_I = -g_p \mu_k \frac{\vec{I}}{\hbar}. \tag{4}$$

The angular momentum quantum number m_F has only one possible value $m_F = 0$ for $F = 0$, but three possible values $m_F = -1, 0, 1$ for $F = 1$. Such states can also be seen as superpositions of the combinations of the electron angular momentum quantum number m_J and the nuclear angular momentum quantum number m_I. A superposition can only exist between states, that correspond to the same m_F though. In an atom with $J = 1/2$ and $I = 1/2$ superpositions are composed like

$$\begin{aligned}
|F = 1, m_F = 1\rangle &= |m_J = 1/2; m_I = 1/2\rangle \\
|F = 1, m_F = 0\rangle &= \frac{1}{\sqrt{2}} \left(|1/2; -1/2\rangle + |-1/2; 1/2\rangle\right) \\
|F = 1, m_F = -1\rangle &= |-1/2; -1/2\rangle \\
|F = 0, m_F = 0\rangle &= \frac{1}{\sqrt{2}} \left(|1/2; -1/2\rangle - |-1/2; 1/2\rangle\right).
\end{aligned} \tag{5}$$

The states with $m_F = 0$ are called "mixed" states because they are a superposition of two spin states, while the states with $m_F = \pm 1$ are called "pure" states.

2.1.5 Zeeman effect

Each state corresponding to a specific F can be split into $2F+1$ degenerated substates, which are each assigned to a value of the quantum number m_F in the range of $-F \leq m_F \leq F$. This quantum number represents the projection of the total angular momentum $\vec{F}$ onto the main quantization axis z. Because of the charge distribution in the atom, the angular momentum $\vec{F}$ corresponds to a magnetic dipole,

which can interact with an external magnetic field $\vec{B}$ and create separate energy levels for each Zeeman state corresponding to an F and m_F if $\vec{B} \neq \vec{0}$.

In the Paschen-Back region with B-fields higher than a critical field

$$B_c = \frac{\Delta E_{\mathrm{HFS}}}{2\mu_B} \tag{6}$$

[9, p. 19] the eigenstates converge to the energies of atoms with pure electron spin states and a nuclear spin interacting with the combined magnetic field of the external field and the electron field (see fig. 2). This is why in the Paschen-Back region a huge split is created by the electron angular momentum J with a large magnetic moment and a small split is created by the nuclear spin I which has a much smaller magnetic moment.

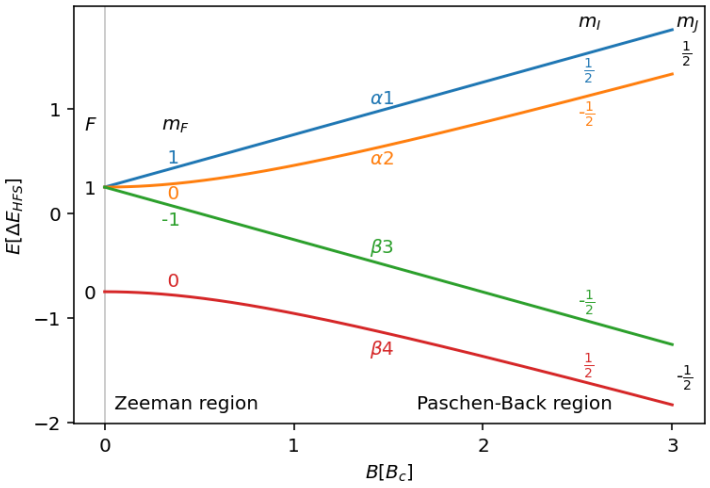

Figure 2: Breit-Rabi diagram of hydrogen in the $2S_{1/2}$ state.

In the Zeeman region with weaker magnetic fields, i.e. $B < B_C$ the eigenstates are no longer necessarily the states with pure m_J- and m_I-combinations; instead the m_J- and m_I-combinations which add up to the same total angular momentum quantum number m_F mix and form superpositions. For $B = 0$, this corresponds to the hyperfine energy levels of the possible values of F.

For an easier description of these states a new convention is established. First the states are numbered from highest to lowest energy. In case of a fine structure state $2S_{1/2}$, the Zeeman sub-states that have an $m_J = 1/2$ i.e. an electron spin parallel to the external B-field, get the prefix "α" and the states with $m_J = -1/2$, i.e. an electron spin antiparallel to the external B-field get the prefix "β" (see figs. 2 and 3). The sub-states of the $2P_{1/2}$-state are labeled with "e" and "f" (see fig. 3) instead.

2.2 Spinfilter

The purpose of a Spinfilter is to quench metastable hydrogen atoms to the ground state but to let atoms in specific Zeeman states pass through (see section 3.5). Existing spinfilters operate at B-field strengths, where the β- and e-branches are energetically close to each other.

This energetic degeneration enables an additional electric field to couple these states via Stark effect to each other and induce transitions of the atoms in the β-states into the e-states, from where they decay to the $1S_{1/2}$ ground state (see fig. 4). The remaining metastable atoms have a polarized angular momentum of the electron J, when only α-state atoms with $m_J = 1/2$ pass through.

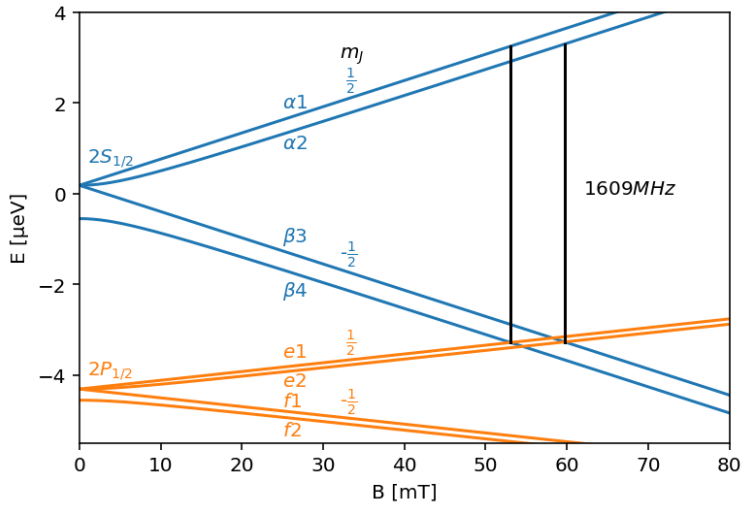

Figure 3: Breit-Rabi diagram of hydrogen in the $2P_{1/2}$- and metastable $2S_{1/2}$-state.

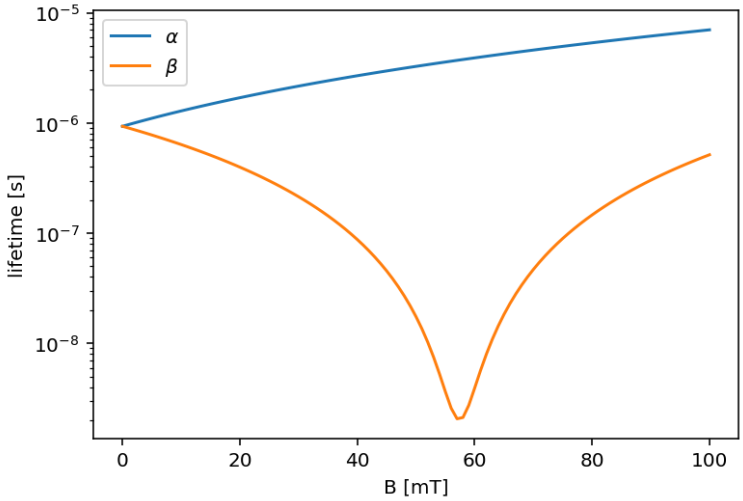

Figure 4: Lifetime of metastable hydrogen atoms in an electric field of $E = 20\ {}^{V}/_{cm}$ depending on the magnetic field B.

To also polarize the nuclear spin, radiation with a frequency of $f = 1609\ MHz$ is applied and induces transitions between the α- and e-states (see fig. 3), which allows them also to decay. If the magnetic field B is tuned precisely to the value, where either the $\alpha 1$-$e1$-transition or the $\alpha 2$-$e2$-transition is resonant, the atoms that were in the corresponding α-state before entering the spinfilter are able to oscillate between the α- and e-state and have a chance, not to decay into the ground state (see fig. 5).

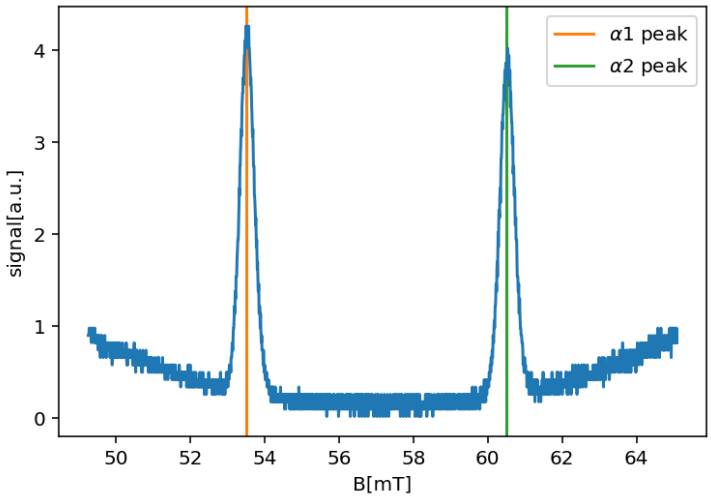

Figure 5: Intensity of metastable hydrogen atoms of an unpolarized beam after passing through a spinfilter depending on the magnetic field B.

Because the β-states are always quenched in such a spinfilter design, they are not able to be separated in such a spinfilter and only α-states can easily be observed.

2.3 Sona-transition unit

2.3.1 Classical Sona transitions

Initially, the Sona-transition unit was invented to produce nuclear polarized beams of metastable hydrogen atoms [1]. To do so, a beam of metastable hydrogen atoms would get electron spin polarized by quenching the β-states with magnetic and electric fields the same way they are quenched in a spinfilter. If the B-field strength is turned negative (see fig. 6), the direction of the magnetic field is flipped from parallel to antiparallel to the beam axis. During this process the $\alpha 1$- and $\beta 3$-states switch binding energies and the occupation numbers of these states are exchanged. This would enable the production and measurement of metastable hydrogen atoms in the $\beta 3$-state by combining a spinfilter set to $\alpha 1$ and a Sona-transition unit to switch between the $\alpha 1$- and $\beta 3$-state [1].

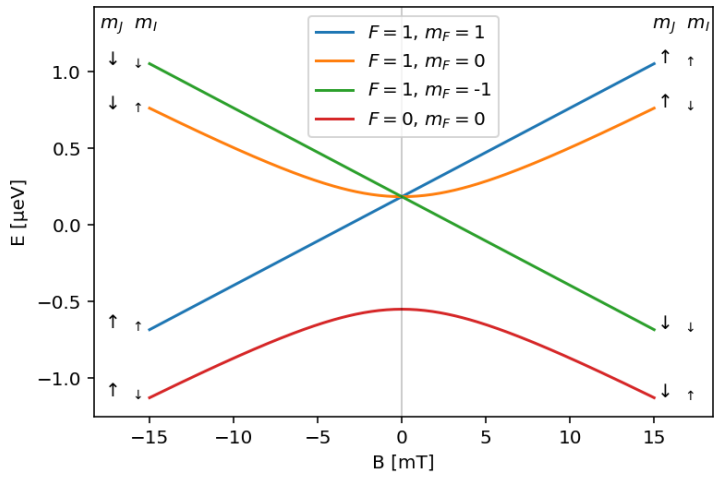

Figure 6: Zero-crossing of the energy levels of 2S-hydrogen atoms with the electron angular momentum $J = 1/2$ and nuclear spin $I = 1/2$.

To prevent precession of the spins while moving through an area with weak and diffuse B-fields, magnets with opposing polarity had been placed before and after the zero-crossing, creating a nearly linear gradient of the longitudinal magnetic field (see figs. 7 and 8). For the classical adiabatic Sona transition, the inversion of the orientation of the B-field. One should also keep in mind, that the orientation of the magnetic fields in each spinfilter should be aligned with the

Sona magnet closer to it. Otherwise more zero-crossings are created disturbing the measurement.

2.3.2 B-fields of the longitudinal Sona-transition unit design

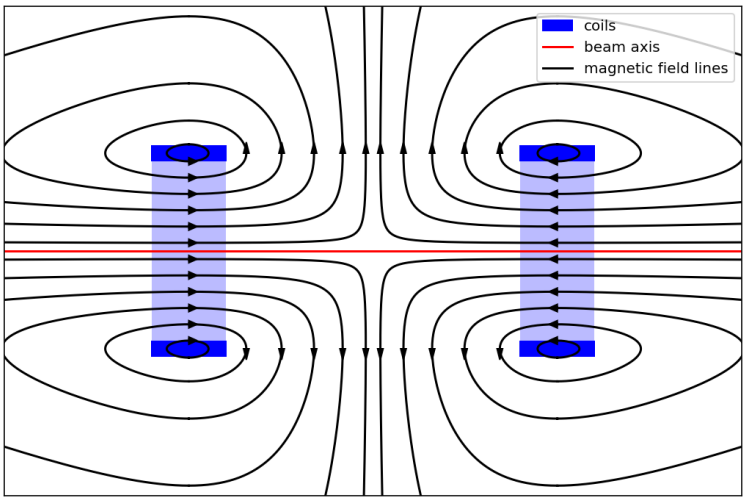

Figure 7: Scheme of the B-field of a longitudinal Sona-transition unit.

The magnets creating the opposing magnetic fields around a zero-crossing are solenoid coils, that are aligned to the beam axis but have opposing polarities. They generate magnetic field lines heading towards each other. Magnetic field lines can not just end, so they have to be diverted to the side (see fig. 7). Therefore, in an apparatus with a rotational symmetry like a longitudinal Sona-transition unit, a radial component is created, where the longitudinal field strength changes. Further, the strength of the radial component increases with the distance to the symmetry axis r, as more field lines have to be diverted when considering a larger radius. On the other hand, in a perfectly symmetrical setup, no radial or transversal B-field component exists on the beam axis with $r = 0$ and only the longitudinal component remains.

For the calculation of an estimated radial field, it is assumed that the longitudinal magnetic field B_z is homogeneous over the cross section of the beam and the whole field has a rotational symmetry. Under these conditions the amount of longitudinal field component dB_z ending within an infinitesimal length dz and a circular cross section has to exit this infinitesimal cylinder through its mantle as the radial magnetic field component B_r.

This consideration is equivalent to using the Gaussian law for magnetism

$$\vec{\nabla} \cdot \vec{B} = 0 \tag{7}$$

to find an approximated radial component for a longitudinal magnetic field with varying strength. The result of both derivations is

$$B_r = -\frac{dB_z}{dz} \cdot \frac{r}{2}. \tag{8}$$

This equation can be used to create approximations of the transversal component of the magnetic field near the beam axis in the longitudinal Sona-transition unit. Figure 8 shows an example of an extrapolation from a measurement using this method.

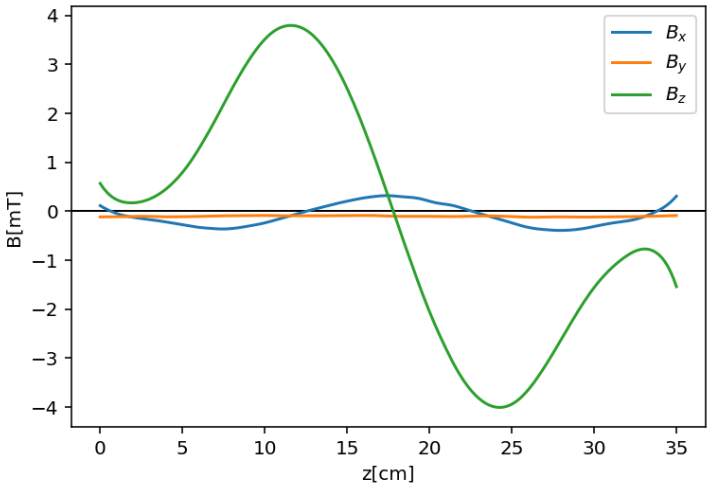

Figure 8: B-field of a longitudinal Sona-transition unit 1 cm off the beam axis in x-direction.

2.3.3 Okorokov effect

Several research groups conducted experiments trying to utilize a Sona-transition unit [3] or similar apparatuses [2] and some of them observed oscillations when changing the current in the Sona-transition unit.

A recent explanation is, that atoms passing a polarity inversion of the magnetic field experience similar fields like when they are interacting photons (see fig. 8). Therefore, the magnetic fields are acting as photons on the magnetic dipole of the atoms [4]. I.e., the spatially oscillating magnetic field appears in the system at rest of the atoms as a singe incoming electromagnetic field oscillation. Here, the electric field component is induced by the magnetic field changing in time following the Maxwell equations. This photon effect is called Okorokov effect, which initially got discovered for particles experiencing periodic fields in crystals [5][6].

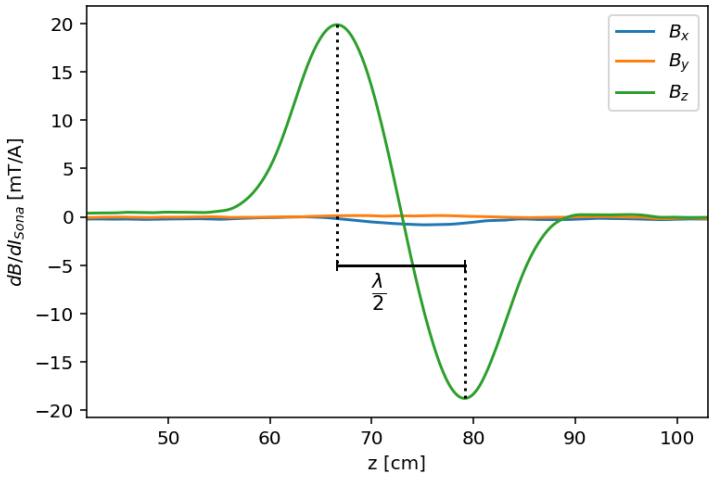

Figure 9: B-field of a longitudinal Sona-transition unit on the center ray in relation to the current. The half wavelength between the maximum and the minimum is additionally drawn in.

The wavelength λ of this magnetic wave (see fig. 9) can be converted to a photon energy E_γ using

$$f = \frac{v}{\lambda}, \tag{9}$$

$$E_\gamma = h \cdot f \tag{10}$$

and the velocity of the particle v. The observed oscillations result from resonances at several values of the energy differences $\Delta E_{\alpha 1,\alpha 2}$ and $\Delta E_{\alpha 2,\beta 3}$ between the $\alpha 1$, $\alpha 2$ and $\beta 3$ Zeeman state. For small fields $B < B_C$ (see fig. 2) these states have smaller energetic differences between each other than they have to the fourth state $\beta 4$, because at $B = 0$ they degenerate to the substates $m_F = -1, 0, 1$ of $F = 1$. Under these conditions the $\beta 4$-states is the $F = 0$, $m_F = 0$-state, that is separated from the others energetically by the hyperfine structure energy ΔE_{HFS}.

$\alpha 1\alpha 2$- and $\alpha 2\beta 3$-transitions are $\Delta m_F = \pm 1$-transitions, that are induced by the radial component of the field oscillations. For this reason the radial field, that is highly dependent on the position in the beam (see eq. (8)), of longitudinal Sona-transition units is crucial for the Okorokov effect.

If the Δm_F between two Zeeman states is ± 1, the absorption of an odd number $2\,n+1$ of photons can induce a transition. The spin angular momenta, which can be ± 1 for each photon need to add up to Δm_F, which is not possible for an even number of photons. The transition can only occur, if the energy difference $\Delta E_{\alpha 1,\alpha 2}$ or $\Delta E_{\alpha 2,\beta 3}$ is resonant, i.e. corresponds to the energy of the absorbed photons, which is $2\,n+1$ times the single photon Energy E_γ.

The magnetic field strengths at which this condition is met differ for $\alpha 1\alpha 2$- and $\alpha 2\beta 3$-resonances, because the energy difference of this resonances behave differently (see fig. 10).

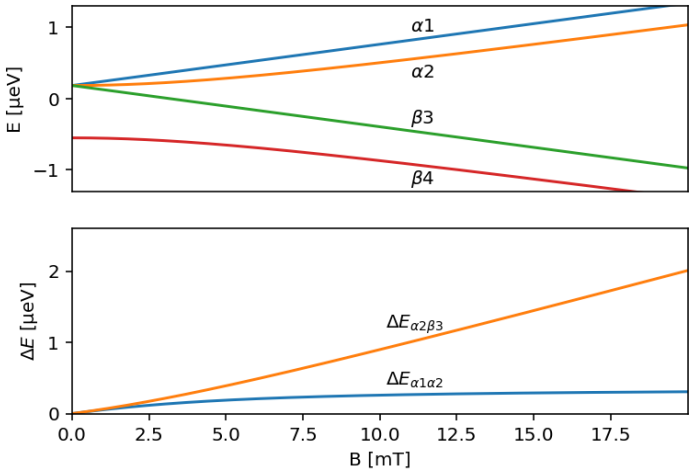

Figure 10: Energy differences in the Breit-Rabi diagram of metastable $2S_{1/2}$ hydrogen.

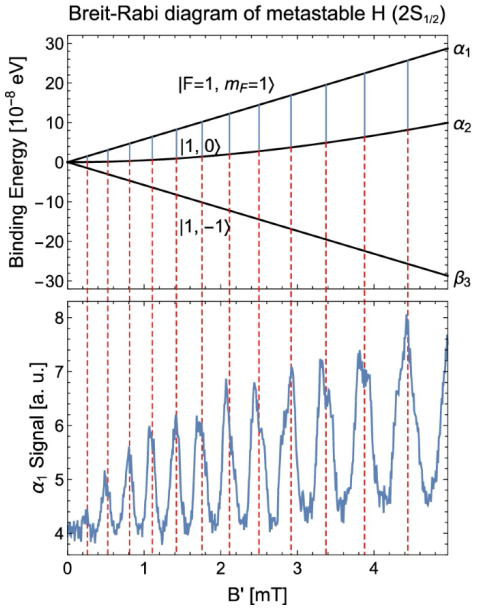

Figure 11: Measurement with both spinfilters set to $\alpha 1$, compared to the $2\,n+1$-photon resonances (source: [4, Graphical abstract]).

Attempts have been made to match the peaks or valleys of the oscillations to resonances (see fig. 11). These attempts had a low precision, as many transitions

happen at the same time (see fig. 12), which distorts the peaks. This implies that the effect of the probability of one transition changes depending on the resonance of the other transition. Thus simple analyses these Sona spectra are insufficient for achieving high precision.

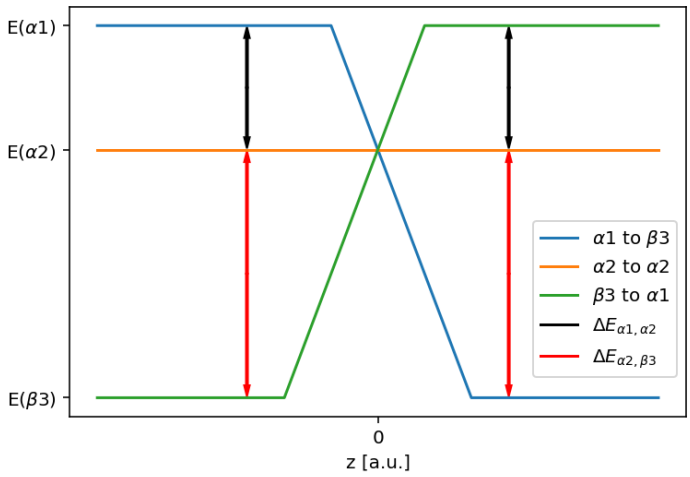

Figure 12: Scheme of multi-photon induced transitions in a Sona-transition unit.

2.3.4 Precession of angular momenta and magnetic moments

An alternative but equivalent concept to the more intuitive photon- or Okorokov-effect image is the concept of spins and other angular momenta being rotated in space by external magnetic fields and magnetic fields within the atom. To calculate the time evolution of a system of Zeeman states interacting with external B-fields, the Schrödinger equation needs to get solved for this system. To calculate the behavior of a known ensemble of particles, the density operator formalism can be used to describe the system in an orthonormal basis of eigenstates.

With this formalism the Schrödinger equation is transformed into the von Neumann equation

$$\frac{d\hat{\rho}}{dt} = -\frac{i}{\hbar}[\hat{H}, \hat{\rho}] \tag{11}$$

with the density operator $\hat{\rho}$ and Hamilton operator $\hat{H}$. With given initial states and magnetic fields over time a numerical solver for differential equations can simulate the time evolution of spin states.

The von Neumann equation (see eq. (11)) gets exploited to simulate the spin dynamics of metastable hydrogen atoms in the Sona region. It is written as a set of coupled differential equations in the uncoupled representation $|m_J, m_I\rangle$ for a

numerical approach. Using Clebsch-Gordon coefficients this basis can easily be converted back and forth into the coupled representation, which consists of four states characterized by $F = 1,0$ and $m_F \in \mathbb{Z},\ |m_F| \leq F$ for hydrogen atoms with $J = 1/2$ and $I = 1/2$ (see eq. (5)).

The Hamilton operator, an essential part of the von Neumann equation, of the spin and angular-momentum system of a hydrogen atom, which has its electron in a given shell $n \in \mathbb{N}$, is described by

$$\hat{H} = \Delta E_{\text{Lamb}} \frac{\vec{L}\cdot\vec{S}}{\hbar^2} + A\frac{\vec{I}\cdot\vec{J}}{\hbar^2} + \left(g_j \mu_B \frac{\vec{J}}{\hbar} - g_I \mu_k \frac{\vec{I}}{\hbar}\right)\cdot\vec{B} \tag{12}$$

(source: [10, p.16, eq. (75)]).

It contains a term describing the Lamb shift, which is an interaction between the spin $\vec{S}$ and orbital angular momentum $\vec{L}$, a second term describing the hyperfine structure as an interaction between the nuclear spin $\vec{I}$ and the total angular momentum of the electron $\vec{J}$ and a last term describing the Zeeman effect as an interaction of $\vec{I}$ and $\vec{J}$ with the external magnetic field $\vec{B}$.

The commutator in the von Neumann equation can be written as

$$[\hat{H},\hat{\rho}] = \hat{H}\cdot\hat{\rho} - \hat{\rho}\cdot\hat{H}. \tag{13}$$

To write the von Neumann equation as a calculable equation each term of the Hamilton operator has to be multiplied with the density operator like in

$$\begin{aligned}
&\langle m_J, m_I | J_+ \cdot \hat{\rho} \left| m_J', m_I' \right\rangle \\
&= \left\langle m_J', m_I' \right| \left(J_+ \cdot \hat{\rho}\right)^\dagger |m_J, m_I\rangle^* \\
&= \left\langle m_J', m_I' \right| \hat{\rho}^\dagger J_+^\dagger |m_J, m_I\rangle \qquad |J_+^\dagger = J_-,\ \hat{\rho}^\dagger = \hat{\rho} \\
&= \left\langle m_J', m_I' \right| \hat{\rho} J_- |m_J, m_I\rangle \\
&= c_{J-} \cdot \left\langle m_J', m_I' \right| \hat{\rho} |m_J, m_I\rangle \\
&= c_{J-} \cdot \langle m_J, m_I | \hat{\rho}^\dagger \left| m_J', m_I' \right\rangle \qquad |\hat{\rho}^\dagger = \hat{\rho} \\
&= c_{J-} \cdot \langle m_J, m_I | \hat{\rho} \left| m_J', m_I' \right\rangle \\
&= c_{J-} \cdot \hat{\rho}_{m_J, m_I; m_J', m_I'},
\end{aligned} \tag{14}$$

where J_+ is used as an example to calculate the product with $\hat{\rho}$ in the $\langle m_J, m_I | m_J', m_I' \rangle$-base representation. The factor c_{J-} is an example for the abbreviation of the term

$$c_{x\pm} = \sqrt{x(x+1-m_x(m_x \pm 1))}, \tag{15}$$

that exists as c_{J+}, c_{J-}, c_{I+} and c_{I-}. After repeating similar calculations for all terms, the differential equation for metastable hydrogen in a magnetic field is found to be

$$
\begin{aligned}
\dot{\hat{\rho}}_{m_J,m_I;m_J',m_I'} &= \langle m_J, m_I | \, \dot{\hat{\rho}} \, | m_J', m_I' \rangle \\
&= \frac{i}{\hbar} \{ {}^{A}/_{2} \cdot c_{J-}' \cdot c_{I+}' \cdot \hat{\rho}_{m_J,m_I;m_J'-1,m_I'+1} + {}^{A}/_{2} \cdot c_{J+}' \cdot c_{I-}' \cdot \hat{\rho}_{m_J,m_I;m_J'+1,m_I'-1} \\
&\quad - {}^{A}/_{2} \cdot c_{J+} \cdot c_{I-} \cdot \hat{\rho}_{m_J+1,m_I-1;m_J',m_I'} - {}^{A}/_{2} \cdot c_{J-} \cdot c_{I+} \cdot \hat{\rho}_{m_J-1,m_I+1;m_J',m_I'} \\
&\quad + A \cdot (m_J' \cdot m_I' - m_J \cdot m_I) \cdot \hat{\rho}_{m_J,m_I;m_J',m_I'} \\
&+ g_J \mu_B ([c_{J-}' \cdot \hat{\rho}_{m_J,m_I;m_J'-1,m_I'} + c_{J+}' \cdot \hat{\rho}_{m_J,m_I;m_J'+1,m_I'} \\
&\quad - c_{J-} \cdot \hat{\rho}_{m_J-1,m_I;m_J',m_I'} - c_{J+} \cdot \hat{\rho}_{m_J+1,m_I;m_J',m_I'}] \cdot {}^{B_x}/_{2} \\
&\quad + [c_{J-}' \cdot \hat{\rho}_{m_J,m_I;m_J'-1,m_I'} - c_{J+}' \cdot \hat{\rho}_{m_J,m_I;m_J'+1,m_I'} \\
&\quad + c_{J-} \cdot \hat{\rho}_{m_J-1,m_I;m_J',m_I'} - c_{J+} \cdot \hat{\rho}_{m_J+1,m_I;m_J',m_I'}] \cdot {}^{iB_y}/_{2} \\
&\quad + (m_J' - m_J) \cdot B_z \cdot \hat{\rho}_{m_J,m_I;m_J',m_I'}) \\
&+ g_I \mu_k ([- c_{I-}' \cdot \hat{\rho}_{m_J,m_I;m_J',m_I'-1} - c_{I+}' \cdot \hat{\rho}_{m_J,m_I;m_J',m_I'+1} \\
&\quad + c_{I-} + \cdot \hat{\rho}_{m_J,m_I-1;m_J',m_I'} + c_{I+} \cdot \hat{\rho}_{m_J,m_I+1;m_J',m_I'}] \cdot {}^{B_x}/_{2} \\
&\quad + [- c_{I-}' \cdot \hat{\rho}_{m_J,m_I;m_J',m_I'-1} + c_{I+}' \cdot \hat{\rho}_{m_J,m_I;m_J',m_I'+1} \\
&\quad + c_{I-} \cdot \hat{\rho}_{m_J,m_I-1;m_J',m_I'} - c_{I+} \cdot \hat{\rho}_{m_J,m_I+1;m_J',m_I'}] \cdot {}^{iB_y}/_{2} \\
&\quad + (m_I - m_I') \cdot B_z \cdot \hat{\rho}_{m_J,m_I;m_J',m_I'}) \} .
\end{aligned}
\tag{16}
$$

In the simulations conducted in this thesis only atoms in the metastable $2S$ state with $l = 0$ were simulated, therefore, the Lamb term becomes zero and irrelevant for the simulations. The Stark effect quenching metastable atoms through the $2P_{1/2}$ to ground state is also neglected in the simulations, because for small magnetic fields the lifetime of Zeeman states does not differ significantly (see fig. 4) and, therefore, the ratio between the occupation numbers would not change when the Stark effect is included. The magnetic field varies throughout the beam cross section, creating differences in the simulations of the development of the spin systems along multiple rays through the beam pipe. Those simulations are weighted corresponding to a fitted or assumed beam density distribution.

2.3.5 Fit of Simulations

The approached attempt in this thesis is to simulate the spin dynamics of metastable hydrogen atoms passing through the Sona-transition unit and trying to match the results to measured Sona spectra. For this purpose first of all the magnetic field $\vec{B}(x,y,z(t))$ of the Sona transition must be optimized. In a next step the g-factors of the electron and proton, which are essential for the simulation can be used as a fit parameter as a new way to determine their values.

2.3.6 Time reversal

A particle that enters an apparatus like a Sona-transition unit in an arbitrary initial state 1 has probability $P_{1,\,2}$ to be measured in an arbitrary final state 2 when leaving it. An important rule in quantum mechanics is, that processes can run in reverse just as they can run forward. Therefore, another particle of the same kind that passes through the apparatus in the reverse direction and starts in state 2 will have the same probability $P_{1,\,2}$ to leave the apparatus in state 1.

In the conducted experiments, the first spinfilter specifies Zeeman state 1 of metastable atoms entering the Sona-transition unit and the second spinfilter measures the amount of atoms leaving it in state 2.

If the Sona-transition unit is symmetrical, swapping the spinfilter settings is equivalent to a time reversal. The reference system is allowed to be rotated around the particle trajectory so that various types of symmetry can fulfill the conditions for being analogous to a time reversal. For example single coil pair and double coil pair transversal Sona-transition units have different types of symmetry (see fig. 13), that can both work the same in reverse.

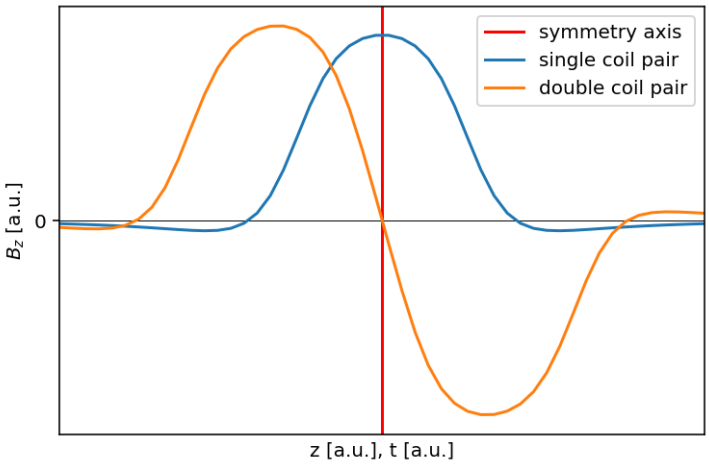

Figure 13: Sketch of possible magnetic fields in x-direction in a transversal Sona-transition unit.

With spinfilters one can measure or produce the $\alpha 1$- and $\alpha 2$-state of metastable hydrogen. Therefore, it is possible to verify the predictions of the time reversal by setting a spinfilter before the Sona-transition unit to $\alpha 1$ and another spinfilter behind it to $\alpha 2$ for a measurement and repeating the process for swapped spinfilter settings.

3 Experimental setup

The setup used for the experiments of this thesis is displayed in figure 14. The first components from the ECR source to the cesium cell are used to produce a beam of metastable hydrogen atoms. The adjacent spinfilter 1 is then used to spin polarize this beam. To measure the effect of the Sona-transition unit on the spin polarization, the amount of metastable atoms in various spin states is measured with spinfilter 2 and the Quench chamber with a photomultiplier.

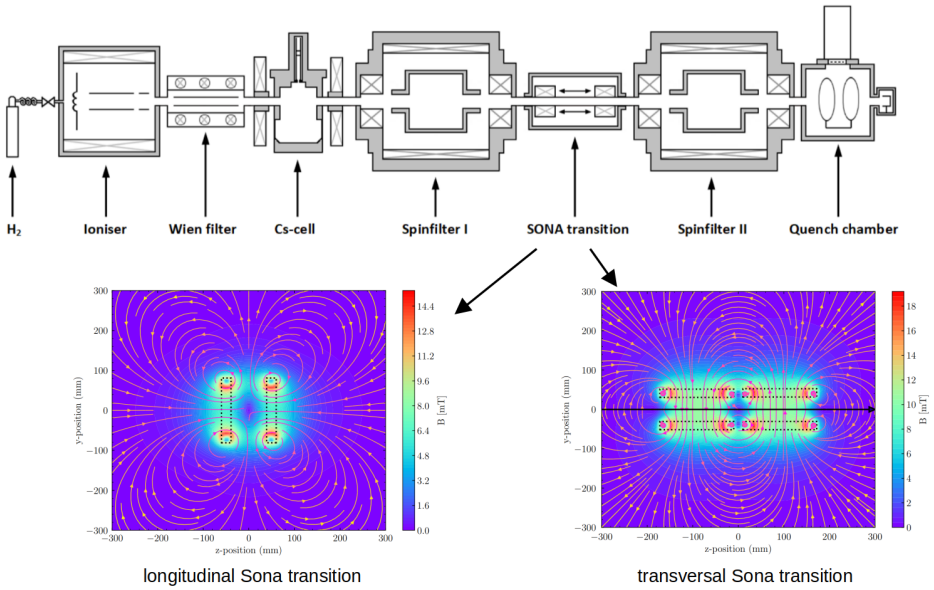

Figure 14: Sketch of the full setup, including examples of the magnetic field in a longitudinal and transversal Sona-transition unit (sources: [7][11]).

In this thesis the settings of the spinfilters are often labeled as a combined setting. For example the $\alpha 2 \alpha 1$-spinfilter setting is equivalent to spinfilter 1 being set to $\alpha 2$ and spinfilter 2 being set to $\alpha 1$.

3.1 ECR ion-source

As a particle beam is needed for the experiments, an **e**lectron-**c**yclotron-**r**esonance (ECR) ion source is used to produce a proton beam. With magnetic fields it keeps electrons on a closed orbit and accelerates them with a radio frequency field. Hydrogen gas flowing into the ECR source gets ionized by these electrons. The resulting surplus of electrons is absorbed by the metal walls of the chamber, while protons leave it through the opening towards the experiment. While doing so the protons are accelerated because the ECR source is put on an electric potential of

several hundred to few thousand volts. Afterwards, the protons have a kinetic energy of the same number of electron volts.

3.2 Wien filter

The proton beam produced in the ECR source enters a Wien filter, where it experiences the opposing electric and magnetic forces $\vec{F}_E = q \cdot \vec{E}$ and $\vec{F}_B = q \cdot \vec{v} \times \vec{B}$. To ensure, that the forces act in opposite directions, the electric and magnetic field have to be orthogonal to each other and the beam direction. An ion can pass the Wien filter without deflection, if the forces acting on an atom cancel out, leading to the velocity condition

$$v = \frac{E}{B}. \tag{17}$$

This way the Wien filter extracts ions of a given velocity.

As ions with the electric charge q get accelerated by the extraction potential U_{ECR} of the ECR source to the kinetic energy $E_{\mathrm{kin}} = U_{\mathrm{ECR}} \cdot q$, their velocity

$$v = \sqrt{\frac{2 \cdot E_{\mathrm{kin}}}{m}} = \sqrt{\frac{2 \cdot U_{\mathrm{ECR}} \cdot q}{m}} \tag{18}$$

depends on their mass m. Assuming a known ionization level, which for hydrogen ions can only be a single ionization $q = e$, a Wien filter can be used to separate ion masses.

In the case of this thesis the Wien filter settings are tuned to the mass and charge of protons (H^+, $m = 1u$), so that ions like H_2^+ ($m = 2u$), H_3^+ ($m = 1u$) or ions of rest gases like nitrogen ($m = 7u$ or $m = 14u$) or oxygen ($m = 8u$ or $m = 16u$) are deflected.

3.3 Beam optics and focusing

After leaving the ECR source, the proton beam passes through some metal rings, which are connected to power supplies setting their electrical potential. This can focus or defocus the beam. To produce an optimally focused beam, the voltages of these lenses and the capacitor plates of the Wien filter are optimized by maximizing the current induced by the ions hitting a Faraday cup at the end of the beam pipe behind the quench chamber. After turning on the production of metastable hydrogen atoms in the cesium cell (see section 3.4) one can reoptimize the beam by maximizing the photomultiplier signal produced by quenched metastable hydrogen (see section 3.7). The settings for an optimal photomultiplier signal are not necessarily the same as the settings, that optimize the number of ions hitting a Faraday cup at the end of the beam line behind the quench chamber.

3.4 Cesium cell

Parts of the proton beam are neutralized in a cesium cell after passing the Wien filter. Here the electropositive properties of cesium are used to transfer its valence electron to protons via the reaction

$$Cs + H^+ \rightarrow Cs^+ + H. \tag{19}$$

The neutralized protons turn into hydrogen atoms of which up to 30% [9, p. 43] are in the metastable $2S_{1/2}$-state (see section 2.1). Cesium, which has a low melting temperature of 28 $°C$, is heated at the bottom of the cesium cell to create vapor pressure. The upper part of the cesium cell is kept at 60 $°C$, so that the cesium can condense and drip back to the bottom. For an optimal amount of collisions between cesium atoms and protons, cesium at the bottom of the cesium cell is heated to 160 $°C$. This temperature creates an optimal partial pressure of cesium vapor of about 0.1 *mbar* to maximize the production of metastable hydrogen atoms.

3.5 Spinfilter

A spinfilter uses electric and magnetic fields and a radio frequency to deexcite metastable hydrogen atoms to the ground state and let only atoms of one specific spin or angular-momentum configuration pass unchanged (see section 2.2).

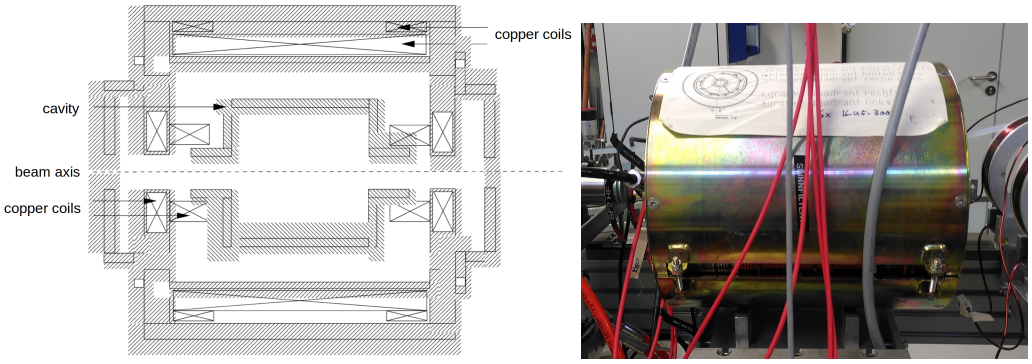

Figure 15: Sketch of spinfilter (left, source: [9]) and photo of spinfilter (right).

To produce the necessary radio frequency of 1609 MHz in a spinfilter, it has a tuned cylindrical cavity with an antenna connected to an RF generator. The required electrical fields need a division of the cavity into electrically insulated quadrants, of which two opposing quadrants are connected to DC-power supplies of opposite polarity. The other two quadrants are grounded. This way the quadrants with opposing voltages create an electrical field. The magnetic field is created by coils surrounding the cavity.

3.6 Sona-transition unit

3.6.1 Longitudinal design

In previous experiments, a longitudinal Sona-transition unit was developed that produced a magnetic field a close to a sine shape as possible [12]. This setup is shown in figure 16 and an example for the magnetic field experienced by an atom passing through it can be seen in figure 8. To shield it from external magnetic fields the Sona-transition unit is surrounded by three layers of μ-metal.

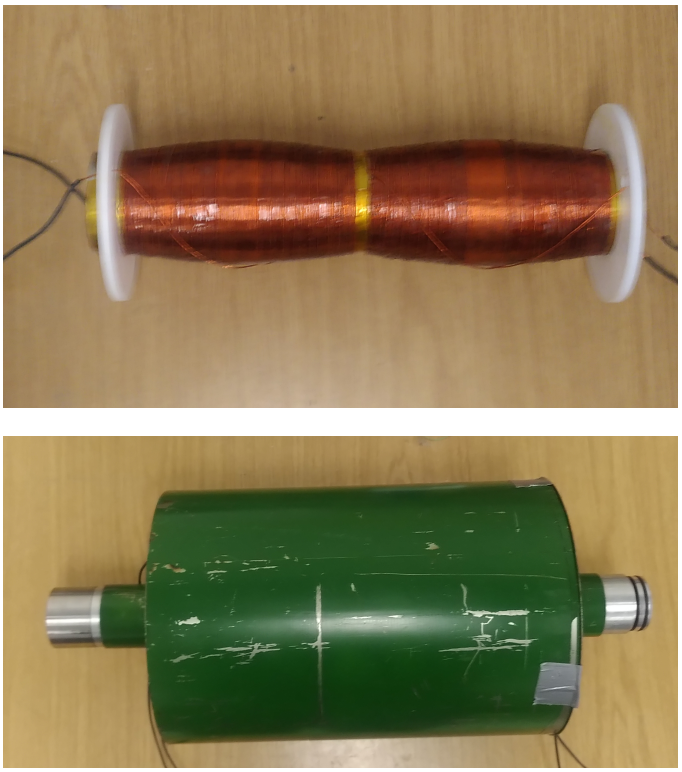

Figure 16: Photo of a longitudinal design Sona-transition unit without (top) and with shielding (bottom).

3.6.2 Transversal design

Because the behavior of the atoms in the Sona-transition unit is critically dependent on the radial component of the magnetic field, another type of Sona-transition unit has been proposed and built [11], which primarily produces a transversal magnetic field in the area of the atomic beam.

The transversal Sona-transition unit had been designed to produce a B-field x-component with a zero-value in the center and a minimum or maximum before

and after (see fig. 48). To create this field, two coil pairs have been put around the beam line transversal to the beam axis and attached electrically in series with opposite polarity. This way one coil pair produces the maximum and the other one the minimum of the B-field x-component. In the exact center the magnetic field of both coil pairs cancel out.

First measurements with this double coil pair Sona-transition unit indicated, that a double coil pair might be less effective or at least just as effective and more complex, than a single coil pair (see sections 5.2.1 and 5.2.2). Therefore, for many experiments only a single coil pair is used. For those measurements with a single coil pair Sona-transition unit, one coil pair, i.e. two coils with their center on the same axis orthogonal to the beam axis, is used, while the other coil pair is disconnected electrically.

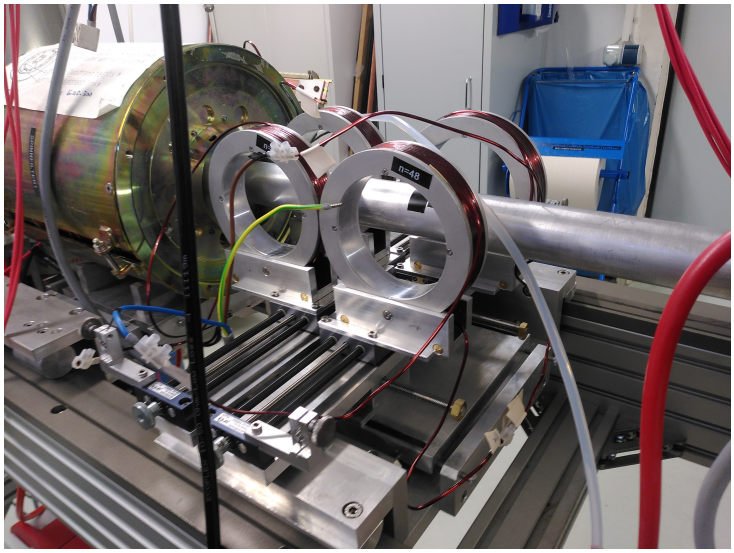

Figure 17: Photo of the transversal Sona-transition unit. Here the coil pair on the left was not attached electrically and the right coil pair was used as a "single coil pair" in the central position between the two spinfilters.

The magnetic field of a transversal Sona-transition unit can be simulated easier than a longitudinal design with variable loop densities along the beam axis. Therefore, such a simulation of the magnetic fields is used for the simulation of the spin state development instead of interpolations of measurements. In the actual measurement other distances, like the easily measurable distance to a spinfilter get measured with a folding rule or a caliper. The more intuitive parameters displayed in figure 18 are calculated afterwards using the distance between the spinfilters and the outer diameter of the beam pipe. In this figure is also shown how the coils of a single and double coil pair Sona transition unit are arranged.

The parameters that are labeled in this sketch are varied in section 5.2.

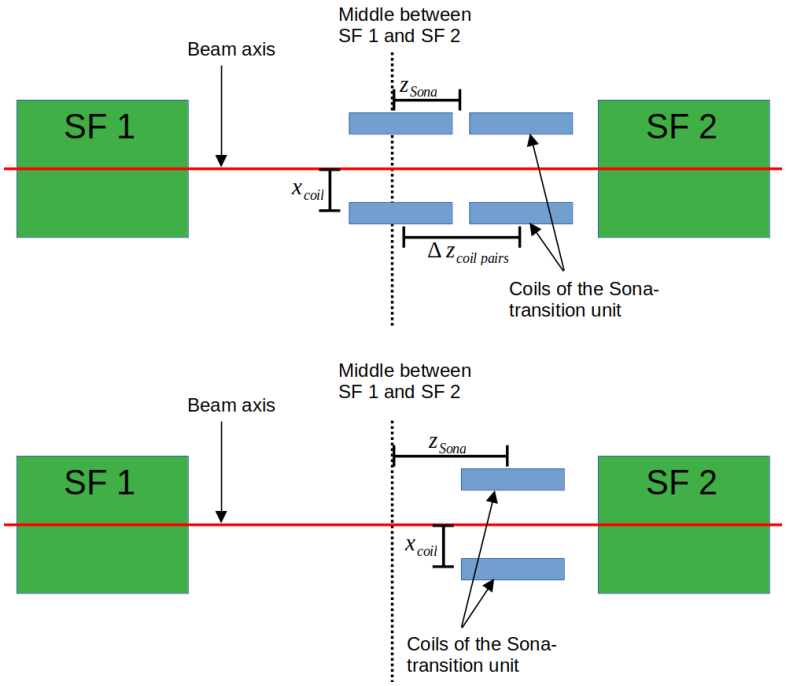

Figure 18: Sketch of a transversal design Sona-transition unit with two coil pairs (top) and with one coil pair (bottom) in between the two spinfilters (SF).

3.7 Quench chamber with photomultiplier

The beam of metastable atoms reaching the quench chamber passes an area with a strong electric field and is quenched to the ground state due to the Stark effect. The energy difference of 10.25 eV is emitted via a Lyman-α photon with a wavelength of 121 nm. These UV-photons can be detected by a photomultiplier and their intensity is registered by electronics and correlated to the current settings of the spinfilters and the Sona-transition unit. Photons entering the photomultiplier are hitting a photocathode creating a free electron each by kicking them out via Einsteins photoeffect. For signal amplification this electrons are directed on a cascade of dynodes, each dynode on a higher electric potential than the last one. As a result the electrons are accelerated from one dynode to the next and on impact produce multiple free electrons for the following stage. This increases the current of electrons until it is measurable by a digital oscilloscope.

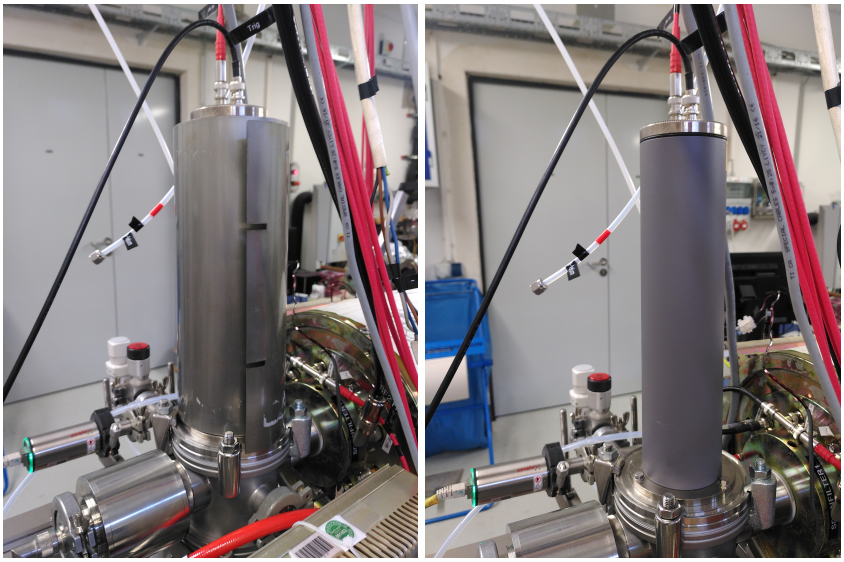

Figure 19: Photomultiplier (PMT) with (left) and without (right) magnetic shielding.

In previous experiments, an unexpected effect was observed when ramping over the magnetic field strength of the second spinfilter to create images such as in figure 5. This spinfilter is visible on the bottom right of the images in figure 19. As it turned out, an internal magnetic shielding of the photomultiplier was missing, making its sensitivity for incoming photons dependent on external magnetic fields, diverting the free electrons inside. Therefore, the spinfilter nearby disturbs its efficiency. Even worse, its disturbance increases with the increased magnetic fields necessary to change from the $\alpha 1$- to the $\alpha 2$-spinfilter setting (see fig. 5). As a countermeasure, magnetic shielding available from previous Sona-transition unit iterations (compare to section 3.6.1) was added.

3.8 Magnetic field measurements

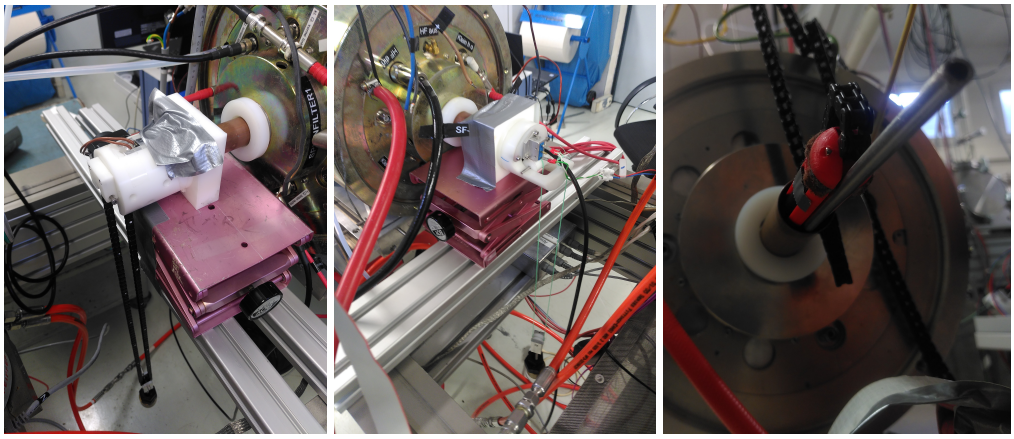

Figure 20: B-field measuring system: Chain pulley system with step motor (left), string pulley system and the cable of the B-field probe (middle) and sled with B-field probe on a guiding rail (right).

To measure the magnetic field inside the setup, a recently built apparatus to automatize this process is used [13]. It uses a step motor and a chain to move a sled with a B-field sensor through a pipe (see fig. 20, right) and to set and measure its position along the pipe axis, which is defined to be the z-axis. Because the chain can only hold its length precisely when in tension, the sled is pulled by a string and a pulley system from the other end of the pipe (see fig. 20, middle). To minimize the force on the step motor, a similar pulley system is installed on the chain as well (see fig. 20, left). The sled containing the B-field meter must not rotate while being pulled through the pipe. Therefore, an additional rail is put into the pipe and fixed on both ends to prevent a rotation around the z-axis. For the measurements of magnetic fields in this thesis, the pipe is put through the arrangement of two spinfilters with a Sona-transition unit in between.

4 Measurements with a longitudinal Sona transition

4.1 Magnetic field measurements

The magnetic field of the longitudinal Sona-transition unit, including the spinfilters before and after, used for this thesis had already been measured when developing the device described in section 3.8 [13]. Three measurements are used to extrapolate the magnetic field in space and for other currents I_{Sona}. The first measurement is conducted with a Sona current $I_{\text{Sona}} = 0.2\ A$ but without currents in the spinfilters (see fig. 21, top left). The second measurement uses the same Sona current but additionally the current in the spinfilters was turned on (see fig. 21, top right). At last the background is measured without any currents, so that mainly the B-field of magnetized iron in the spinfilters is visible in the data (see fig. 21, bottom).

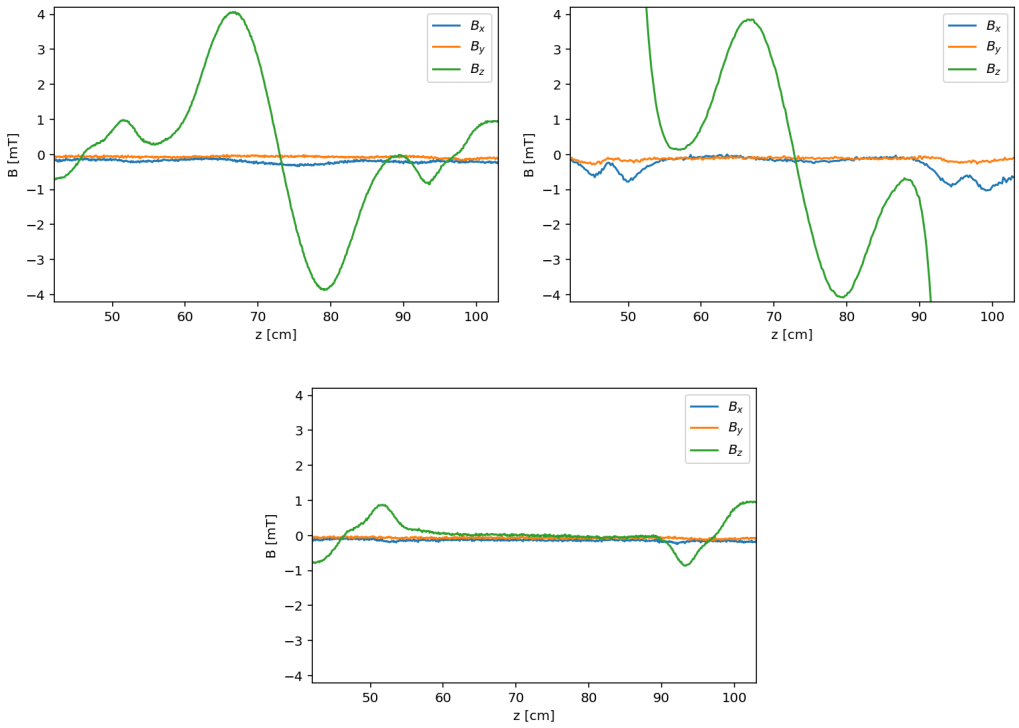

Figure 21: Measurement with $I_{Sona} = 0.2\ A$ (top left), measurement with SF1 and SF2 on and $I_{Sona} = 0.2\ A$ (top right) and background measurement (bottom). The origin of the data are measurements conducted for [13].

To be able to produce a simulation of spin precessions (see section 2.3.4) these measurements have to be turned into continuous functions, that are defined at any

point in the simulated areas. To create such function, a Gaussian curve is placed around the position corresponding to the argument of the function and used to weight the measurement points. Then the average of the weighted data points are the result of the function at that position.

The measurements (see fig. 21 and fig. 69 in the appendix) were used to calculate the magnetic field in the of the Sona-transition region for any current I_{Sona} in the Sona-transition unit. First the influence of the Sona current $d\vec{B}/dI_{\text{Sona}}$ (see fig. 22, left) is calculated by subtracting the measurement without any currents (fig. 21, bottom) from the measurement with a Sona current and dividing the result by $I_{\text{Sona}} = 0.2\ A$ Secondly a background magnetic field $\vec{B}_0(z)$ (see fig. 22, right), that is mainly determined by the magnetic field of the spinfilters is calculated. To do so the influence of the spinfilter current is calculated as the difference between the measurements with a Sona current without (fig. 21, top left) and with spinfilter currents (fig. 21, top right) and added to the measurement without any currents (fig. 21, bottom).

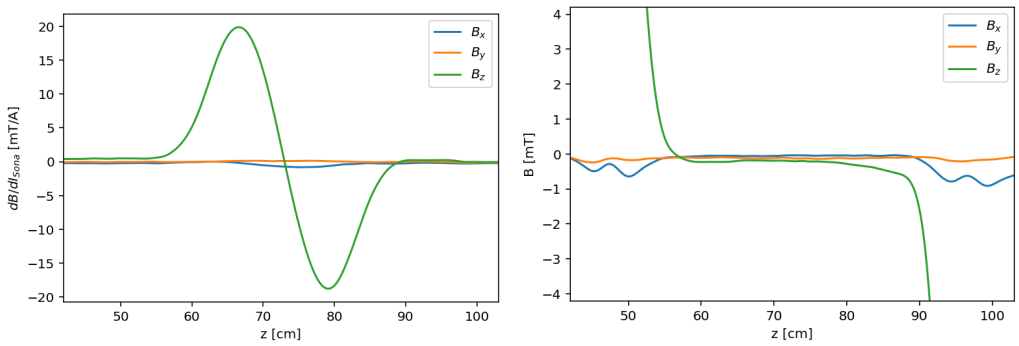

Figure 22: Dependence of the B-field on I_{Sona} (left) and the B-field for $I_{Sona} = 0\ A$ (right). The dependence on I_{Sona} is the difference between the measurement with $I_{Sona} = 0.2\ A$ and the background measurement from fig. 21 divided by 0.2 A. To find the B-field for $I_{Sona} = 0\ A$, the measurements for $I_{Sona} = 0.2\ A$ from fig. 21 with and without spinfilters were subtracted from each other to include the influence of the spinfilter current. Additionally the general background from from fig. 21 is also added.

The longitudinal Sona-transition unit is one solid object (see fig. 16). Therefore, no geometric parameters could be varied for measurements investigating dependencies of the Sona oscillations, while this could be done for transversal Sona-transition units (see section 5).

4.2 Fit of simulations to a measurement

As an attempt to find a simulation that matches as good as possible to a conducted measurement, a fit is done. In each iteration step it conducts a simulation with changed parameters and for a given set of values for Sona currents I_{sim}. Then it calculates the difference between the measurement and simulation for each I_{sim} and tries to minimize the squared sum of these differences.

To find a match between the measurement and simulations, parameters of the simulation are varied, until an optimum is found. The first parameters, that are varied, are t_0 and Υ, that translate the time of the measurement t, saved by the digital oscilloscope, to a current $I_{\text{Sona}}(t) = (t - t_0) \cdot \Upsilon$.

A second type of parameters vary the weight of the measurements in figure 21, especially the background fields and also the exact start and end point of the simulation.

Third the beam distribution gets varied. To do so, the weights w_i of the simulations along multiple parallel rays throughout the beam pipe cross section are changed. Depending on the position $\vec{x_i} = \binom{x_i}{y_i}$ of a simulated ray i in the beam pipe relative to the pipe´s center, the ray is weighted with

$$w_i = e^{-\frac{1}{2} \cdot \left| (\vec{x_i} - \vec{x_0})/\sigma \right|^2}. \tag{20}$$

The variable fit parameters are the central position $\vec{x_0} = \binom{x_0}{y_0}$ of the beam relative to the beam pipe center and the distribution width of the beam σ.

At last the simulated intensities of other Zeeman states are added with smaller weights to the expected Zeeman state. These weights are used as parameters to check, whether the apparatus behind the Sona-transition unit is actually only sensitive to one Zeeman state or whether the spinfilter also lets other Zeeman states pass through in small amounts.

4.2.1 Results

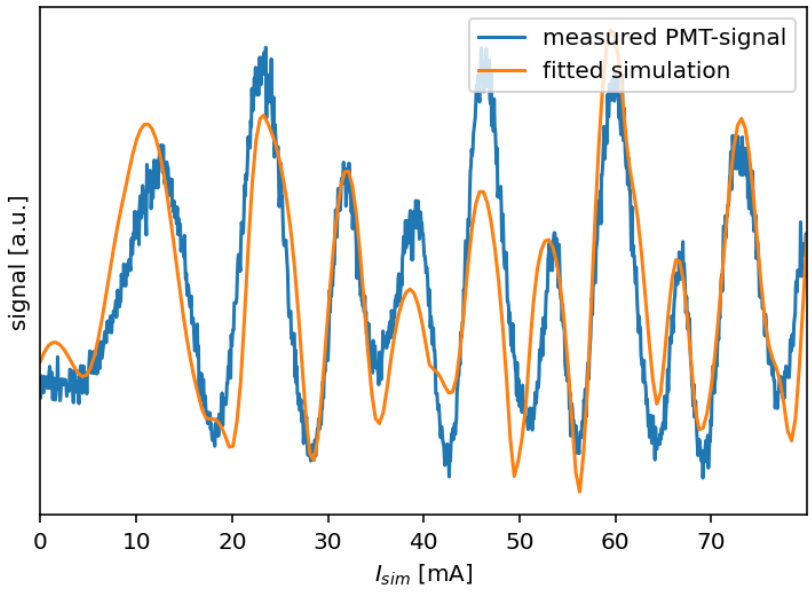

Figure 23: Simulation and measurement fitted to each other with $\alpha 2\alpha 1$*-settings. On the x-axis the simulation current* I_{sim} *is displayed. This is an important distinction, as the calculated current of the measurement is bigger by a factor larger than* 2*.*

The fit gives a surprising value for the time to current factor Υ, which was found to be 31.7 $\frac{mA}{s}$ instead of the expected 81.3 $\frac{mA}{s}$ measured before in a calibration measurement. The expected value is deducted from the ramp signal, that gets saved with the measured PMT signal. Thus, one must question the validity of the found fit result between simulation and measurement.

The resulting fit parameters of the beam distribution have values of $x_0 = 23.6\ mm$, $y_0 = -10.6\ mm$ and $\sigma = 0.6\ mm$. The values for x_0 and y_0 seem a bit large but might be reasonable if the sensor used for the magnetic field measurement had been positioned off axis. It is also possible, that the position in the beam axis is preferred by the fit due to random effects making the simulation more similar to the measurement with this settings, because other fit parameters might have a far lager impact. On the other hand the radial distribution width σ seems to be far too small to be realistic. A possible explanation might be, that the distribution of the beam intensity is less gaussian and more cylindrical than assumed. If simulations of rays outside the cylinder with actual beam intensity deviate relatively much from the measurement and the rays within this cylinder, the fit prefers not to include these rays and decreases σ beyond the actual radius.

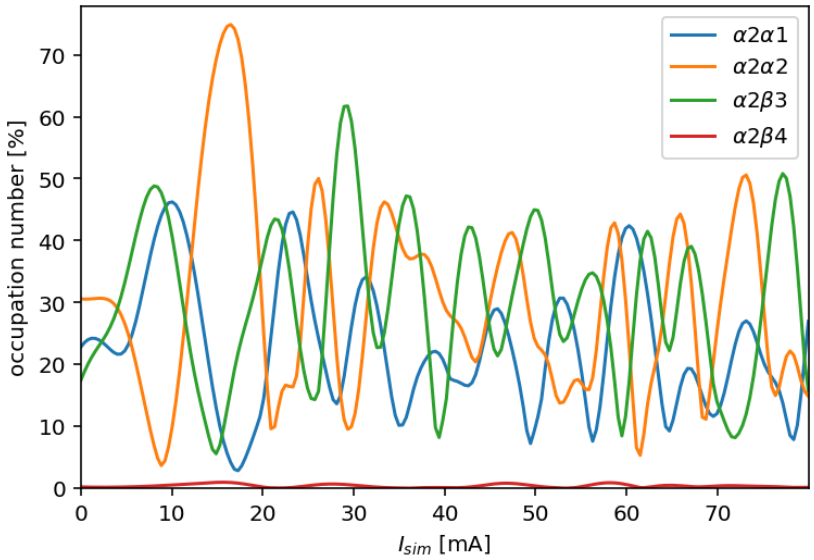

Figure 24: Full result of the simulation starting with the $\alpha 2$-state, fitted to a measurement with $\alpha 2\alpha 1$-settings. On the x-axis the simulation current I_{sim} is displayed. This is an important distinction, as the calculated current of the measurement is bigger by a factor larger than 2.

The fitted parameters, that vary the not renormalized additional weight of the simulations of the four Zeeman states, are 33.3 % for the $\alpha 2\alpha 2$- and $\alpha 2\beta 3$-simulation and 0 % for the $\alpha 2\beta 4$-simulation and represent the weight relative to the main simulation for $\alpha 2\alpha 1$-settings. These values are the maximum (33%) and minimum (0%) of the fitting range. After weighting and adding these simulations, the sum is renormalized. Therefore, these results are equivalent to for example 0 % for the $\alpha 2\alpha 2$- and $\alpha 2\beta 3$-simulation and -50 % for the $\alpha 2\beta 4$-simulation. In this case it is even reasonable to represent the fit result as such, because the $\alpha 2\beta 4$-simulation gives very small values (see fig. 24), that are used to compensate random fluctuations and, therefore, can also be negative with a relative high absolute value.

To evaluate the precision of the simulation fit to the measured data, the resulting fit parameters have been used to simulate the transitions with the spinfilter settings $\alpha 1\alpha 1$, $\alpha 1\alpha 2$, $\alpha 2\alpha 1$ and $\alpha 2\alpha 2$ (see fig. 25). The only other change of this simulations is, that the fitted corrections for the sensitivity of the spinfilter to the four Zeeman states are ignored, which causes small deviations between figure 23 and the bottom left image of figure 25. Except the $\alpha 2\alpha 1$-measurement, that is used to fit the result of the simulation with variable parameters, measurements for $\alpha 1\alpha 1$, $\alpha 1\alpha 2$ and $\alpha 2\alpha 2$ have also been conducted. the results of these simulations and measurements are compared in figure 25.

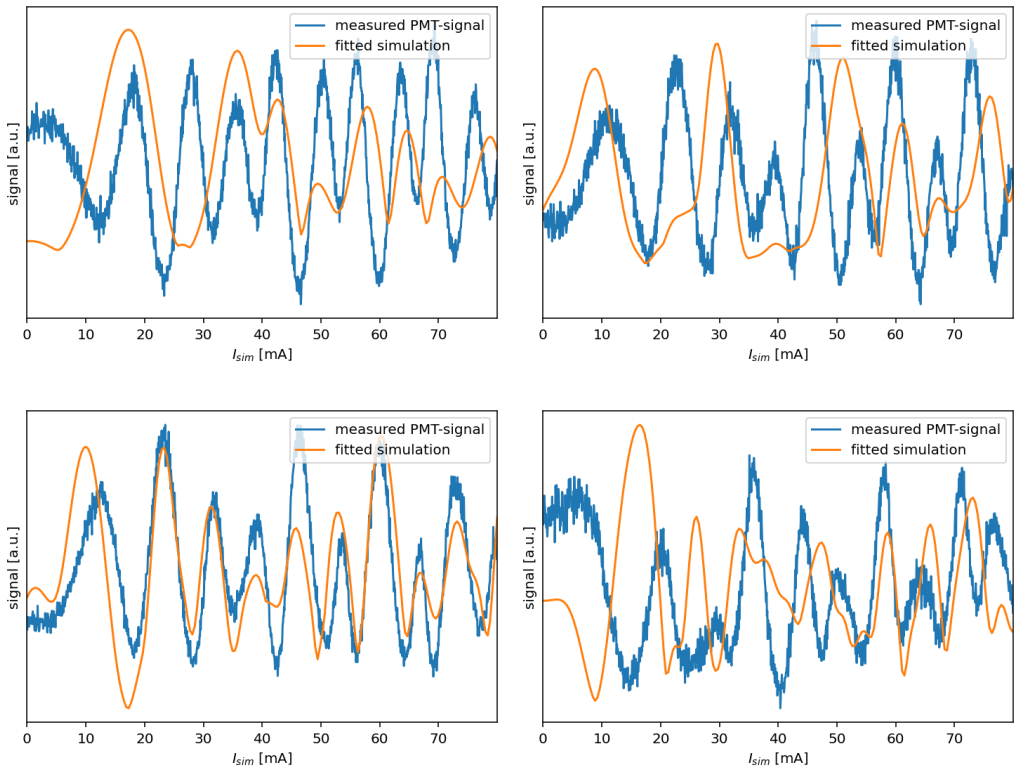

Figure 25: Measurements and simulations with $\alpha 1\alpha 1$*- (top left),* $\alpha 1\alpha 2$*- (top right),* $\alpha 2\alpha 1$*- (bottom left) and* $\alpha 2\alpha 2$*-spinfilter settings (bottom right). The simulations used parameters, that resulted from a fit of the* $\alpha 2\alpha 1$*-settings. On the x-axis the simulation current* I_{sim} *is displayed.*

The $\alpha 1\alpha 1$-measurement and simulation fit well together, as the peaks are at similar positions but have very different heights. Only the second peak at $I_{\text{Sona}} = 25\ mA$ to $30\ mT$ seems to be suppressed or small in the simulation.

For the $\alpha 1\alpha 2$-measurement, some peaks are also shifted, suppressed or enhanced in the simulation. For example, the peaks at about $I_{\text{Sona}} = 25\ mA$ and $40\ mT$ are visible but suppressed. The peaks above $55\ mT$ fit quite well and only between $45\ mA$ and $55\ mT$ it seems like two peaks from the measurement were shifted towards each other in the simulation into one big peak.

The peak positions of the simulation and measurement of $\alpha 2\alpha 2$ fit together above $50\ mT$, although the peak heights do not fit. The peak of the measurement at $45\ mT$ seems to be shifted towards slightly higher currents. Apart from the peaks at $35\ mT$, here the peaks cannot be matched well for lower currents of $\alpha 2\alpha 2$.

The precision of the simulations gets investigated further, because the simulated graphs still look quite different from the measurements. As an example, a

Simulation is conducted, that includes a change of the magnetic field, that corresponds to changing the spinfilter settings from the $\alpha 1$-setting to $\alpha 2$ (see fig. 26).

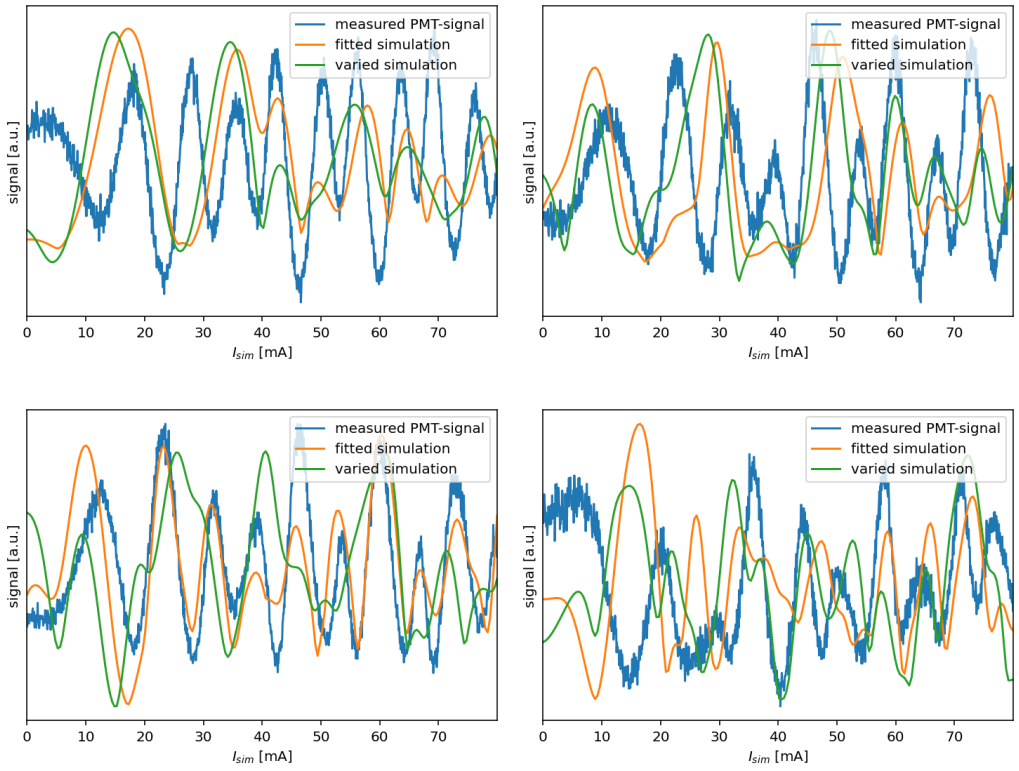

Figure 26: Measurements and simulations with $\alpha 1\alpha 1$- (top left), $\alpha 1\alpha 2$- (top right), $\alpha 2\alpha 1$- (bottom left) and $\alpha 2\alpha 2$-spinfilter settings (bottom right). The simulations used parameters, that resulted from a fit of the $\alpha 2\alpha 1$-settings. A second simulation is plotted, using a magnetic field, assuming a changed spinfilter setting. On the x-axis the simulation current I_{sim} is displayed.

One can see, that at various points the simulations using varied magnetic fields look significantly different than the unvaried simulation. Various peaks and dips have been suppressed, increased or shifted by the variation. The type of change is not necessarily expected to be the same as in the real measurement because the magnetic field, that was fitted, had a limited number of parameters, so that the actual magnetic field might not even been possible to achieve by varying the given parameters. Due to these differences other changes, like an estimated B-field change from a different spinfilter setting, might influence the result differently.

It can be concluded, that small deviations from the real magnetic field can already make a huge difference in the patterns of the simulated Sona oscillations.

In actual measurements the stray fields of the spinfilters are always changed to measure different Zeeman states, causing a change of hight for the peaks of the Sona oscillations. On the other hand the positions of the peaks are not impacted much, because the effective B-field B_{eff} is not changed much by the stray fields of the spinfilters.

4.3 Simulations for varying the kinetic energies

When the measurements from section 4.2 were conducted, they were conducted only at a kinetic energy of 1.5 keV. Later, when measurements with various kinetic energies have been conducted for transversal Sona-transition units and analyzed, it turned out that the measurements are sensible to different kinetic energies. Unfortunately at this point it was not feasible anymore to conduct such measurements, as at that moment the setup got rebuild for other experiments. Therefore, only simulations could get analyzed.

These simulations were done without any background magnetic field, as there are no measurements to compare to. Instead this simulations shall represent the physical effects with as little disturbance as possible.

4.3.1 Fitting the energy differences of the Breit-Rabi diagram

To check the possibility of matching the photon image to measurements and simulations, the position of the first peaks of the $\alpha 1 \alpha 1$ simulations are searched for in figure 27 (left). Afterwards the theoretical positions of the $\alpha 1 \alpha 2$-resonances (see section 2.3.3) are fitted to the measured peaks by varying the assumed wavelength of the Sona-transition unit λ and the quotient between the effective magnetic field and Sona current $\kappa = \frac{B_{\text{eff}}}{I_{\text{Sona}}}$ (see fig. 27, right).

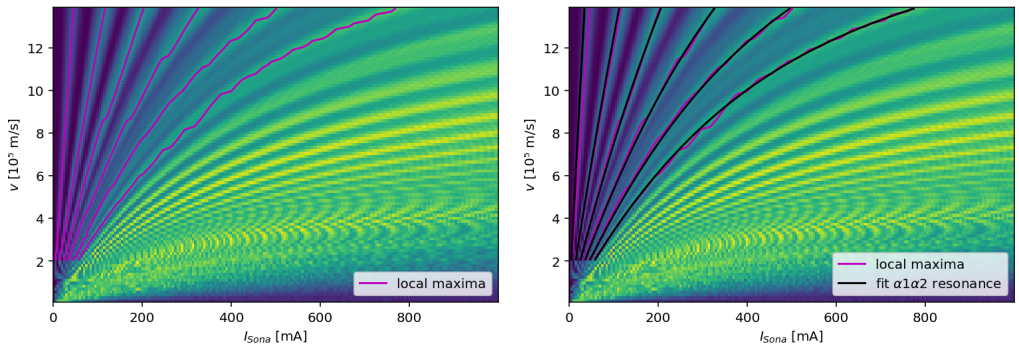

Figure 27: Fit of the $\alpha 1 \alpha 2$-resonances depending on κ and λ to the patterns of the $\alpha 1 \alpha 1$-simulation.

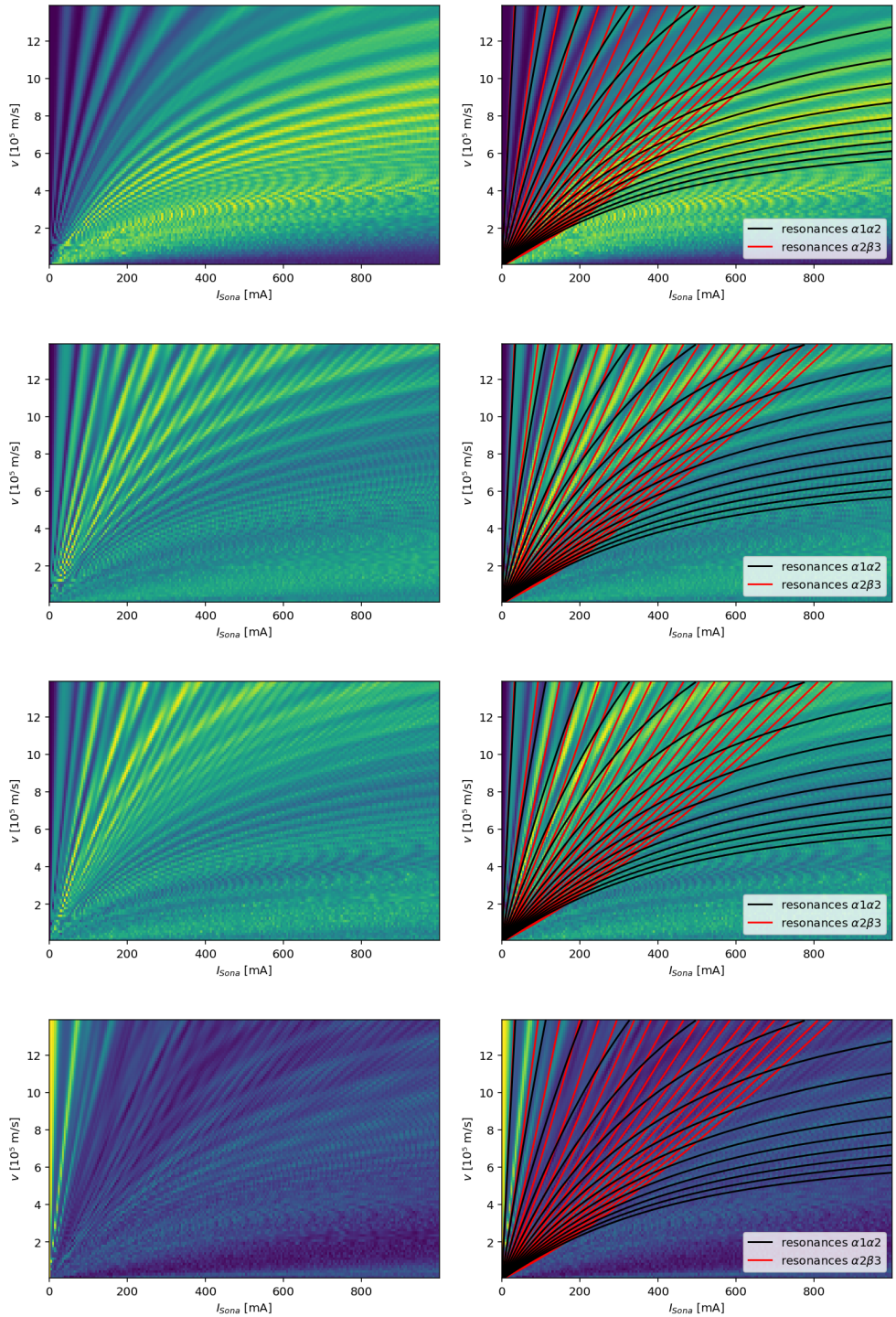

Figure 28: Extended simulation for $\alpha 1\alpha 1$, $\alpha 1\alpha 2$, $\alpha 2\alpha 1$ *and* $\alpha 2\alpha 2$ *(top to bottom), including* $\alpha 1\alpha 2$*-(black) and* $\alpha 2\beta 3$*- (red) resonances (right). The* κ *and* λ *are fitted to the* $\alpha 1\alpha 2$*-patterns of the* $\alpha 1\alpha 1$*-simulation.*

To verify the result of this fit, the found λ and κ are used to predict the position of $\alpha 2\beta 3$- and further $\alpha 1\alpha 2$-resonances. Those resonances can, according to figure 12, cause peaks or dips, if they can cause a population or depopulation of a state. Therefore, one expects, that patterns in simulations and measurements follow the calculated resonance positions, which was checked in figure 28.Additionally to the four spinfilter settings in simulated in this figure, which are measurable with existing spinfilters, the final occupation numbers of the β-states are displayed in figure 70 in the appendix.

In the images displaying the $\alpha 1\alpha 1$-simulation in figure 28, one can not recognize the $\alpha 2\beta 3$ resonances well because of the amount of transitions that would be necessary to populate or depopulate the $\alpha 1$-state via $\alpha 2\beta 3$-transition. These transitions can be traced in figure 12. In all other images of figure 28 the $\alpha 2\beta 3$-resonances are recognizable in the visible patterns, even though these pattern shift slightly relative to each other. On the other hand, the $\alpha 1\alpha 2$-resonances fit to the patterns for all examined spinfilter settings. Even for the higher order resonances, that are extrapolated and not directly fitted, the expected resonances fit to the pattern in the images.

4.3.2 Comparison of the results for $\alpha 1\alpha 2$- and $\alpha 2\alpha 1$-settings

Theoretically the results for measurements for switched spinfilter settings should be the same (see section 2.3.6). One can see in 29, that the simulations for $\alpha 1\alpha 2$ and $\alpha 2\alpha 1$ are very similar but not perfectly equal.

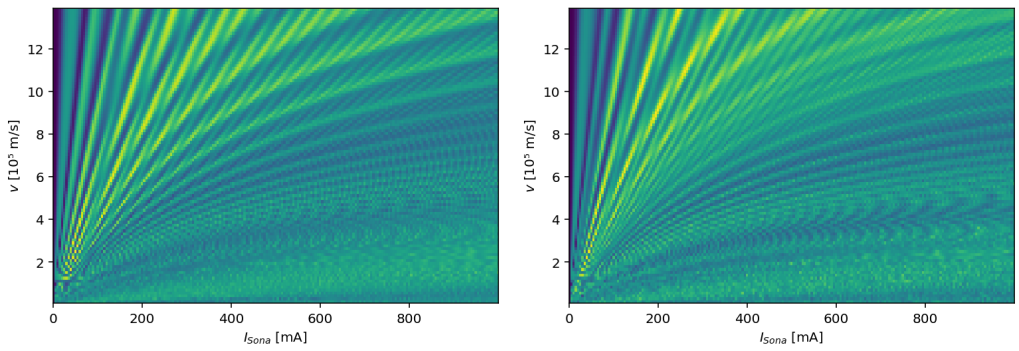

Figure 29: Comparison of simulations at various kinetic energies with the spinfilter settings $\alpha 1\alpha 2$ (left) and $\alpha 2\alpha 1$ (right).

The reason that the simulations are not perfectly equal is, that the necessary conditions are also not perfectly met. One condition for this equality is, that the magnetic field is symmetrical, which is not the case for simulations of the longitudinal Sona-transition unit. Here the magnetic field that is used for the simulation

is derived from measurements, that cannot be perfectly symmetrical. On the other hand the simulations of transversal Sona-transition units are perfectly equal (see section 5.4.3), because the magnetic fields used for the simulations are simulated perfectly symmetrical (see section 5.1).

Generally, both simulations match quite well to each other. The only specifically recognizable difference is, that the $\alpha 1\alpha 2$-resonances of the $\alpha 2\alpha 1$-simulation seem to be split into double peaks for high velocities v and high I_{Sona}, while they do not in the $\alpha 1\alpha 2$-simulation. A possible reason is, that the magnetic field might correspond to two overlapping photons with slightly different wavelengths, instead of one or more photons with the exact same wavelength. Due to the asymmetry of the magnetic field and the swap of the spinfilter settings, these photons have a differently weighted influence on the occupation numbers at the resonances.

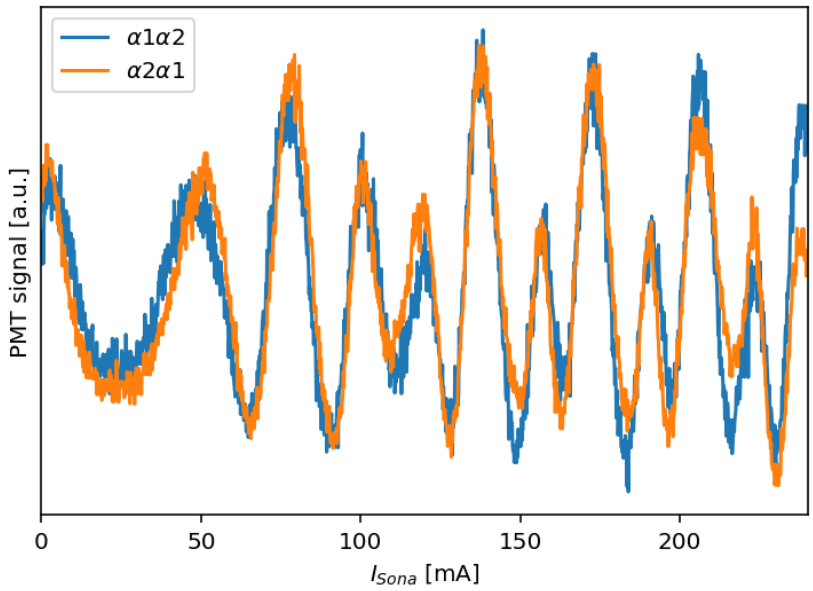

Figure 30: Comparison between the measurements with $\alpha 1\alpha 2$- and $\alpha 2\alpha 1$-settings.

The results of the measurements conducted with $\alpha 1\alpha 2$- and $\alpha 2\alpha 1$-settings for $E_{\text{kin}} = 1.5\ keV$ (see fig. 30) are also very similar supporting the prediction in section 2.3.6.

5 Measurements with transversal Sona transitions

5.1 Magnetic field measurements

In contrast to the magnetic fields longitudinal Sona-transition unit from section 4, which has a longitudinal coil with varying winding density per length (see fig. 16), the transversal Sona-transition unit consists of two or four simple coils. For an easier and faster computation of the magnetic fields, the coils were assumed to be perfectly circular conductors with a point like cross section. To validate the applicability of such simulations, several measurements of the magnetic fields have been conducted with a single coil pair and a double coil pair as described in section 3.8. For the simulation of such magnetic fields the positions of the coils was given to functions of the python library "magpylib", which used this information to calculate the resulting magnetic field.

5.1.1 Calibration

If a measurement is conducted with a current in the Sona-transition unit $I_{\text{Sona}} \neq 0$ turned on, the pattern of the transversal magnetic field can be recognized both in the $B_{\text{x raw}}$-component and the $B_{\text{y raw}}$-component, because the magnetic field sensor on the sled, the sled in the pipe or both are rotated around the z-axis (see figs. 20 and 31).

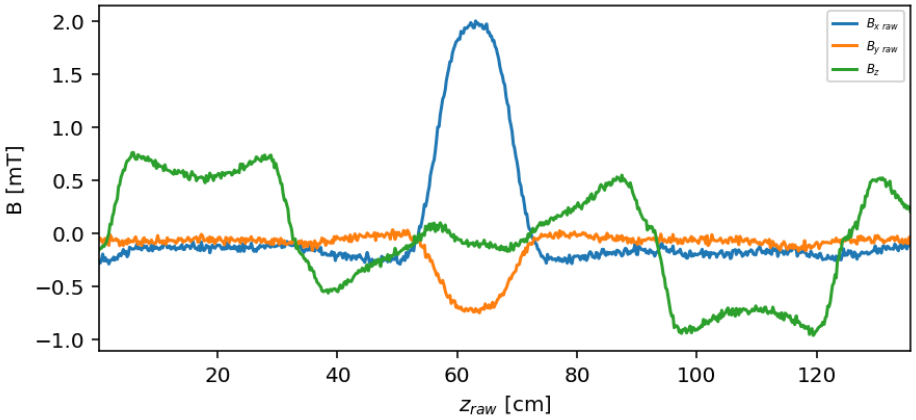

Figure 31: Raw measurement of the magnetic field in a single coil transversal Sona-transition unit in the middle between the two spinfilters.

To compensate such rotations around the z-axis, a fit performs the rotational transformation

$$\begin{pmatrix} B_x \\ B_y \end{pmatrix} = \begin{pmatrix} \cos(\varphi) & -\sin(\varphi) \\ \sin(\varphi) & \cos(\varphi) \end{pmatrix} \cdot \begin{pmatrix} B_{\text{x raw}} \\ B_{\text{y raw}} \end{pmatrix} \tag{21}$$

by such an angle φ, that the B_y-component in the area in between the spinfilters is as constant as possible (see fig. 32).

A simple minimization of the B_y-component is not desirable, as there are background magnetic fields, such as the geomagnetic field. If at least one spinfilter is turned on, its relative strong magnetic field of more than 50 mT is partly but significantly recognizable in the B_x- and B_y-component (e.g. see figs. 34 and 35), due to imperfections of the spinfilter alignment or the B-field sensor. Therefore, the data taken in the spinfilters is not suitable to calibrate the rotation correction around the z-axis for the best alignment with the Sona-transition unit. The resulting correction angle is for most measurements between 15 ° and 20 °.

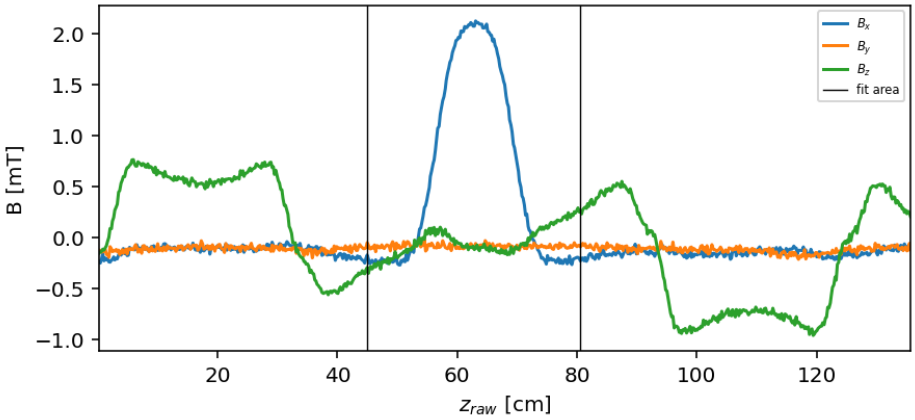

Figure 32: Measurement of the magnetic field in a single coil transversal Sona-transition unit in the middle between the two spinfilters. The x- and y-component are rotationally transformed so that the magnetic field of the transition unit in the fit area points along the x-axis.

For a more vivid definition of the z-axis parallel to the beam, the z-position is redefined to have $z = 0\ cm$ at the center between the spinfilters. To find this center in the magnetic field measurements, the standard measurement with one coil pair is used for calibration by fitting a simulation of of the z-component. For compensation of the geomagnetic field, a constant background is added as a fit parameter (see fig. 33). This measurement is used as the base for all measurement series using single coil pair Sona-transition units. All measurements of these series use the same parameters as the basic measurement and are only changed by the parameter explicitly varied, which can be the coil pair position z_{Sona} or the distance of the coils from the beam axis x_{coil}. Therefore, each of these series contains the basic measurement, which has not been repeated for every series but just been used multiple times. Similarly there is also a basic measurement for the double coil pair, that has been used in series varying z_{Sona} and the distance between the

coil pair positions $\Delta z_{\text{coil pairs}}$. Measurements of the background with $I_{\text{Sona}} = 0\ A$ (see figs. 34 and 35) have also been conducted only once and were not repeated multiple times for various measurement series such as the double coil pair and single coil pair Sona-transition units.

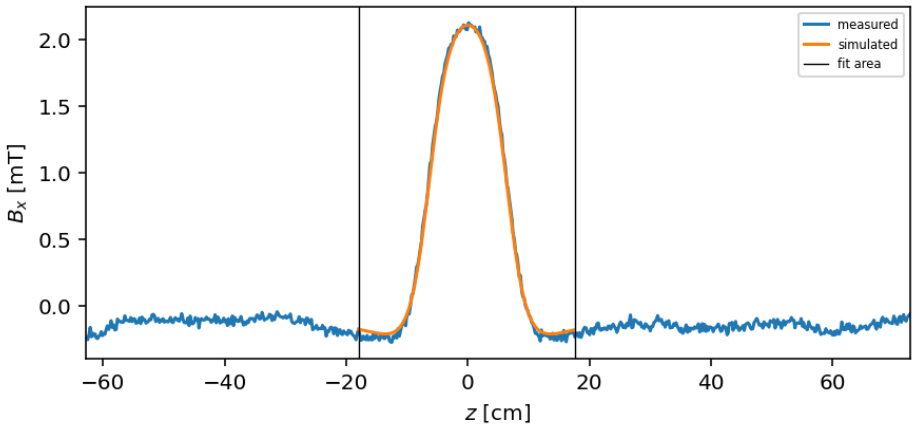

Figure 33: x-component of the rotary transformed, measured magnetic field and a simulated magnetic field for the geometrical settings of a single coil pair Sona-transition unit. In a fit the offset of the z-axis is recalibrated and a homogeneous background field is added to the simulation.

In contrast to the calibrations of the rotation angle around the z-axis, which if possible have been done for all B-field measurements individually, the calibration of the z-axis gets done once and is adopted for all other measurements.

5.1.2 Background measurements and spinfilter influence

To see the isolated influence of the spinfilters on the magnetic field in the Sona-transition region, the magnetic field is measured for all four combinations of the two spinfilters either being turned off or on with a current of 8.1 A (see fig. 34). In the spinfilters a current of 8.1 A corresponds to a magnetic field of 53.5 mT which is at the $\alpha 1$-resonance (see section 2.2).

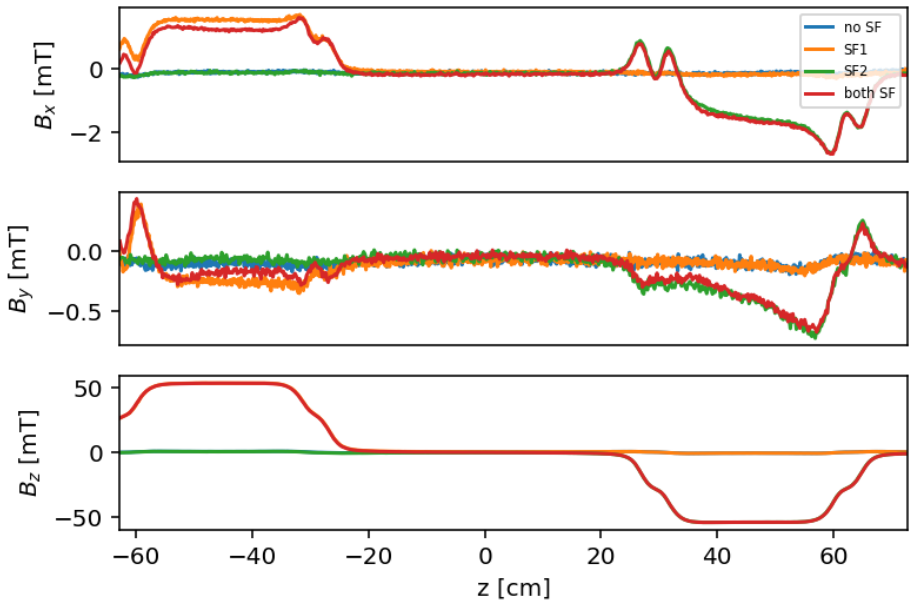

Figure 34: Magnetic field measurements without an active Sona-transition unit along the x-, y- and z-coordinate. All combinations of the spinfilters each turned off or on at 8.1 *A.*

Because the z-component in the turned on spinfilters are with about 53.5 mT far higher (see fig. 34), than the magnetic fields of a Sona-transition unit (e.g. see fig. 36), in figure 35 the same data have been plotted with other boundaries of the displayed magnetic field for a better visualization of the influence in between the spinfilters.

In figure 34 one can see in the x- and y-component a fraction z-component of the spinfilter B-field, due to imprecisions in the alignment of B-field sensor or spinfilters. The graphs of the B_z-component do still show a pattern within a spinfilter, even if it is turned off, which is caused by the magnetization of iron contained in the spinfilters.

In the region of the Sona-transition unit at $|z| \lesssim 25$ cm one can see, that a portion of the spinfilter B_z-component reaches into this area. The corresponding influence is measured in the sections 5.2.1 and 5.2.3.

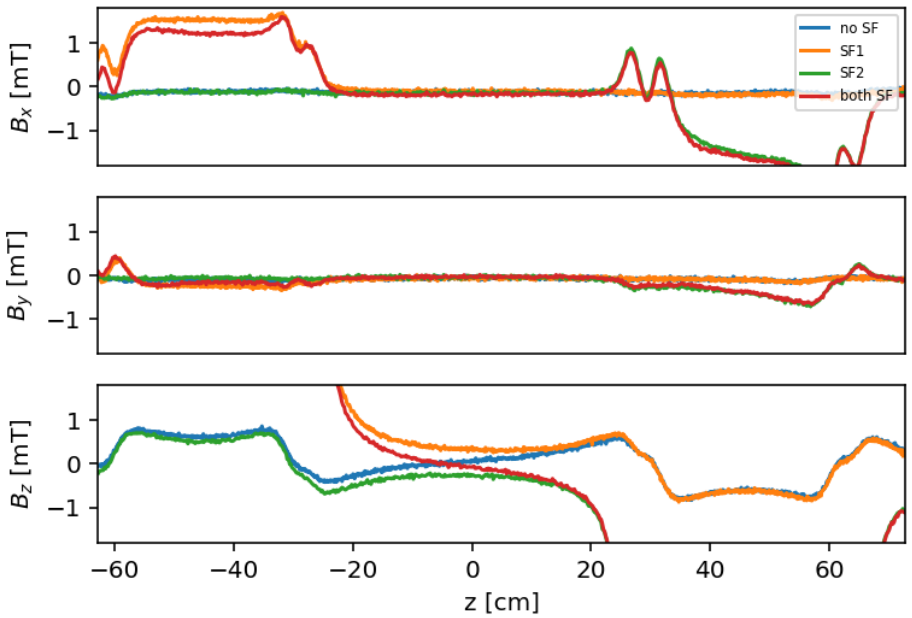

Figure 35: Magnetic field measurements without an active Sona-transition unit along the x-, y- and z-coordinate. All combinations of the spinfilters each turned off or on at 8.1 *A.*

For an actual comparison between the magnetic field strength of the Sona-transition unit and the influence of the spinfilters in the relevant region, a simulation and the magnetic field measurement with and without the spinfilter field are shown in figures 36 and 37 with a typical Sona current of $I_{\text{Sona}} = 5\ A$ for a single and double coil pair setup. The full measurements including the magnetic field in the spinfilters and the single coil pair measurement with the other coil pair can be found in section C of the appendix.

One can see, that the spinfilter has a negligible influence on the x- and y-component. Only the off-center B_z has a magnitude comparable with the B-field of the Sona-transition unit.

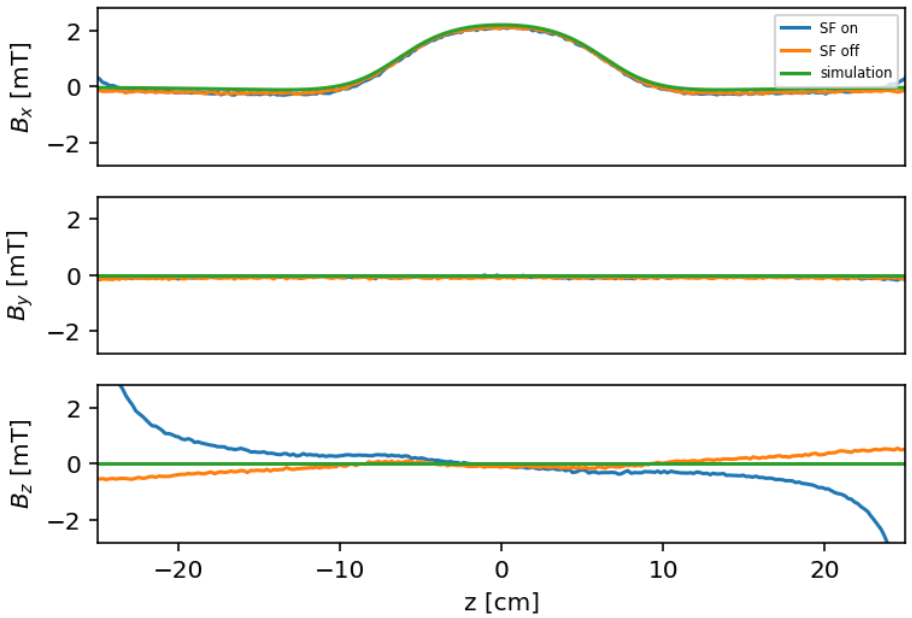

Figure 36: Magnetic field measurements in the Sona-transition unit region with single coil pair 1 and $I_{Sona} = 5$ A.

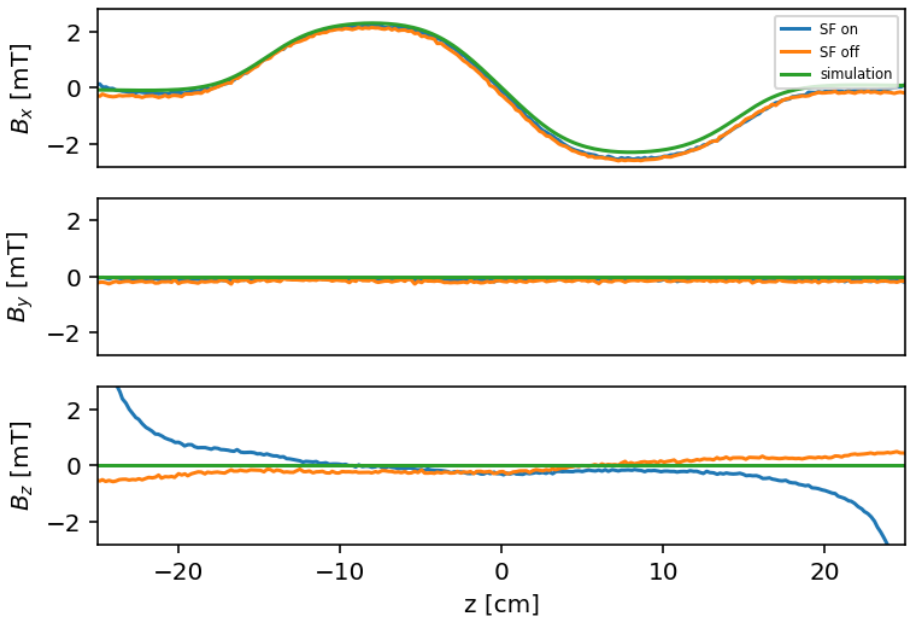

Figure 37: Magnetic field measurements in the Sona-transition unit region with the coil pair, i.e. both single coil pairs combined and $I_{Sona} = 5$ A.

5.1.3 Variation of the current in a Sona-transition unit

To verify the linearity between the Sona current I_{Sona} and the magnetic field strength in the Sona-transition unit, the magnetic field is measured for multiple values of I_{Sona} and plotted in figure 38 for the single coil pair Sona-transition unit. Additionally, simulations of the magnetic field in the center of the beam pipe (see section 2.3.4) have been added to the figure. The parameters for this simulation have been taken from geometrical measurements of the coils. To simplify and accelerate the computation of the simulation, each coil is approximated to be a one dimensional circular conductor with the current I_{Sona} multiplied with the number of windings of the real coil.

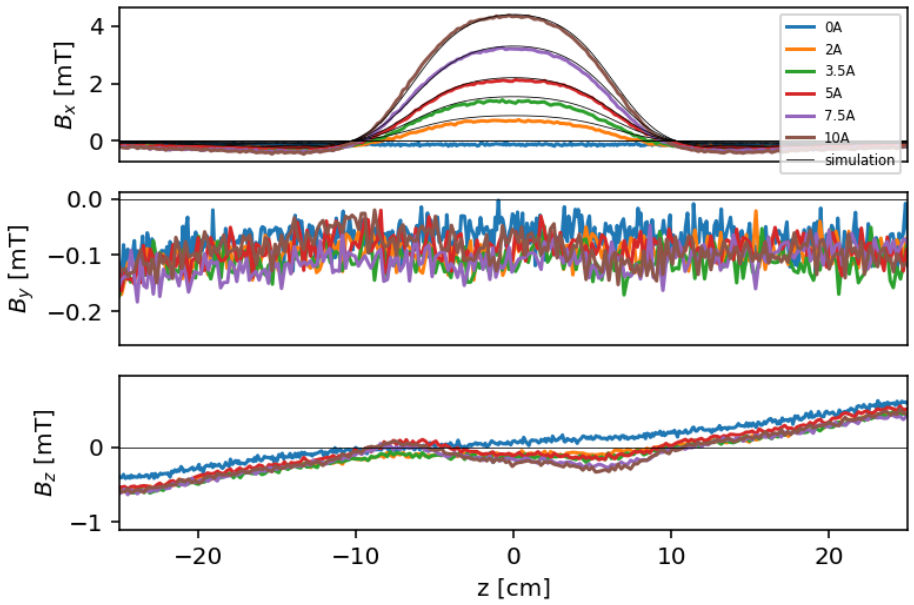

Figure 38: Magnetic field measurements in the region of the single coil pair Sona-transition unit for multiple values of I_{Sona}. The magnetic field of the spinfilters is turned off.

The y-component does not differ significantly at all in between the different I_{Sona}, although it is not perfectly zero, which may be explained by background magnetic fields like the geomagnetic field.

In the z-component one can recognize the pattern of the magnetization of the iron in the turned off spinfilters, which has similarities to the corresponding graph in figure 35. Due to symmetry reasons the y- and z-component of the magnetic field on the beam axis must be zero. The slight differences in between the measurements of the z-component might be caused by an offset of the measurement

points from the beam axis. Another reason might be a difference of the magnetization in between the measurements.

On a first glance, the x-component of the magnetic field seems to match the simulation. In figure 39 the residuals are displayed.

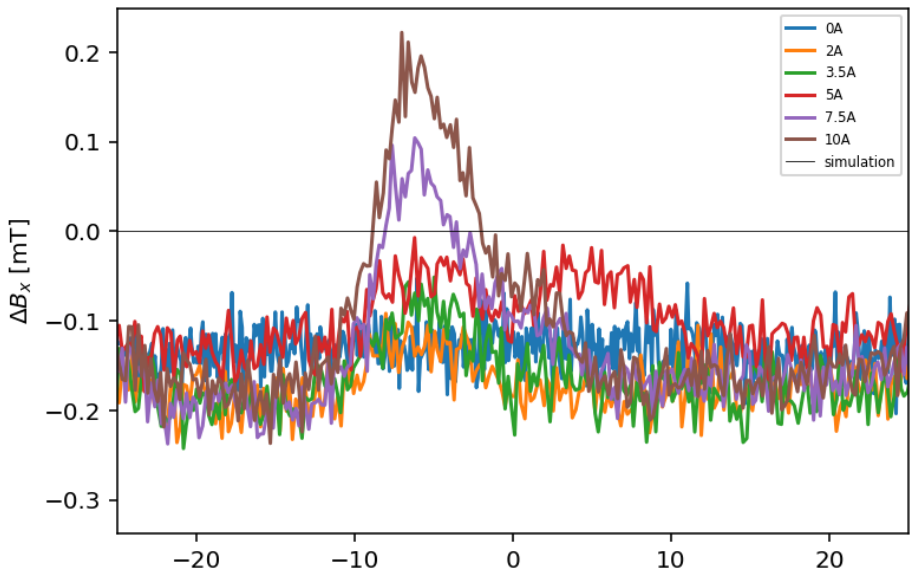

Figure 39: Residuals of the x-component between measurements of the magnetic field in a single coil pair Sona-transition unit for multiple I_{Sona} and unfitted corresponding simulations.

After fitting the simulation to the data by varying a background value and an offset of the z-position for each measurement and a correction of the coil diameter and its distance to the beam axis for all measurements together, the resulting residuals are shown in figure 40. With a $\chi^2/dof = 0.66$ the fit seems reasonable. A possible reason, for $\chi^2/dof < 1$ is, that the digitization error is in the same order of magnitude as the statistical uncertainty on the measurement of a B-field value. This might cause the saved values of multiple measurements at the same place to be torn apart by digitization and, therefore, an overestimation of the uncertainty of the measurement.

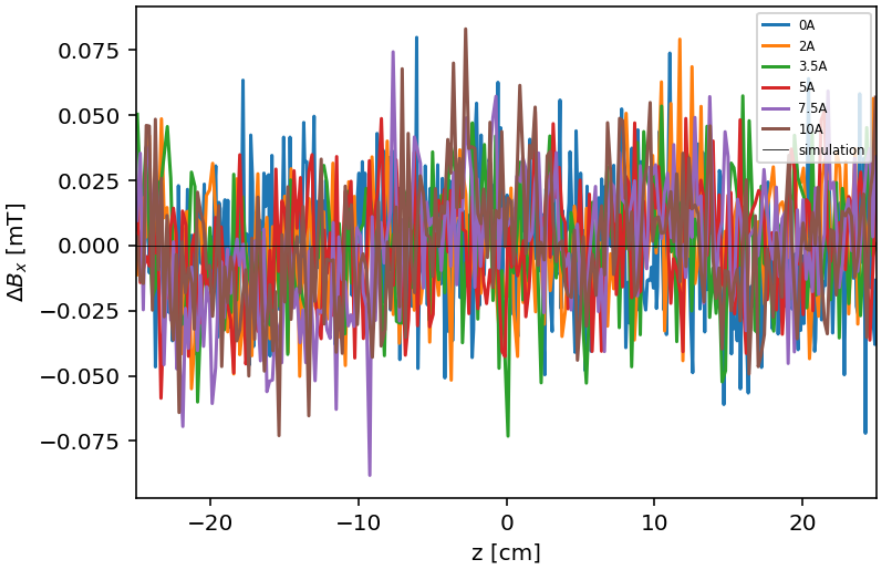

Figure 40: Residuals between the measured magnetic field for multiple I_{Sona} of the single coil pair Sona-transition unit and a simulation with a fitted background and offset of the z-position of each measurement. All measurements share a common correction of the coil diameter and distance to the beam axis.

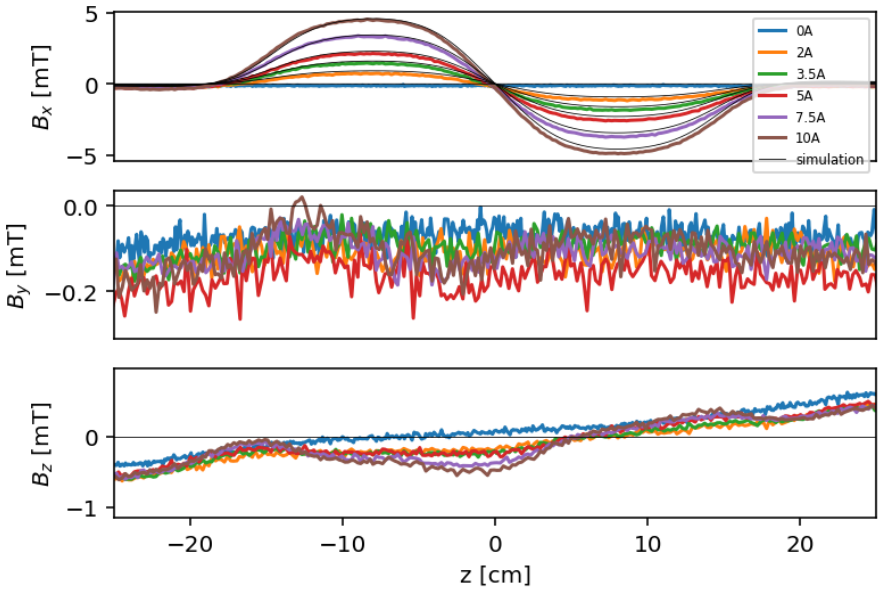

Figure 41: Magnetic field measurements in the region of the double coil pair Sona-transition unit for multiple values of I_{Sona}. The magnetic field of the spinfilters is turned off.

In figure 41 magnetic measurements of the double coil pair Sona-transition unit are displayed for multiple I_{Sona} analogue to 38 and analogue to the figures 39 and 40 the residuals to an unfitted and a fitted simulation of the double coil pair Sona-transition unit are shown in the figures 42 and 43 with similar results.

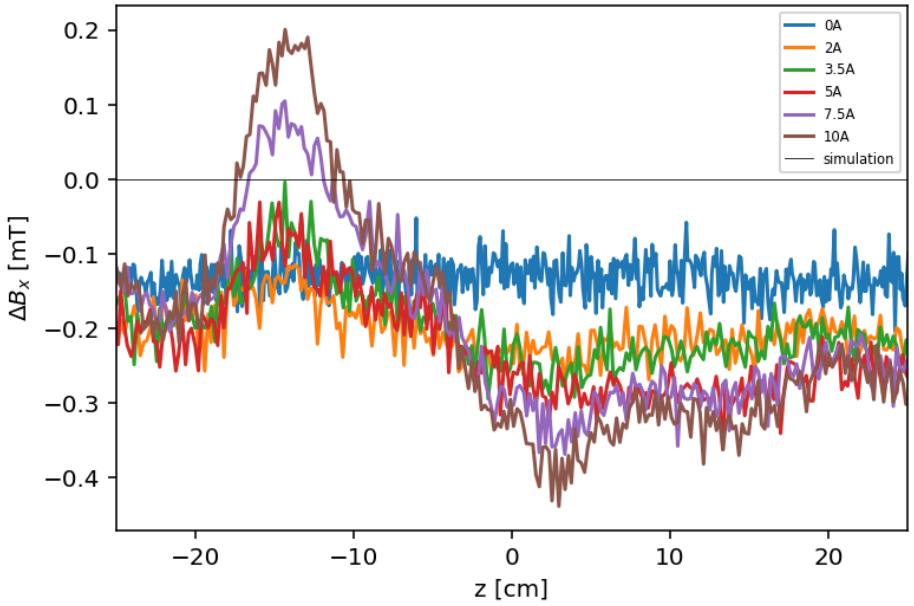

Figure 42: Residuals of the x-component between measurements of the magnetic field in a double coil pair Sona-transition unit for multiple I_{Sona} and unfitted corresponding simulations.

The only difference of figure 43 to its equivalent with a single coil pair Sona-transition unit (see fig. 39) is a slight pattern especially at the edges of the residual plot and a slightly higher $\chi^2/dof = 1.78$. A reason might be, that the fit assumed perfectly symmetrical settings for both coil pairs, which is not necessarily given. For example, the value of distance of the coils to the beam axis x_{coil} might be different for each coil pair or coil.

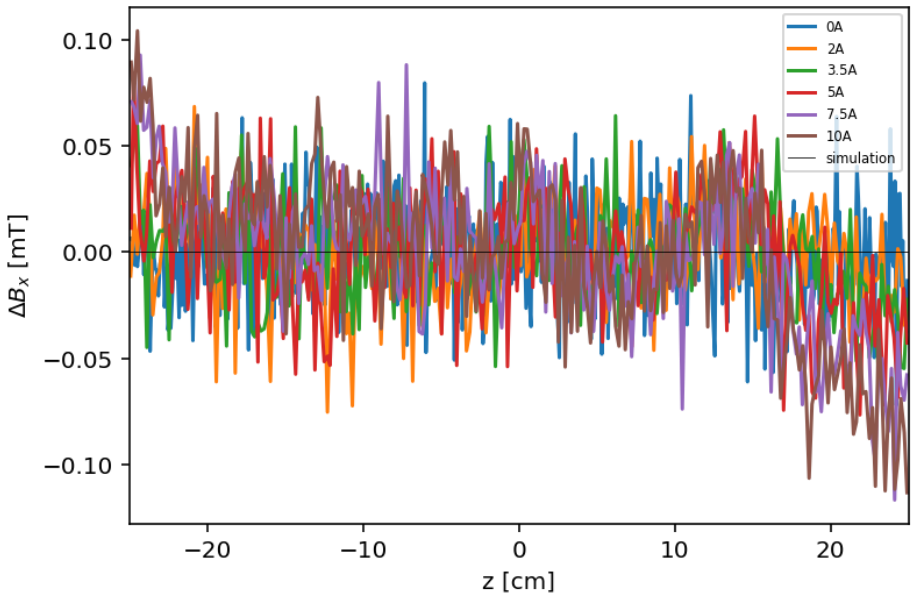

Figure 43: Residuals between the measured magnetic field for multiple I_{Sona} of the double coil pair Sona-transition unit and a simulation with a fitted background and offset of the z-position of each measurement. All measurements share a common correction of the coil diameter, distance to the beam axis and distance between both coil pairs.

5.2 Variation of the coil positions

5.2.1 Variation of the position of two coil pairs together

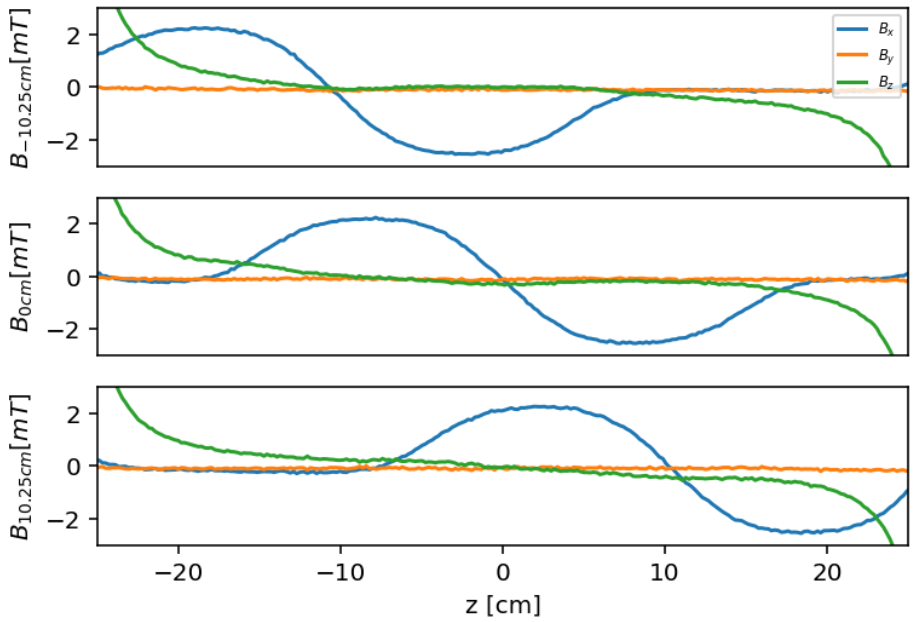

Figure 44: Magnetic field measurements of a double coil pair transversal Sona-transition unit for multiple positions $z_{Sona} = -10.25$ cm (top), 0 cm (middle) and 10.25 cm (bottom) of the transition unit. The positions $z_{Sona} = \pm 10.25$ cm correspond to a coil pair touching a spinfilter. The spinfilters are turned on with the current $I_{SF} = 8.1$ A and the Sona coils with $I_{Sona} = 5$ A.

When the position of the Sona-transition unit is varied, the resulting differences must be caused by the influence of the magnetic fields of the spinfilters before and after the Sona-transition unit (see fig. 44). To find the dependency of the Sona-transition oscillations on the spinfilter influence, a measurement is conducted, varying the position of a transversal Sona-transition unit with two coil pairs along the beam axis parallel to $\vec{e}_z$. In figure 45 the results are shown with the position of the center between both coil pairs z_{Sona} relative to the center between the spinfilters.

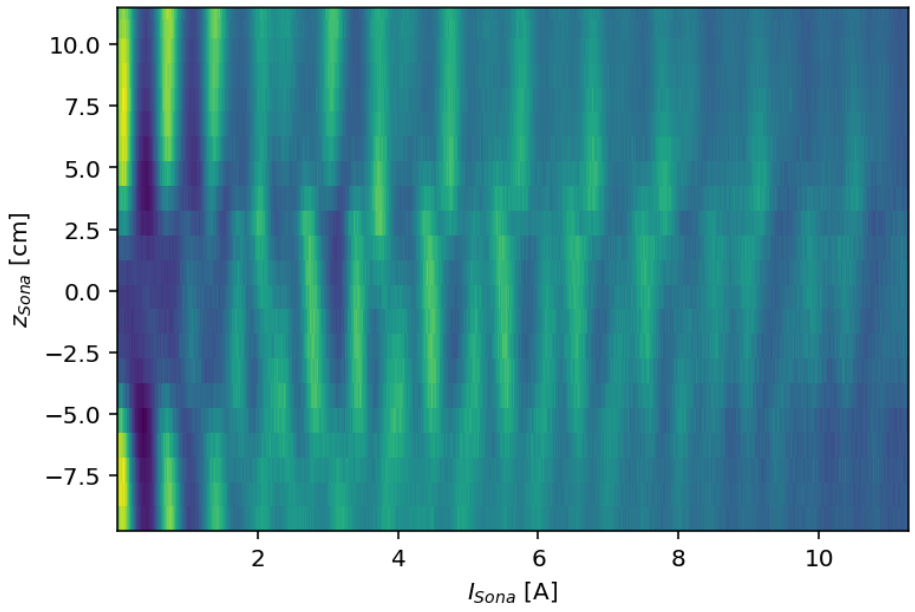

Figure 45: Color map representing the beam intensity of metastable hydrogen after passing through spinfilter 1, set to $\alpha 1$*, a transversal Sona-transition unit with the current* I_{Sona} *and spinfilter 2, set to* $\alpha 1$ *for different* z_{Sona}*.*

In this figure, two breaks of the pattern along horizontal lines can be seen at $z_{\text{Sona}} = -5$ *cm* and 3 *cm*. While the pattern in between these breaks seems not to be very stable, as some peaks even begin and end in the middle of this range, the pattern at $z_{\text{Sona}} \geq 5$ *cm* does only change very little. Because the measurements only started at $z_{\text{Sona}} = -9.25$ *cm*, the consistency of the pattern for $z_{\text{Sona}} \leq -5$ *cm* is more difficult to judge, but seems to be given also within said boundaries. A reason for the patterns not being symmetrical around $z_{\text{Sona}} = 0$ *cm* might be, that the spinfilters are slightly different constructed and their most outer edges, from which the center in between are measured, do not necessarily correspond to the same point of their magnetic field.

Another interesting correlation is the similarity of the pattern for $z_{\text{Sona}} \geq 5$ *cm* and the pattern visible in figure 51, which is showing a similar measurement, but with only a single coil pair instead of a double coil pair. For a better comparison the oscillations of the PMT-signals for the double coil pair position $z_{\text{Sona}} = 10.75$ *cm* and the single coil pair position $z_{\text{Sona}} = 2.5$ *cm* are both plotted in figure 46. For the corresponding settings, one coil pair of the double coil pair is put at the same place as the single coil pair.

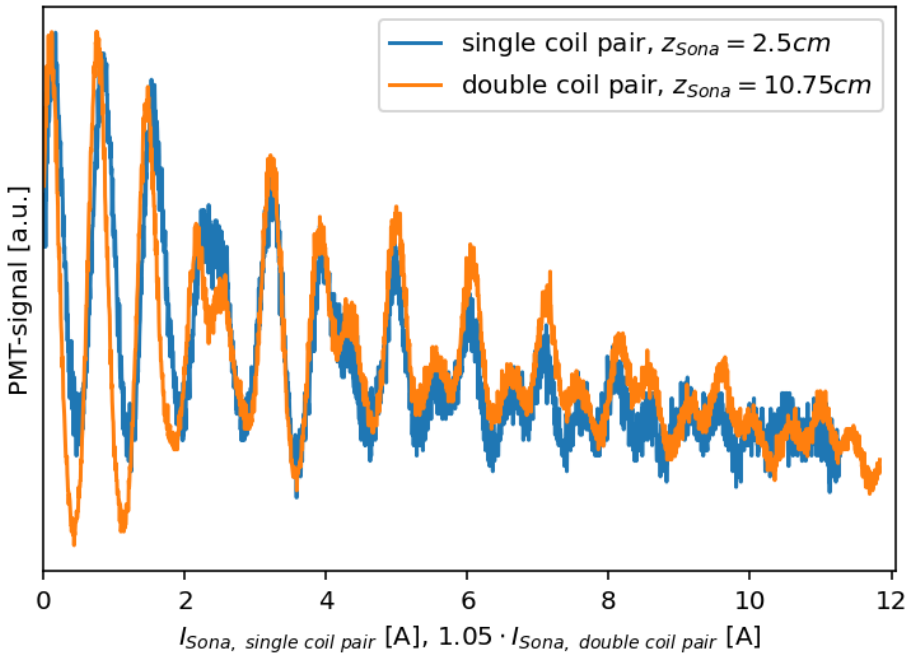

Figure 46: Comparison of measurements with a single coil pair and a double coil pair.

These data samples of a single and double coil pair do also match well when displayed in the same plot. Only one correction is needed, i.e. the axis of the current in the double coil pair $I_{\text{Sona, double coil pair}}$ has to be stretched by a factor of 1.05.

The similarity of these datasets seems to indicate, that the closeness to a spinfilter deactivates the effect of one of the two coil pairs. The reason for this might be the at this point relatively strong longitudinal field created by the spinfilter. In the image of precessing of angular momenta and magnetic moments (see section 2.3.4) a dominant longitudinal component would mainly prevent the precession around transversal magnetic fields. Therefore, it would also prevent the transitions of metastable atoms between the Zeeman states in the coil pair close to a spinfilter, that would otherwise create the oscillations for $-5\ cm \leq z_{\text{Sona}} \leq 3\ cm$ in a Sona-transition unit with a double coil pair. Instead the other coil pair acts as a single coil pair and creates the same oscillations as in figure 51.

The reason, that the experiment perceives the magnetic field of the double coil pair as 5 % stronger, than the single coil pair, seems to be, that some magnetic field lines induced by the coil pair next to the spinfilter pass back in the other direction through the other coil pair and add to its B-field strength.

5.2.2 Variation of the distance between two coil pairs

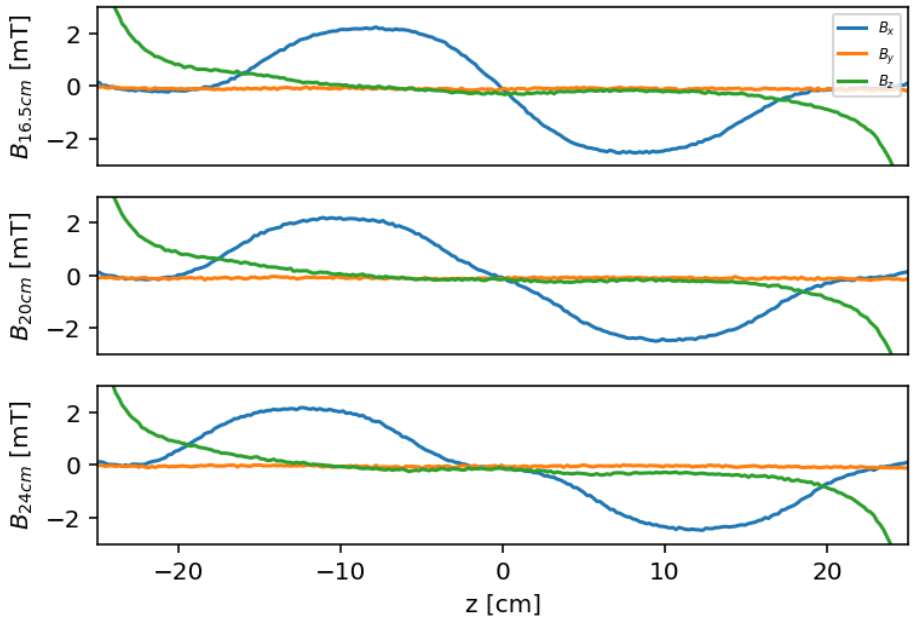

Figure 47: Magnetic field measurements of a double coil pair transversal Sona-transition unit for $\Delta z_{coil\ pairs} = 16.5$ cm (top), 20 cm (middle) and 24 cm (bottom). The spinfilters are turned on with the current $I_{SF} = 8.1$ A and the Sona coils with $I_{Sona} = 5$ A.

In the photon image of the Sona-transition effect, the wavelength of the sine-like curve, representing the magnetic fields, is a critical parameter for characterizing the oscillations created in a Sona-transition unit. Therefore, changing the distance between two coil pair positions $\Delta z_{\text{coil pairs}}$ should have a significant influence on the Sona oscillations, because it determines the distance between the maximum and minimum of B_x (see fig. 47), which theoretically is a half wavelength. Figure 47 shows three measurements of the magnetic field, including the influence of the spinfilter. Simulations of the same magnetic fields are shown in figure 48, that shows the x-component of B-field simulations, that have been used to simulate the Sona oscillations (see fig. 49, right). Here the influence of the spinfilters is not included though.

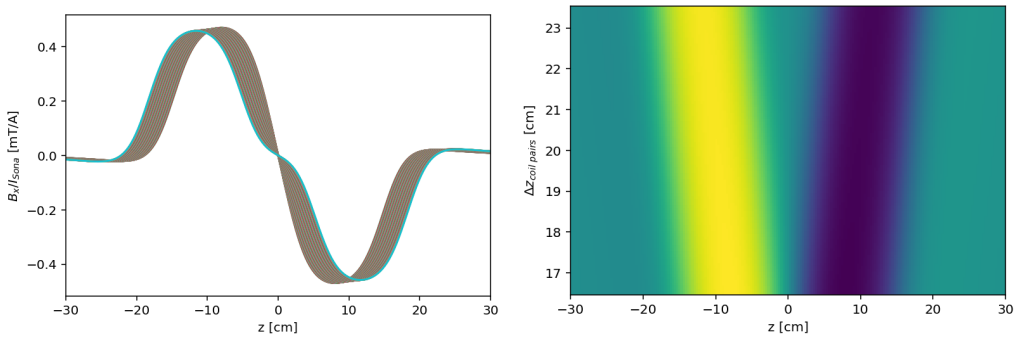

Figure 48: Plot (left) and color map (right) representing x-component of the magnetic field in the beam axis of a transversal Sona-transition unit with two coil pairs, depending on the distance of the centers of these coil pairs $\Delta z_{coil\ pairs}$.

The results of the measurement with a varying distance between the centers of the two coil pairs $\Delta z_{\text{coil pairs}}$ within a double coil pair are displayed in figure 49. One can see, that there is almost no correlation between $\Delta z_{\text{coil pairs}}$ and the pattern of the Sona oscillations, leading to the conclusion, that both coils are acting almost independently on the occupation numbers of the Zeeman states of hydrogen atoms.

The only observable effect caused by the variation of the distance between the coil pairs is a slight stretch of the oscillation pattern towards relatively larger or smaller $\Delta z_{\text{coil pairs}}$.

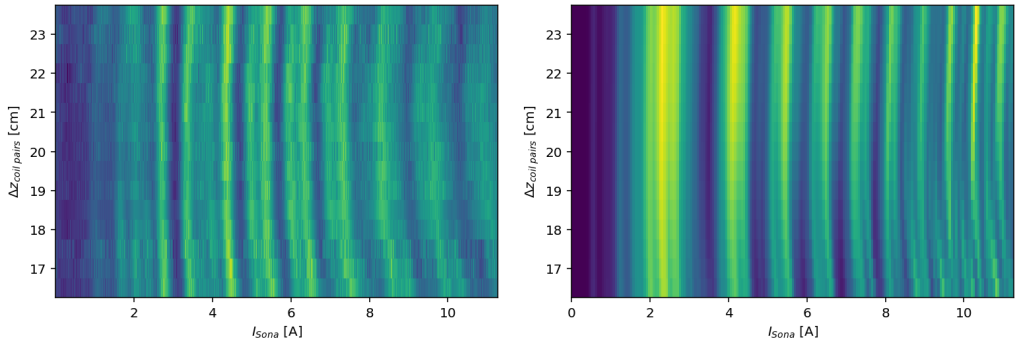

Figure 49: Color map representing the beam intensity of metastable hydrogen after passing through spinfilter 1, set to $\alpha 1$*, a transversal Sona-transition unit with the current* I_{Sona} *and spinfilter 2, set to* $\alpha 1$ *for different* $\Delta z_{coil\ pairs}$*. This process is measured (left) and simulated (right).*

The pattern produced by the simulation does look similar, but does not match the measurement perfectly. The reason is probably the influence of the spinfilter

B-field in the Sona-transition unit region, which is ignored in the simulation but gets proven to be influential on such measurements in section 5.2.1.

5.2.3 Variation of the position of a single coil pair

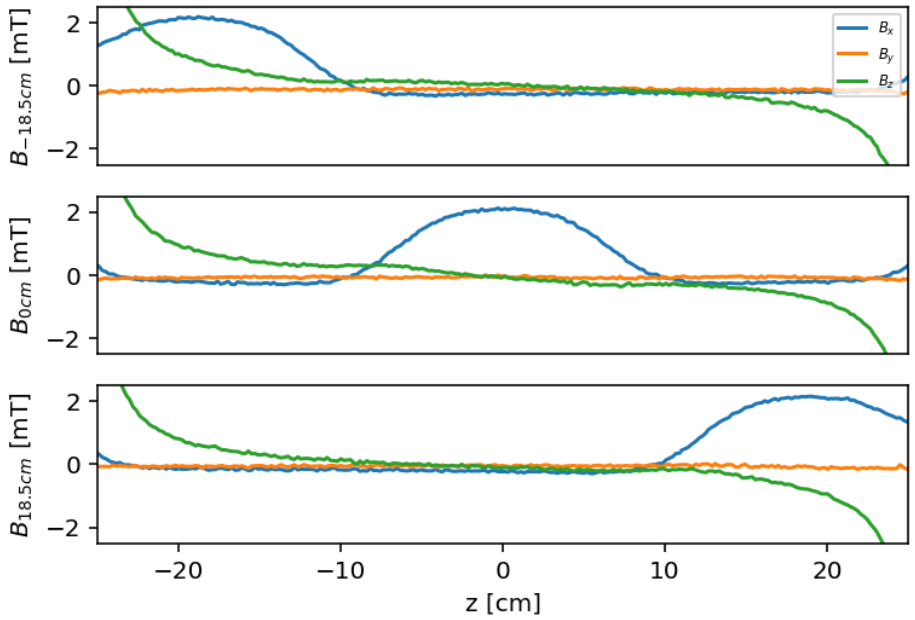

Figure 50: Magnetic field measurements of a single coil pair transversal Sona-transition unit for multiple positions $z_{Sona} = -18.5$ cm (top), 0 cm (middle) and 18.5 cm (bottom) of the transition unit. The positions $z_{Sona} = \pm 10.25$ cm correspond to a coil pair touching a spinfilter. The spinfilters are turned on with the current $I_{SF} = 8.1$ A and the Sona coils with $I_{Sona} = 5$ A.

To see the influence of the spinfilter B-field on a measurement with a single coil pair Sona-transition unit, such a unit is placed at various positions z_{Sona} in between the spinfilters, changing how the spinfilter influences the B-field of the Sona-transition unit (see fig. 50). The measurements with various z_{Sona} are displayed in figure 51.

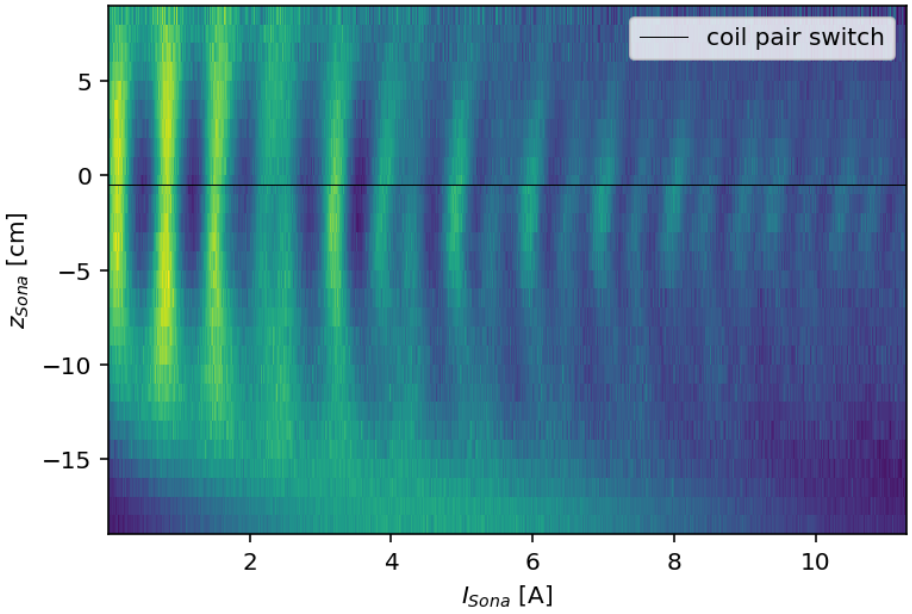

Figure 51: Plot of measurements for 29 positions z_{Sona} of a single coil pair transversal Sona-transition unit. For geometric reasons it is not possible to use one coil pair for all z_{Sona}, therefore a coil pair switch is needed.

One can see, that the pattern does not change much within $|z| \leq 5\ cm$, but gets weaker at the z_{Sona}-positions further out, until it is unrecognizable at $|z| = 15\ cm$. In this outer region one can also see a diagonal pattern from $I_{\text{Sona}} = 0\ A$ and $z_{\text{Sona}} = -10\ cm$ to $I_{\text{Sona}} = 5\ A$ and $z_{\text{Sona}} = -18\ cm$, which seems to mark the transition from a dominant Sona-transition field in the relevant region to a dominant influence of the spinfilter.

Because in reality the single coil pair Sona-transition unit is just one coil pair of the double coil Sona-transition unit (see fig. 17), the geometry of the setup does not allow the measurement for all positions with one coil. Therefore, the coils are switched near the middle ($z_{\text{Sona}} = -0.5\ cm$). Due to uncertainties in the manufacturing or positioning of the coils, there is a slight break in the pattern at the coil switch, although the measurements for both coil pairs at the same place are still very similar (see fig. 52).

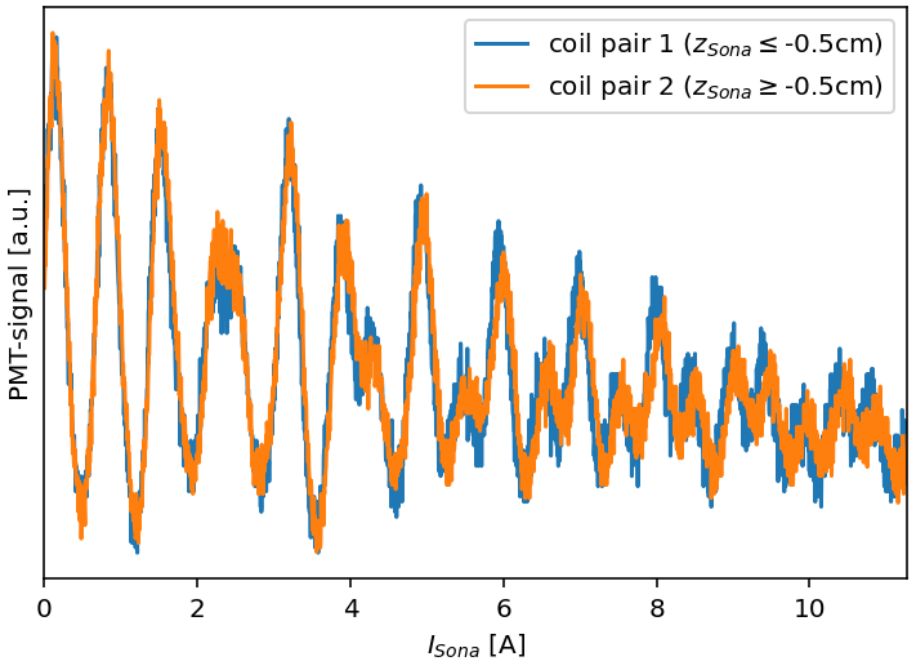

Figure 52: Comparison of measurements with coil pair 1 and 2 at the same position $z_{Sona} = -0.5$ cm and other settings.

5.3 Variation of the distance from the beam axis to the coils

sec: magnetic field trans To investigate the influence of the distance x_{coil} from the beam axis to the coil, corresponding measurements have been conducted. The magnetic field along the beam axis for three examples of x_{coil} have been plotted in figure 53. In figure 77 in the appendix measurements of the magnetic field for the same settings are displayed, but with the spinfilter B-fields turned off.

In the measurements with metastable hydrogen atoms, the fields of the spin-filter could not be turned off, but have been ignored in the simulation of said measurements. Instead the simulations of the magnetic field measurements in figure 54 have been used to simulate the spin propagation.

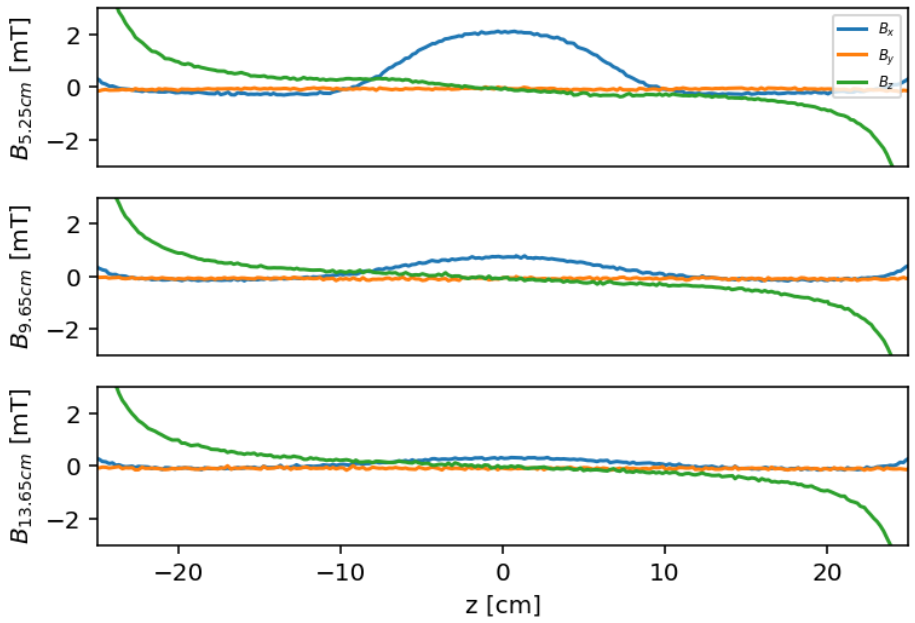

Figure 53: Magnetic field measurements of a single coil pair transversal Sona-transition unit for $x_{coil} = 5.25$ cm (top), 9.65 cm (middle) and 13.65 cm (bottom). The spinfilters are turned on with the current $I_{SF} = 8.1$ A and the Sona coils with $I_{Sona} = 5$ A.

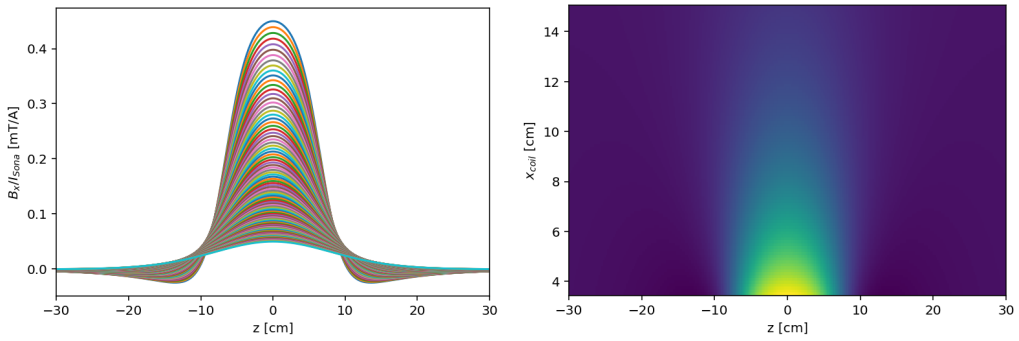

Figure 54: Simulation of the x-component of the magnetic field in a transversal Sona-transition unit with a single coil pair for various x_{coil}.

As an example for the measurements and simulations of the polarized metastable hydrogen atoms passing through the Sona transition, the results of $\alpha 1$ to $\alpha 1$ spinfilter settings are displayed in figure 55. The measurements for the $\alpha 1$ to $\alpha 2$ and $\alpha 2$ to $\alpha 2$ spinfilter settings can be found in figures 79 and 80 in the appendix.

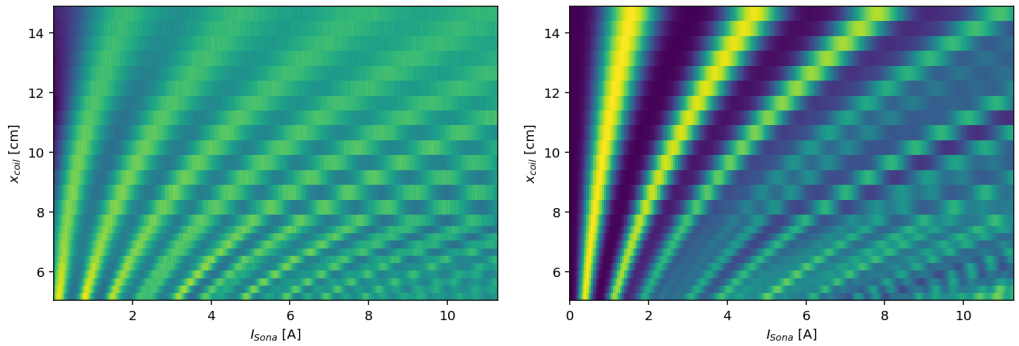

Figure 55: Measurement (left) and simulation (right) of $\alpha 1 \alpha 1$ for various x_{coil}.

The pattern of this measurement and simulation look already similar and show a pattern, that bends towards higher currents I_{Sona} for larger x_{coil}. The reason for this bend is, that at larger distances of the coils from the beam, represented by x_{coil}, the same current produces smaller magnetic fields (see fig. 54), which actually determine the pattern.

5.3.1 Normalizing to the B-field maximum

To correct for the changing correlation between the current I_{Sona} and the magnetic field strength, the x-axis of the diagrams like in figure 55 is changed from I_{Sona} to the maximal magnetic field B_{max} occurring in the simulation (compare figs. 54 and 56).

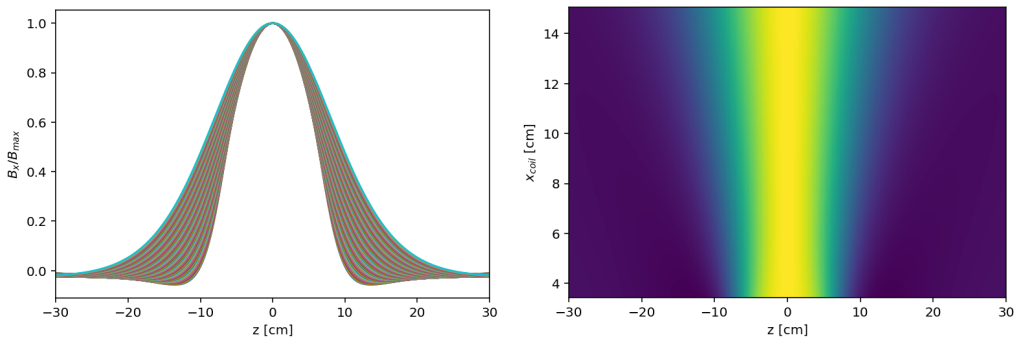

Figure 56: Simulation of the x-component of the magnetic field in a transversal Sona-transition unit with a single coil pair for various x_{coil}. Normed to the maximum value.

The data from figure 55 for $\alpha 1$ to $\alpha 2$ with a changed x-axis is shown as figure 57. Additionally, measurements and simulations with the spinfilter settings $\alpha 1$ to $\alpha 2$ and $\alpha 2$ to $\alpha 2$ are shown in figures 58 and 59.

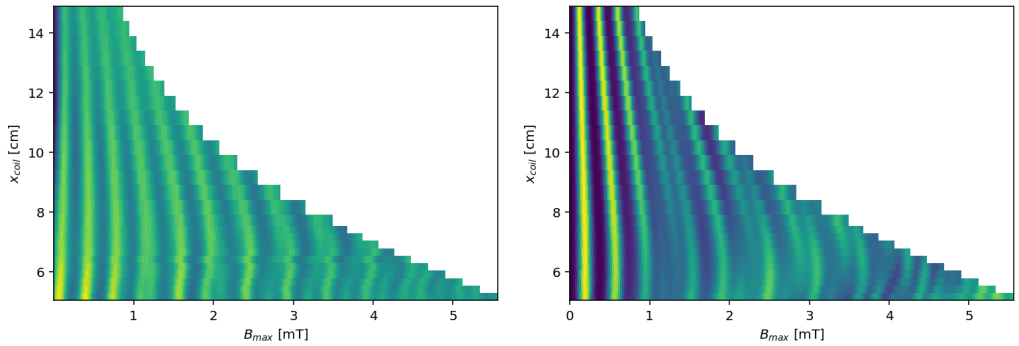

Figure 57: Measurement (left) and simulation (right) of $\alpha 1 \alpha 1$ *for various* x_{coil}.

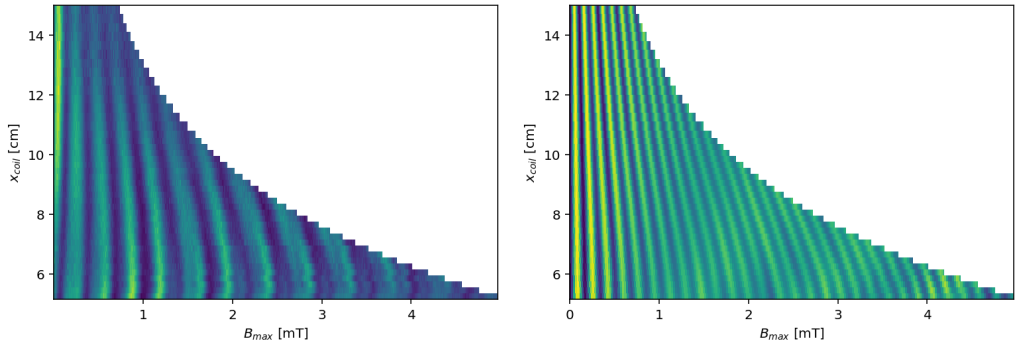

Figure 58: Measurement (left) and simulation (right) of $\alpha 1 \alpha 2$ *for various* x_{coil}.

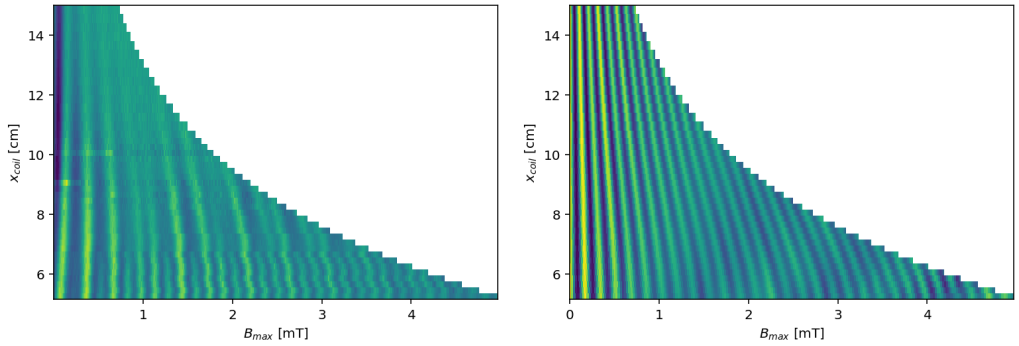

Figure 59: Measurement (left) and simulation (right) of a2a2 for various x_{coil}.

In all of these plots, the patterns are generally vertical, with a tendency to slightly smaller B-fields for larger x_{coil}. The only exception are kinks near the

minimal measured x_{coil}. Figure 56 shows, that the peak in the x-component of the B-field gets wider if the coils are further away from the beam, i.e. x_{coil} is larger. In the photon image of the interaction between magnetic fields and spin objects this means, the wavelength of the photons becomes larger and the energy of the photons diminishes. Therefore, the resonances of multi-photon transitions also have smaller energies for higher x_{coil}, which corresponds in the Breit-Rabi diagram to a smaller magnetic field, which here is represented by B_{max}.

Some measurements have kinks in the patterns for small x_{coil}. For those x_{coil} the coils are very close to the beam, which makes the magnetic field quite inhomogeneous and the assumption of a nearly sine-like transversal component imprecise. These imperfections in the magnetic field might make the assumption of simple photon energies not easily applicable anymore and cause the visible disturbances.

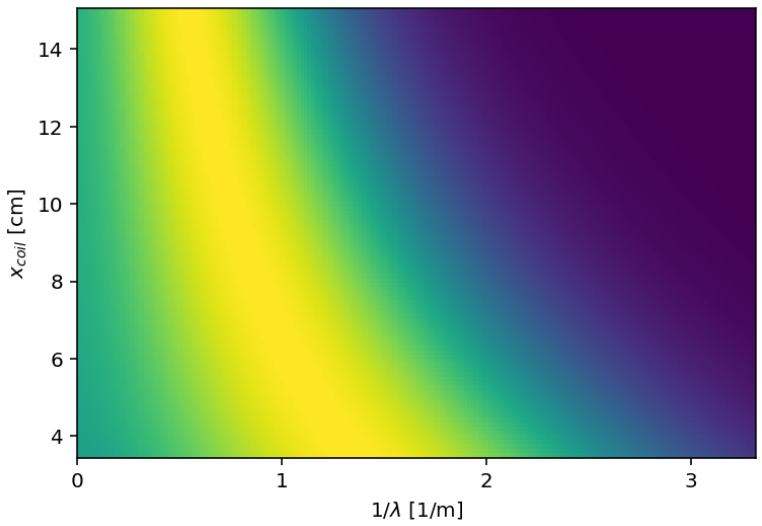

Figure 60: Fourier analysis of the magnetic field in a Sona-transition unit for for various x_{coil}. The Fourier analysis of every x_{coil} is normalized to its maximal amplitude.

5.3.2 Comparison of measurements with $\alpha 1\alpha 2$- and $\alpha 2\alpha 1$-settings

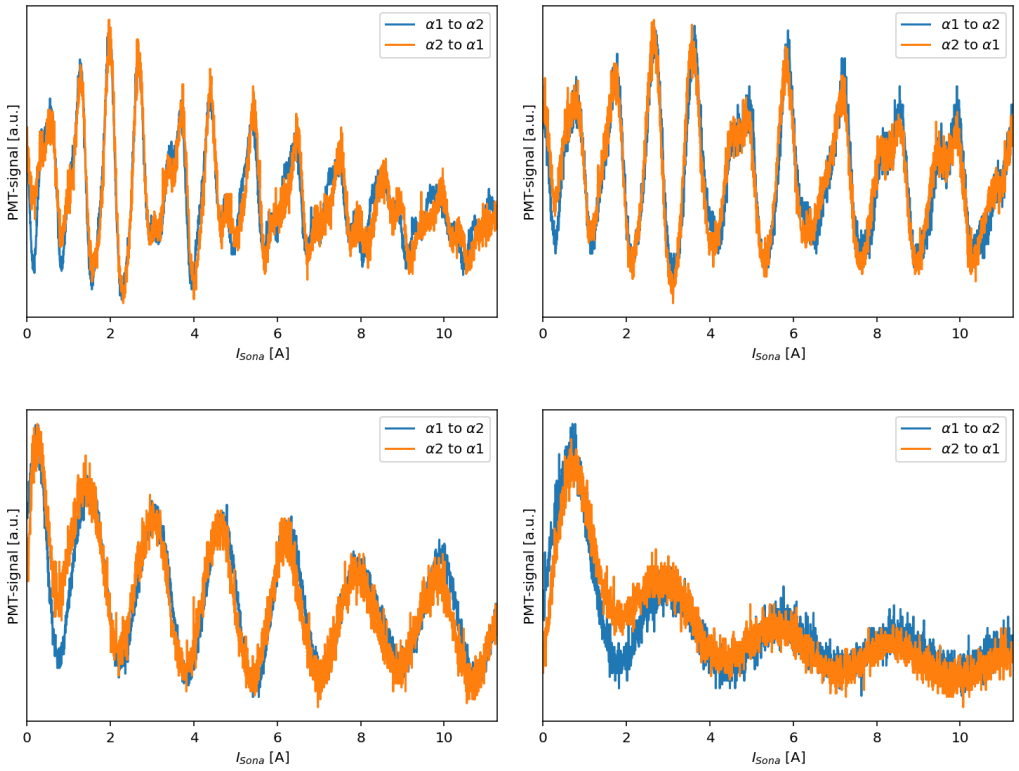

Figure 61: Comparison of Sona oscillations between $\alpha 1$ to $\alpha 2$- and $\alpha 2$ to $\alpha 1$-settings for $x_{coil} = 5.25$ cm (upper left), 6.65 cm (upper right), 9.65 cm (lower left) and 13.65 cm (lower right). The $\alpha 1$ to $\alpha 2$ data are also part of figure 79 and the left plot of figure 58.

From symmetry reasons explained in section 2.3.6 one expects the same result when swapping the spinfilter settings. To verify this, four example measurements have been conducted with spinfilter 1 set to $\alpha 2$ and spinfilter 2 set to $\alpha 1$. In figure 61 these four measurements are compared with the corresponding measurements, that are also part of figures 79 and 58. These comparisons show, that the results are actually very similar.

5.4 Variation of kinetic energy

Because the influence of the possible geometric changes of the existing Sona-transition unit coils on the magnetic wave is quite nonlinear, the frequency of a photon in the photon image can be changed most easily and controlled by varying the velocity or kinetic energy (see eq. (18)). Because the velocity is directly

proportional to the photon energy in the photon image (see eqs. (9) and (10)), in this chapter, the velocity is applied to the vertical axis of the plot, instead of the corresponding kinetic energy (see fig. 62).

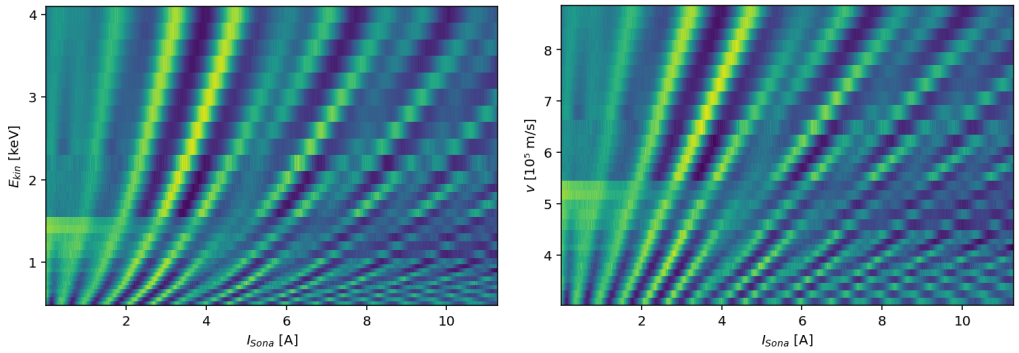

Figure 62: Measurement of $\alpha 1 \alpha 2$ for various E_{kin}, displayed as a function of the kinetic energy (left) and velocity (right).

In some measurements, displayed as horizontal lines, another pattern is visible, which corresponds to higher measured intensities at low currents I_{Sona} (see for example fig. 62). This is caused by an effect in the spinfilters. Because the transit time of particles is smaller for higher kinetic energies, the effect of the electric fields in a spinfilter diminishes as well. One useful side effect of the electric fields, other than coupling $2S_{1/2}$ and $2P_{1/2}$ states (see section 2.2), is, that ions i.e. protons, that are not neutralized in the cesium cell and would cause a background signal in the photomultiplier by hitting the wall near the quench region and producing radiation, are diverted already in the first spinfilter. If the diversion of the spinfilters is not strong enough, ions also can be diverted by strong enough transversal magnetic fields. That is why this effect is only relevant at small I_{Sona}. When this effect was noticed while conducting measurements with increasing kinetic energy, the electric field strength was increased in the spinfilters to prevent it for the following measurements.

5.4.1 Comparison measurement and simulation

Measurements of the Sona oscillations with a ramped current I_{Sona} were conducted for all four possible spinfilter settings and various kinetic energies between 0.5 *keV* and 4 *keV*. The same measurements were also simulated. In general the direction of the patterns match between measurement and simulation. For the spinfilter settings $\alpha 1 \alpha 1$ (see fig. 63, top) and $\alpha 2 \alpha 2$ (see fig. 64, bottom) the density of the peaks also fits very well. Therefore, for those spinfilter settings

measurement and simulation fit well together overall. For $\alpha 1 \alpha 1$ one can even recognize disturbances, that exist in both the measurement and simulation and at the highest velocity are visible at about $I_{\text{Sona}} = 4.5\ A$, $7.5\ A$ and $10\ A$. But for $\alpha 2 \alpha 2$ some peaks of the measurement are more pronounced than others, while this is not the case for the simulation.

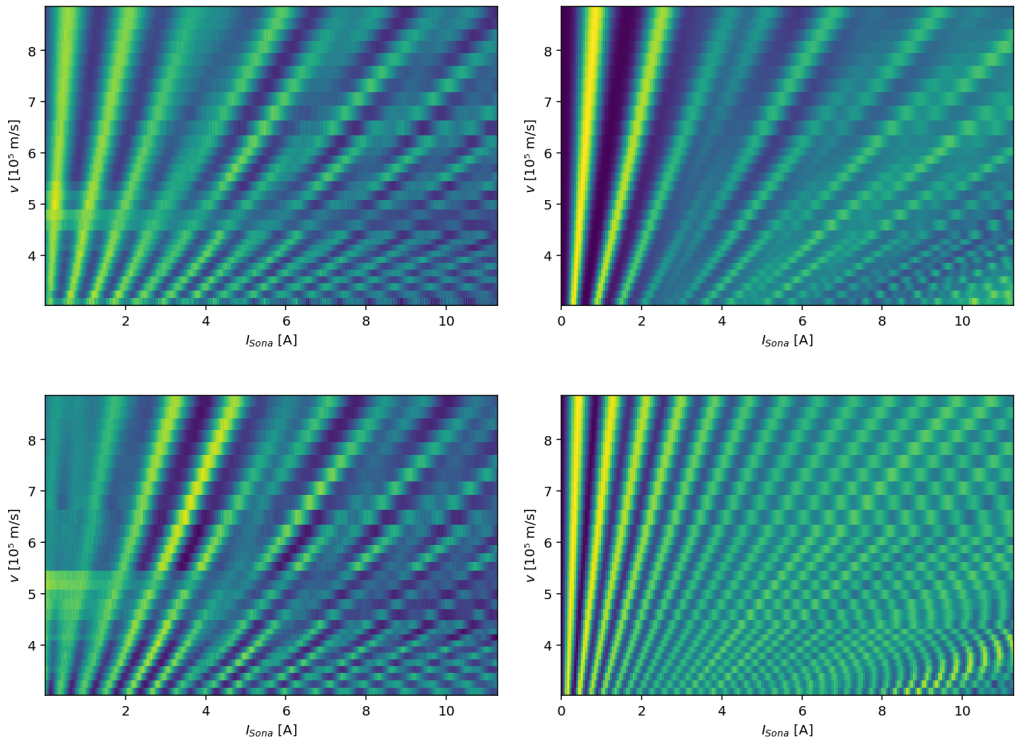

Figure 63: Measurement (left) and simulation (right) of $\alpha 1 \alpha 1$ *(top) and* $\alpha 1 \alpha 2$ *(bottom) for various* E_{kin}*, displayed as a function of the velocity.*

With $\alpha 1 \alpha 2$- (see fig. 63, top) and $\alpha 2 \alpha 1$-settings (see fig. 64, bottom) the pattern density of the simulations is higher than of the measurements. The simulation also misses distortions similar to those for $\alpha 1 \alpha 1$.

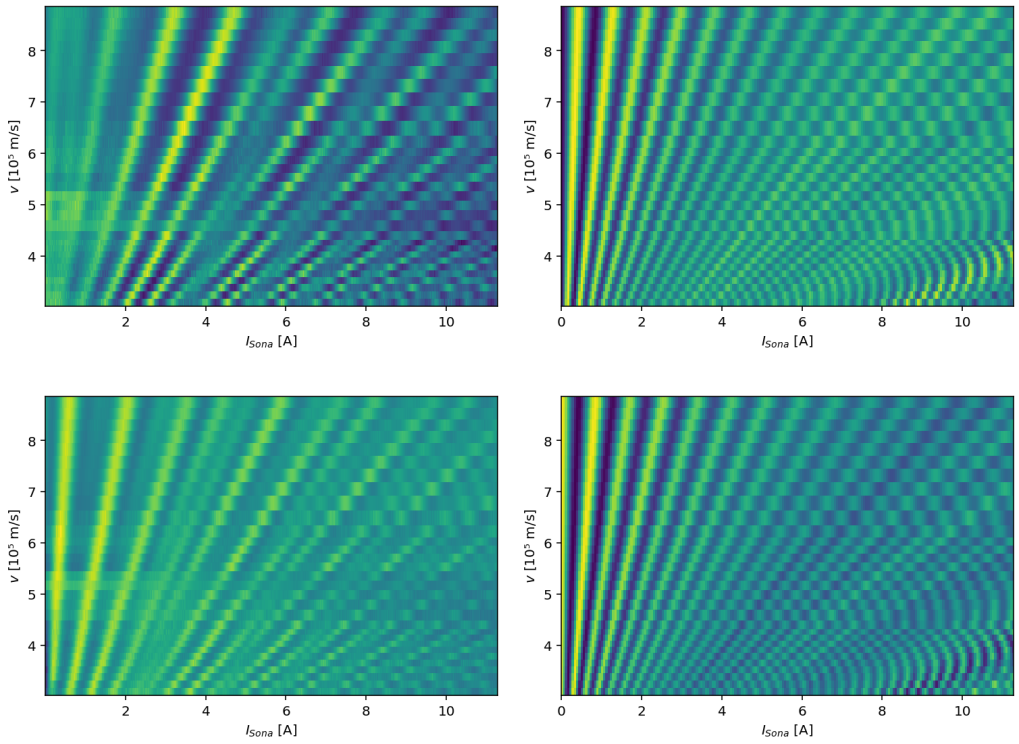

Figure 64: Measurement (left) and simulation (right) of $\alpha 2\alpha 1$ *(top) and* $\alpha 2\alpha 2$ *(bottom) for various* E_{kin}*, displayed as a function of velocity.*

5.4.2 Extended simulation

Because the patterns of the measurements and simulations with a longitudinal Sona-transition unit are very straight, one might assume to be in the region of small magnetic fields, where the energy differences between the Zeeman states is approximately linear. To confirm this hypothesis, the simulation was extended towards higher Sona currents I_{Sona}, i.e. higher magnetic fields in the Sona-transition unit and also towards higher velocities to decrease the pattern density and get a better overview of the first few peaks.

Analogue to section 4.3.1 the resonance energies of $\alpha 1\alpha 2$- and $\alpha 2\beta 3$-transitions depend on the B-field strength (see fig. 10). Unlike in this section, the patterns in the extended simulation the $\alpha 1\alpha 2$-pattern is not as dominant but is overlapped with the $\alpha 2\beta 3$-pattern. Therefore it is more difficult to fit the wavelength λ and the ratio between the effective magnetic field and current $\kappa = \frac{B_{\text{eff}}}{I_{\text{Sona}}}$ so that the resonances match with the patterns. The values $\lambda = 25\ cm$ and $\kappa = 0.34\ {}^{mT}/_{A}$ have been adjusted manually and used to calculate the resonances displayed in figure 65 (right). These values also seem reasonable compared to figure 38.

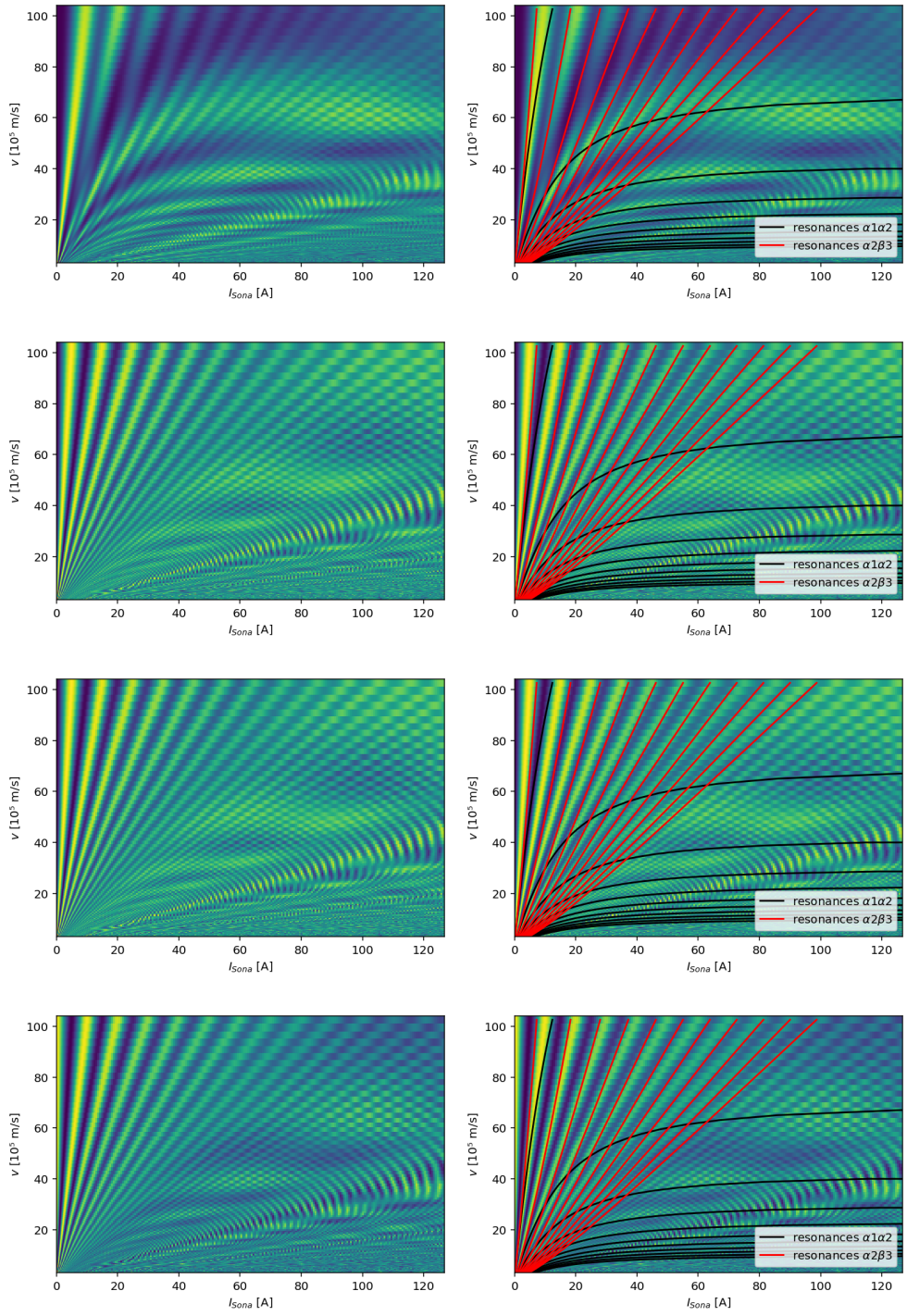

Figure 65: Extended simulation for $\alpha 1\alpha 1$, $\alpha 1\alpha 2$, $\alpha 2\alpha 1$ *and* $\alpha 2\alpha 2$ *(top to bottom), including the resonances for manually fitted* κ *and* λ *(right).*

As the plotted $\alpha 2\beta 3$-resonance shifts relative to the corresponding pattern, the used values of κ and λ might not yet be perfect or the patterns might be distorted by some unknown effect.

The only unexpected result of the extended simulation are diagonal patterns in the bottom right of each plot, that are not explainable with either $\alpha 1\alpha 2$- or $\alpha 2\beta 3$-resonances.

5.4.3 Comparison of measurements and simulations with $\alpha 1\alpha 2$ and $\alpha 2\alpha 1$-settings

When comparing the results of measurements with switched settings of the spinfilter one expects the same result if the Sona-transition unit is symmetrical (see section 2.3.6). Because existing spinfilters can only measure α-states, the swap of spinfilter settings can only be confirmed experimentally for one spinfilter being set to $\alpha 1$ and the other being set to $\alpha 2$ when using hydrogen (protium). The results of such measurements with varying kinetic energy are compared in figure 66. While the measurements are very similar for switched spinfilter settings, the simulation for switched initial and final Zeeman states are exactly the same (see fig. 67). Both results confirm the theoretical prediction.

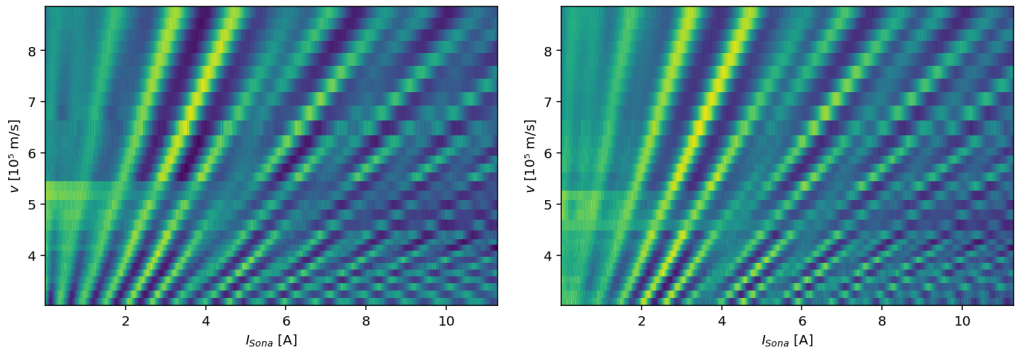

Figure 66: Measurement of $\alpha 1\alpha 2$ (left) and $\alpha 2\alpha 1$ (right) for various E_{kin}, displayed as a function of the velocity.

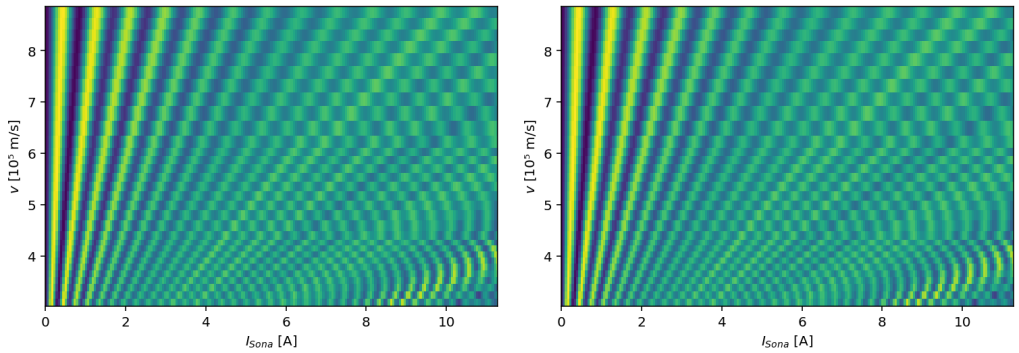

Figure 67: Simulation of $\alpha 1 \alpha 2$ (left) and $\alpha 2 \alpha 1$ (right) for various E_{kin}, displayed as a function of velocity.

The extended simulations also give the same result for $\alpha 1 \alpha 2$ and $\alpha 2 \alpha 1$ (see fig. 68).

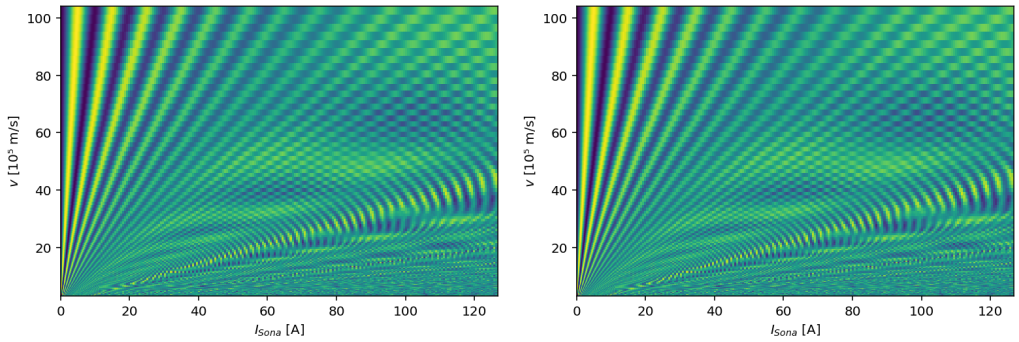

Figure 68: Extended simulation of $\alpha 1 \alpha 2$ (left) and $\alpha 2 \alpha 1$ (right) for various E_{kin}, displayed as a function of velocity.

6 Conclusion and outlook

The objective of this thesis is to conduct first measurements with transversal Sona-transition units and to compare to the older design of a longitudinal Sona-transition unit. Measurements with both kinds of unit are also compared to corresponding simulations.

While a longitudinal Sona-transition unit consists of two electromagnets that are aligned parallel and antiparallel to the beam axis, the initial design of a transversal Sona transition unit uses two coil pairs that each create a magnetic field orthogonal to the beam direction. The coil pairs are placed at different positions of the beam line with opposite orientation to produce a spatially oscillating magnetic field for the beam. After some experiments indicated, that a single coil pair might be sufficient to create the desired effects, one coil pair was deactivated and the rest of the apparatus is used as a single coil pair Sona-transition unit.

To assess the influence of the geometry of a Sona-transition unit, geometric parameters of both Sona-transition units were varied and the resulting impact on the Zeeman state's occupation number analyzed. A visual representation of the parameters is displayed in figure 18.

One important measurement is the variation of the distance between the two coil pairs $\Delta z_{\text{coil pairs}}$ of a double coil pair Sona-transition unit. The theory (see section 2.3.3) predicts, that $\Delta z_{\text{coil pairs}}$ directly correlates to a pattern change of resonances in the resulting Sona oscillation. Surprisingly the simulation and measurement of such a change of the geometry resulted in almost no change of the Sona spectra (see fig. 49). This result is interpreted by regarding the double coil pair as two consecutive but nearly independent single coil pair Sona transition units.

To evaluate the influence of stray fields from spinfilters before and after the Sona-transition unit, the position of the entire Sona-transition unit z_{Sona} along the beam pipe was changed and the corresponding Sona oscillations measured. This was done with a double coil pair- and a single coil pair Sona-transition unit. The oscillations of the single coil pair Sona-transition unit does not change much but vanishes for positions near either spinfilter (see fig. 51). On the other hand the results for the double coil pair Sona-transition unit are quite different. Here two breaks are visible in the Sona oscillation patterns (see fig. 45). Apparently the effect of a coil pair is deactivated if it is too close to a spinfilter, because the longitudinal spinfilter stray field overrides the effect of the transversal coil pair field. Interestingly the pattern of z_{Sona} with a deactivated coil pair is very similar to the pattern of the single coil pair Sona-transition unit (see fig. 46). The pattern is in between the breaks is the interaction between two single coil pair Sona-transitions.

A third type of measurement is conducted by varying the distance of a coil

from the beam axis x_{coil} for a single coil pair Sona-transition unit. The results of this measurement come out as expected and agree with the simulation. Two expected effects were observed. On one hand the overall higher magnetic field for smaller x_{coil} stretch out the according patterns. On the other hand one can see, that the patterns that remain after correcting for the first effect correspond to a change of the wavelength of the oscillating spacial magnetic wave produced by the Sona-transition unit (see section 5.3).

Another expectation, that is confirmed by this thesis, is a conclusion from time reversal independence. The concrete prediction is, that swapping the initial and final state of atoms measured in a Sona-transition unit gives the same result if the magnetic fields inside are symmetrical. This prediction is observed experimentally in both the longitudinal (see section 4.3.2) and transversal (see section 5.4.3) Sona-transition units with good precision. Simulations of a perfectly symmetrical Sona-transition unit found even a perfect match (see figs. 67 and 68).

Overall the simulations fit well to the measurements in both longitudinal and transversal Sona-transition units. For both, extended simulations found that the measurements can analyze the behavior of atoms in the Zeeman region while the behavior in the Paschen-Back region at higher magnetic field strengths can only be simulated because the coils of the Sona-transition units are not designed for higher currents, i.e. higher magnetic fields. For research in this area coils producing higher B-fields should be used. For example they could have thicker wires and more windings or get water cooled.

Another experiment, which does not change the geometry of a Sona-transition unit, utilizes that atoms passing the Sona-transition unit perceive its spatially oscillating magnetic fields differently if they pass it with another velocity. when the atoms are faster, they experience the oscillations with a higher frequency. This frequency corresponds to higher energy photons that cause resonances in the Breit-Rabi diagram. Using this relations one can plot measurements and simulations in a way that directly shows the Sona oscillations as the energy differences in the Breit-Rabi diagram as a function of the magnetic field. The corresponding measurements and simulations of a transversal Sona-transition unit fit well together and give the expected match with the Breit-Rabi diagram energy differences (see section 4.3). For the longitudinal Sona-transition unit a similar simulation is conducted (see section 5.4). Here the patterns also fit well to the Breit-Rabi energies but a measurement with various velocities is not conducted, because the setup was rebuild for other experiments when the necessity for such a measurement became apparent. Such measurements could be done in the future.

An interesting observation in the plots of measurements with various velocity is, that multiple resonances overlap and cause superpositions, that can create extra peaks in measurements with only one velocity. Previous methods that used only atoms of one velocity may misinterpret such peaks as a resonance each, leading

to warped results. When analyzing a plot of measurements with various velocities, one can easily recognize double peaks created by superpositions and conduct spectroscopy in the Breit-Rabi diagram. Such a method may even lead to a new way of measuring g-factors, because the Breit-Rabi energies are directly depending on them.

Generally we can transform electron polarization into nuclear polarization by the methods described in this thesis. If used on a larger scale, techniques using Sona-transition units can produce fuel for polarized fusion or polarized tracers, that can be useful in medicine. In an actual application of the universities of Münster, Crete, Düsseldorf and Ferrara to the european innovation council (EIC) it is foreseen to produce an intense thermic beam of cold HD- or D_2-molecules so that the rotational magnetic moment is $J = 0$. With a powerful infrared laser these molecules are pumped to a dedicated substate m_J so that the rotational angular momentum is polarized. This polarization can now be transferred to the nuclear spin via a Sona transition or by making use of the hyperfine beat of the substates. Here the hyperfine splitting energy is about two orders smaller than for the hydrogen atom, but this is compensated by the much smaller velocity of the molecules, that decreases the photon energy linearly. Afterwards the nuclear polarization can be measured with a Lamb-shift polarimeter to optimize the polarization process. With this method it should be possible to produce 10^{22} polarized molecules per second for further use.

Appendix

A Magnetic field of a longitudinal Sona-transition unit

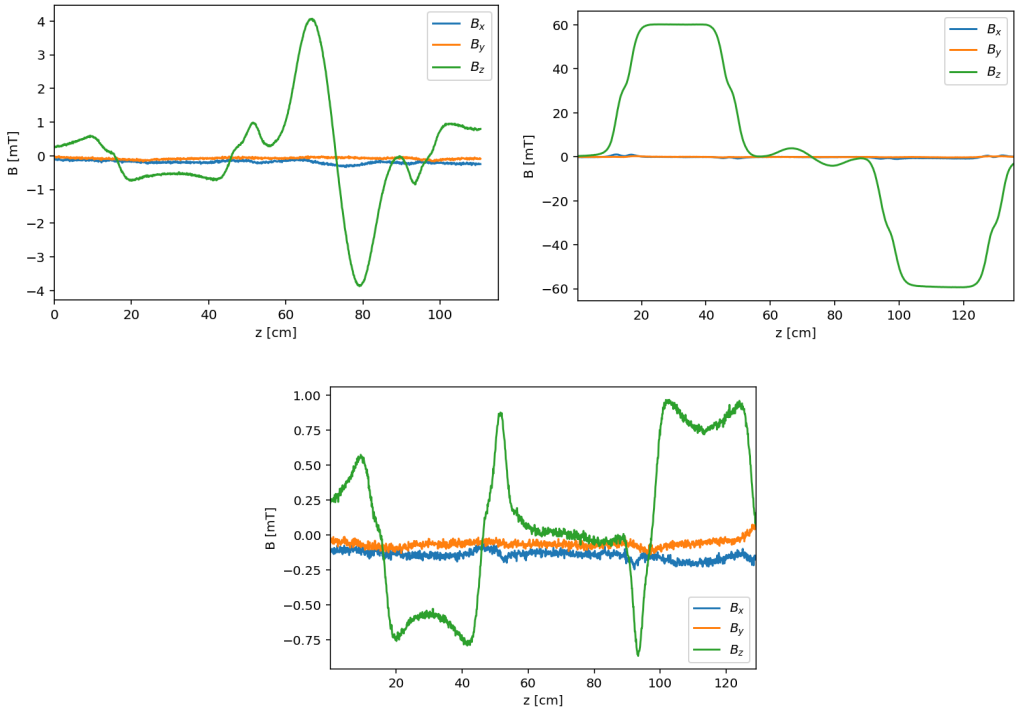

Figure 69: Measurement with $I_{Sona} = 0.2$ A (top left), measurement with SF1 and SF2 on and $I_{Sona} = 0.2$ A (top right)and background measurement (bottom right). The origin of the data are measurements conducted for [13].

B Simulations of a longitudinal Sona-transition unit

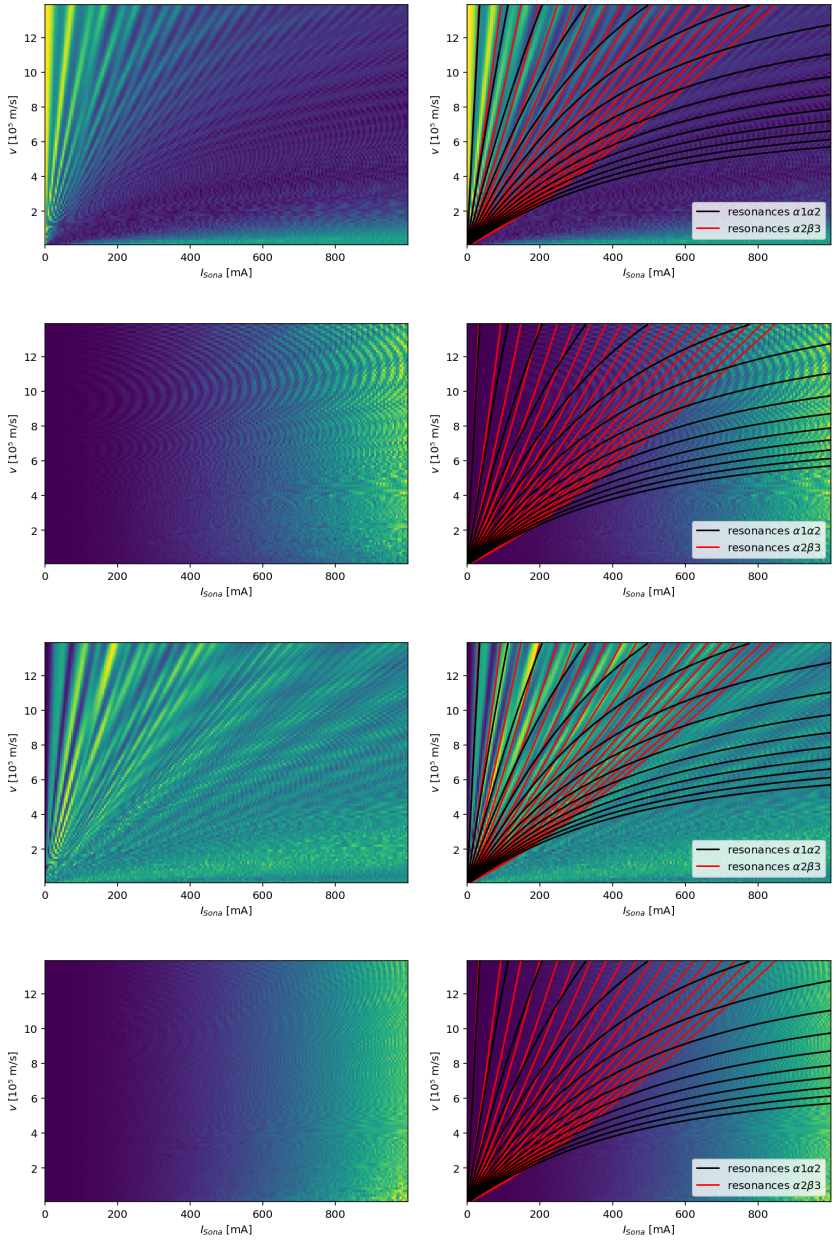

Figure 70: Extended simulation for $\alpha 1\beta 3$, $\alpha 1\beta 4$, $\alpha 2\beta 3$ and $\alpha 2\beta 4$ (top to bottom), including $\alpha 1\alpha 2$- (black) and $\alpha 2\beta 3$- (red) resonances (right). The κ and λ are fitted to the $\alpha 1\alpha 2$-patterns of the $\alpha 1\alpha 1$-simulation. The color gradiant does not match between the images. The by magnitudes smaller intensity of the $\beta 4$-state is therefore not reflected by the colors.

C Magnetic fields of transversal Sona-transition units

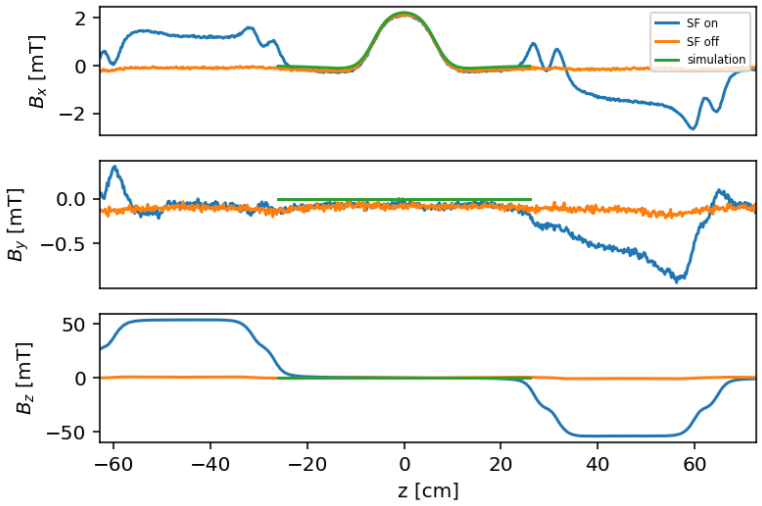

Figure 71: Full magnetic field measurements in the Sona-transition unit and spinfilters with single coil pair 1 and $I_{Sona} = 5$ A.

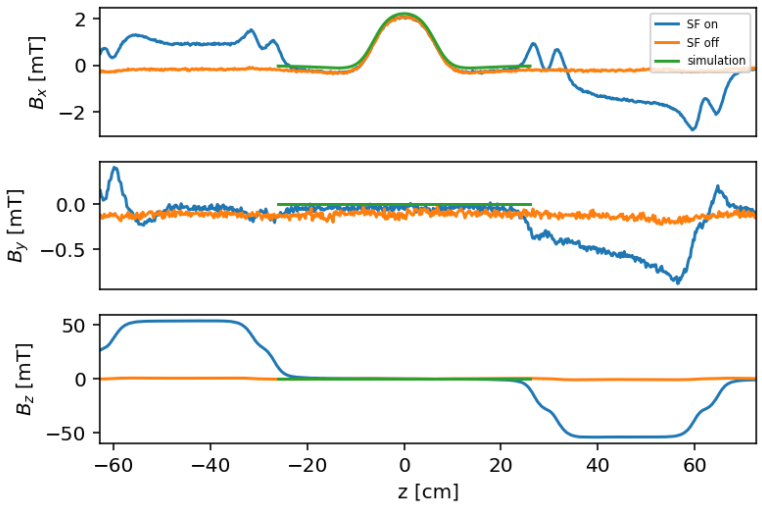

Figure 72: Full magnetic field measurements in the Sona-transition unit and spinfilters with single coil pair 2 and $I_{Sona} = 5$ A.

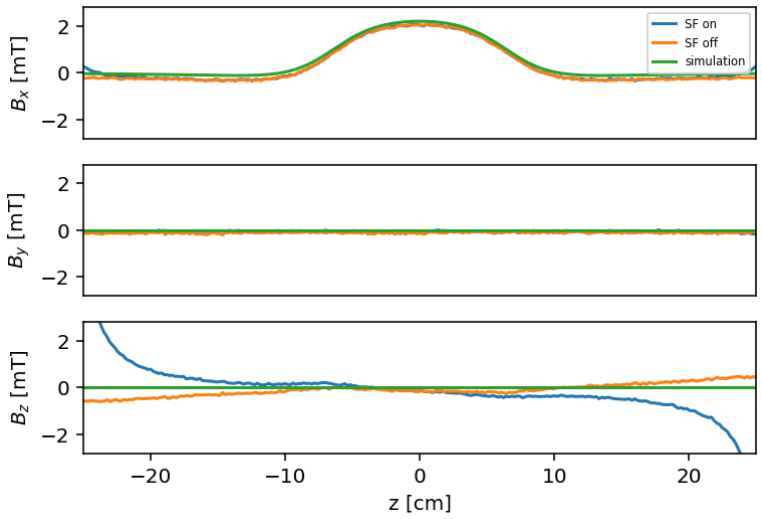

Figure 73: Magnetic field measurements in the Sona-transition unit region with single coil pair 2 and $I_{Sona} = 5$ A.

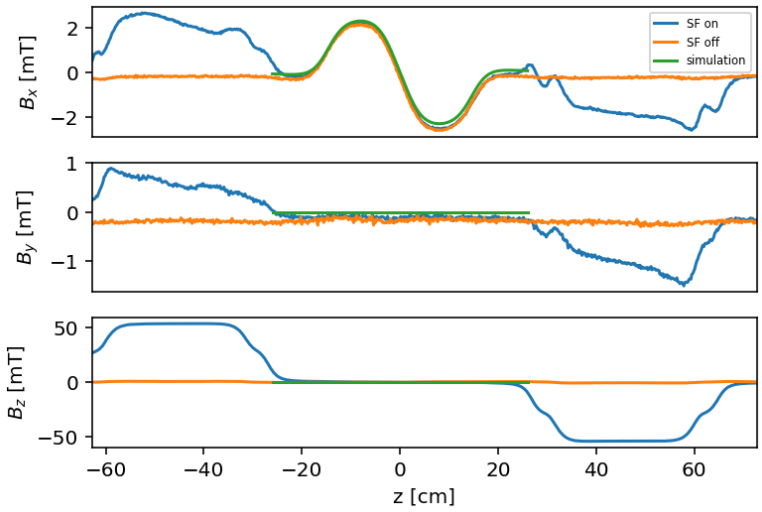

Figure 74: Magnetic field measurements in the Sona-transition unit and spinfilters with the double coil pair, i.e. both single coil pairs combined and $I_{Sona} = 5$ A.

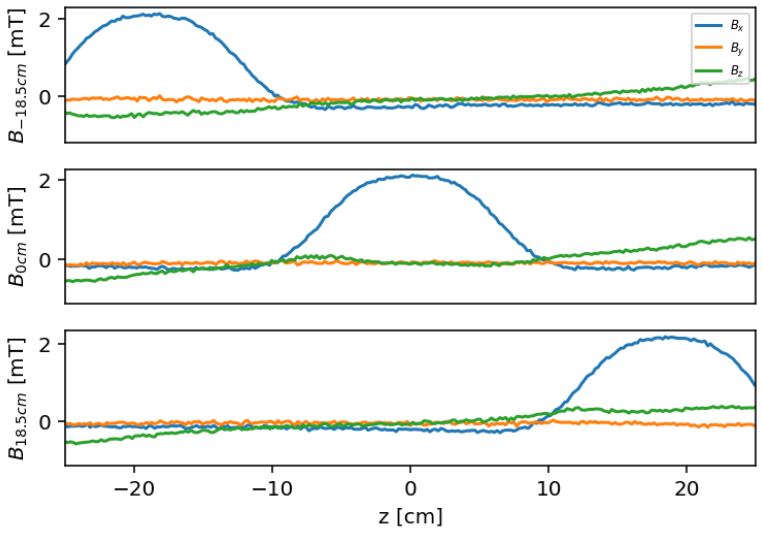

Figure 75: Magnetic field measurements of a single coil pair transversal Sona-transition unit for multiple positions $z_{Sona} = \pm 18.5$ cm and 0 cm of the transition unit. The positions $z_{Sona} = \pm 18.5$ cm correspond to the coil pair touching a spinfilter. The spinfilters are turned off.

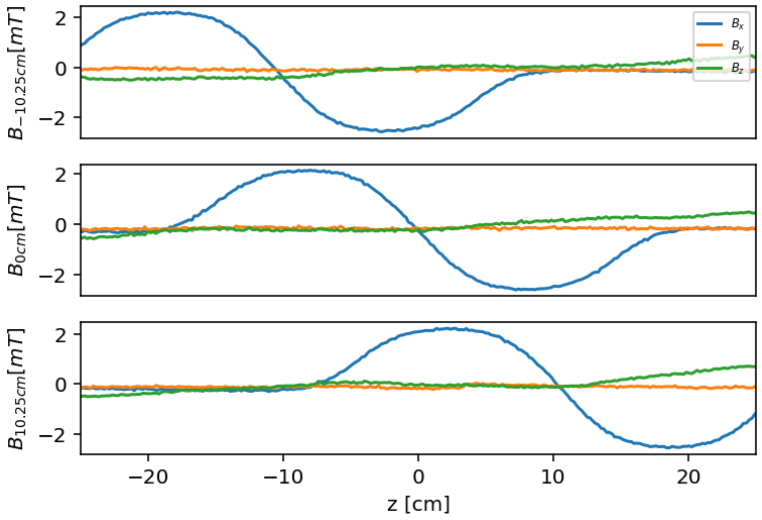

Figure 76: Magnetic field measurements of a double coil pair transversal Sona-transition unit for multiple positions $z_{Sona} = \pm 10.25$ cm and 0 cm of the transition unit. The positions $z_{Sona} = \pm 10.25$ cm correspond to a coil pair touching a spinfilter. The spinfilters are turned off.

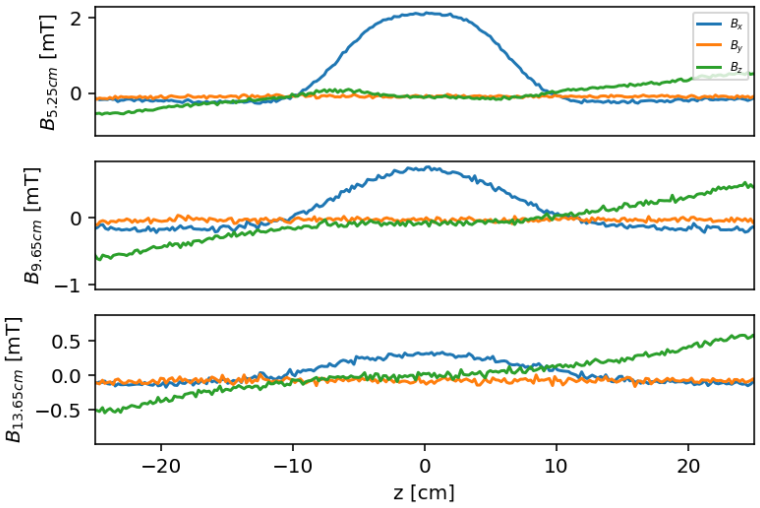

Figure 77: Magnetic field measurements of a single coil pair transversal Sona-transition unit for $x_{coil} = 5.25$ cm (top), 9.65 cm (middle) and 13.65 cm (bottom). The spinfilters are turned off.

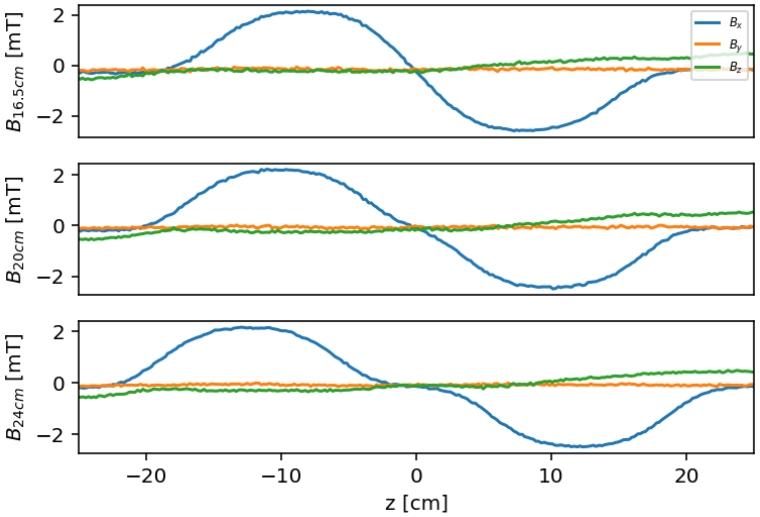

Figure 78: Magnetic field measurements of a double coil pair transversal Sona-transition unit for $\Delta z = 16.5$ cm (top), 20 cm (middle) and 24 cm (bottom). The spinfilters are turned off.

D Measurements and simulations of transversal Sona-transition units

D.1 Variation of the coil distance $x_{\mathbf{coil}}$ from the beam pipe

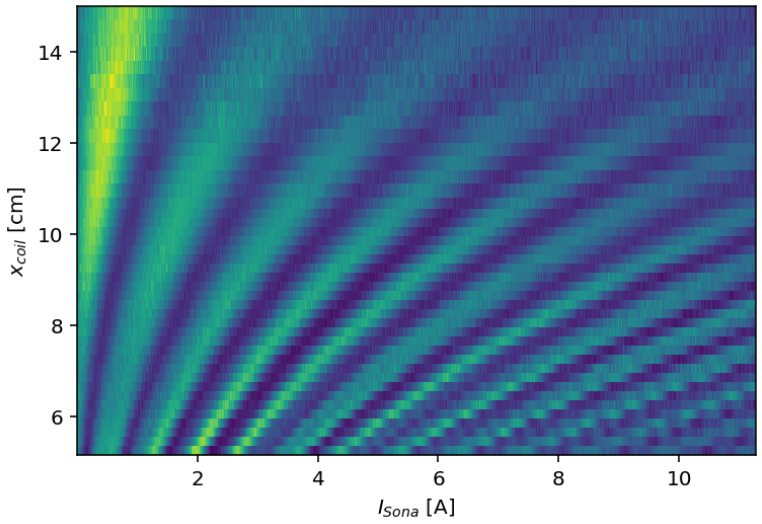

Figure 79: Measurement with a single coil pair for various x_{coil} and the spinfilter settings of $\alpha 1$ to $\alpha 2$.

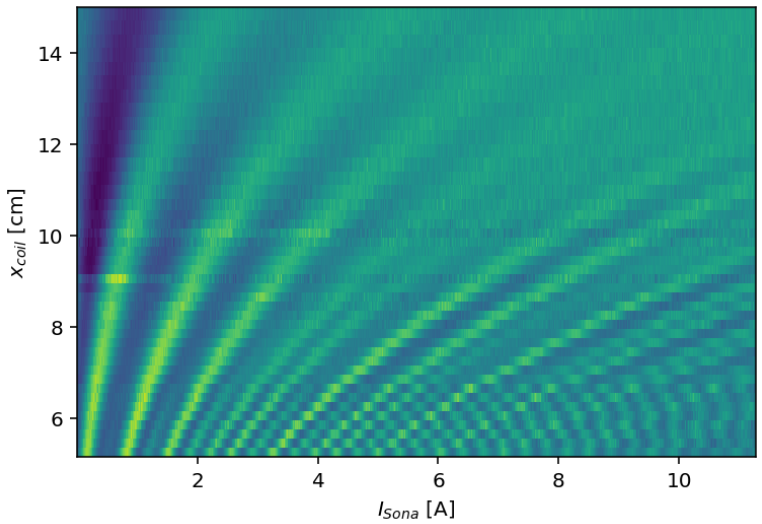

Figure 80: Measurement with a single coil pair for various x_{coil} and the spinfilter settings $\alpha 2$ to $\alpha 2$.

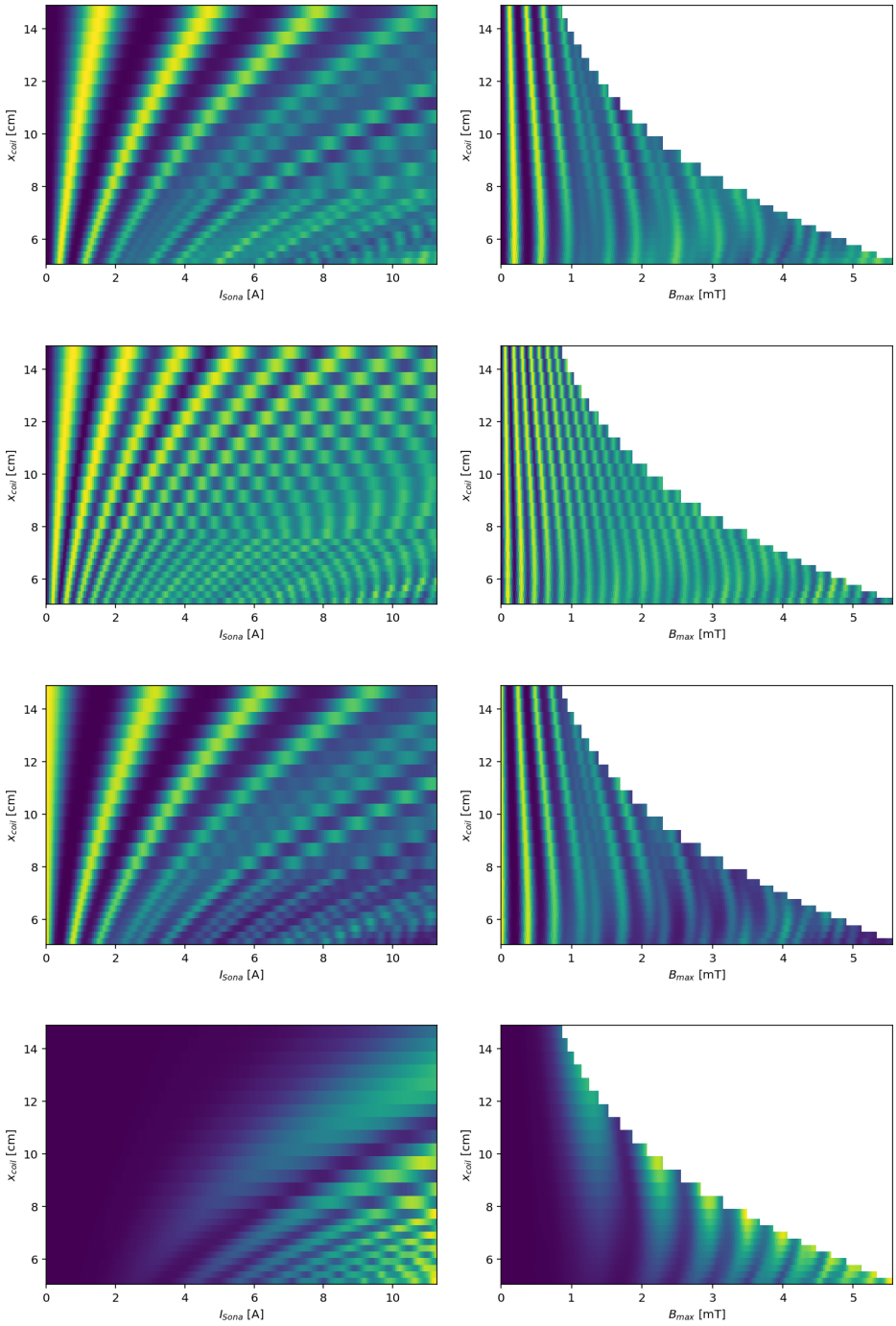

Figure 81: Simulations with $\alpha 1\alpha 1$-, $\alpha 1\alpha 2$-, $\alpha 1\beta 3$- and $\alpha 1\beta 4$-spinfilter settings (top to bottom) and varying x_{coil}. The color gradient does not match in between the images. The by magnitudes smaller intensity of the $\beta 4$-state is therefore not reflected by the colors.

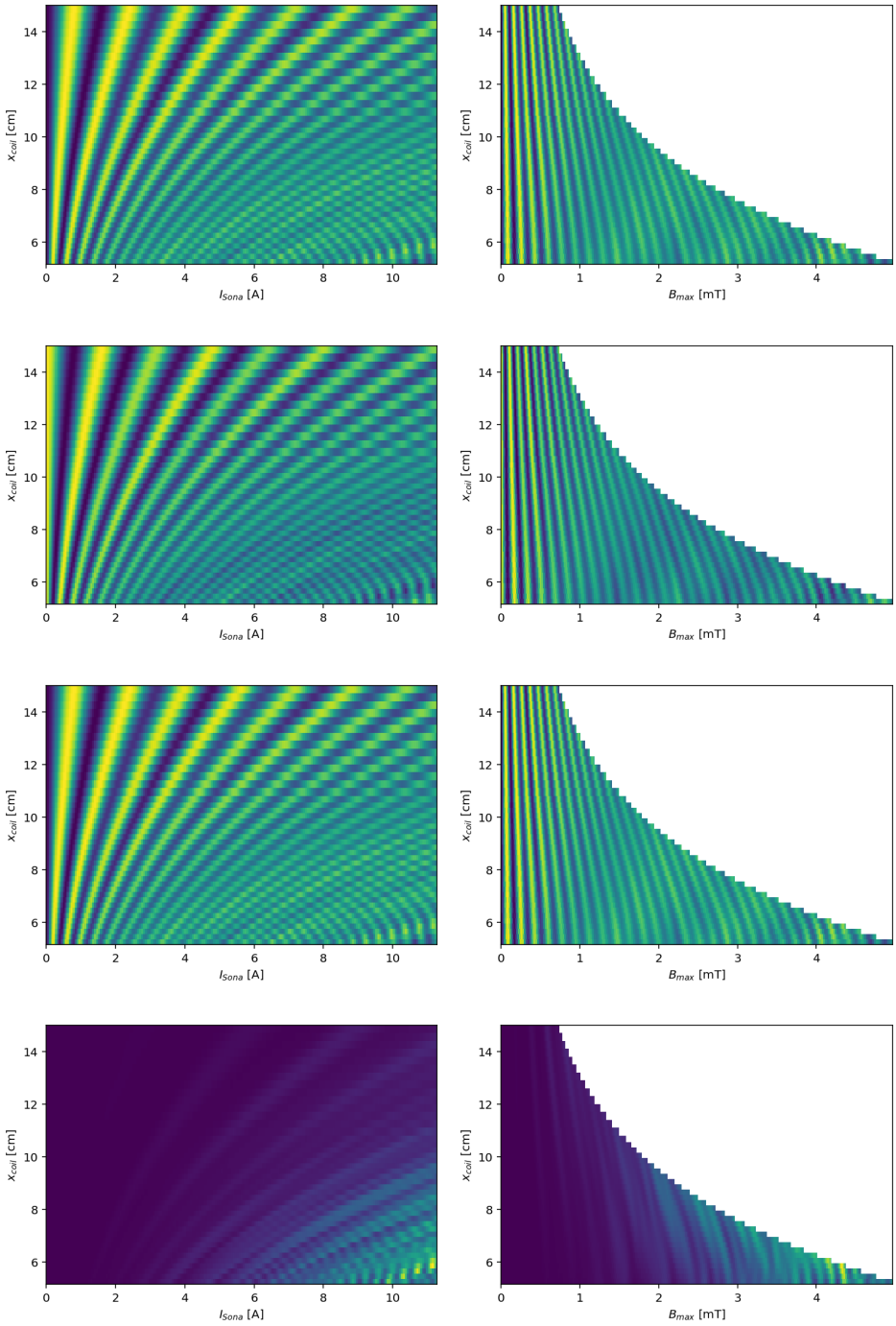

Figure 82: Simulations with α2α1-, α2α2-, α2β3- and α2β4-spinfilter settings (top to bottom) and varying x_{coil}. The color gradient does not match in between the images. The by magnitudes smaller intensity of the β4-state is therefore not reflected by the colors.

D.2 Variation of the kinetic energy

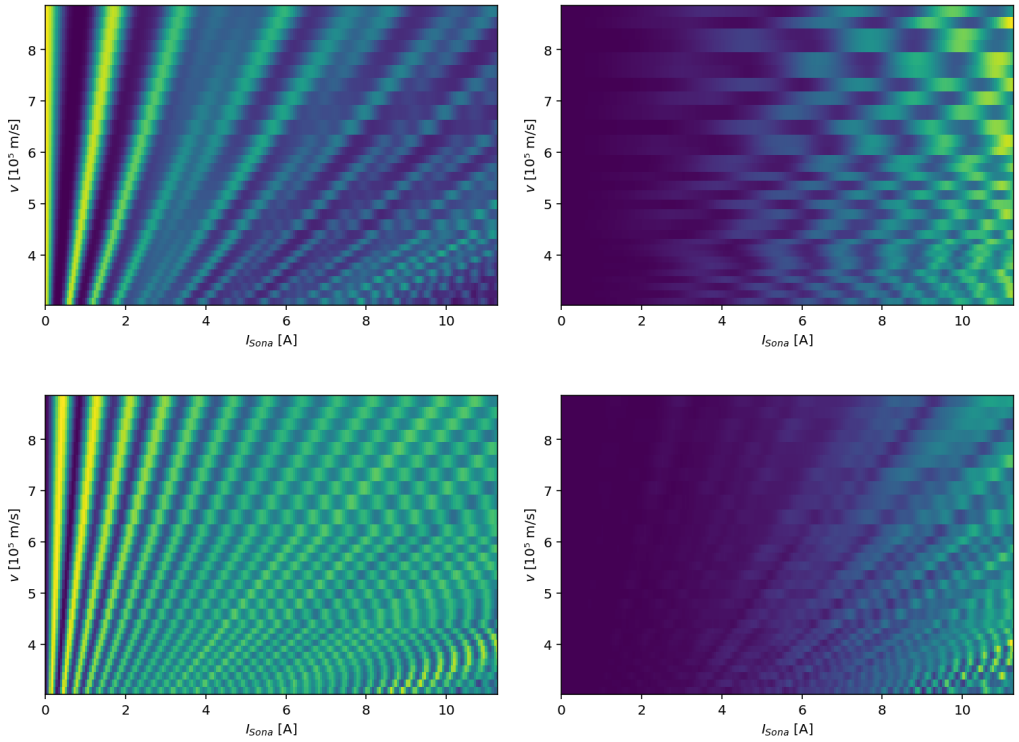

Figure 83: Simulations with $\alpha 1\beta 3$- (top left), $\alpha 1\beta 4$- (top right), $\alpha 2\beta 3$- (bottom left) and $\alpha 2\beta 4$-settings (bottom right) for various E_{kin}, displayed as a function of the velocity. The color gradient does not match in between the images. The by magnitudes smaller intensity of the $\beta 4$-state is therefore not reflected by the colors.

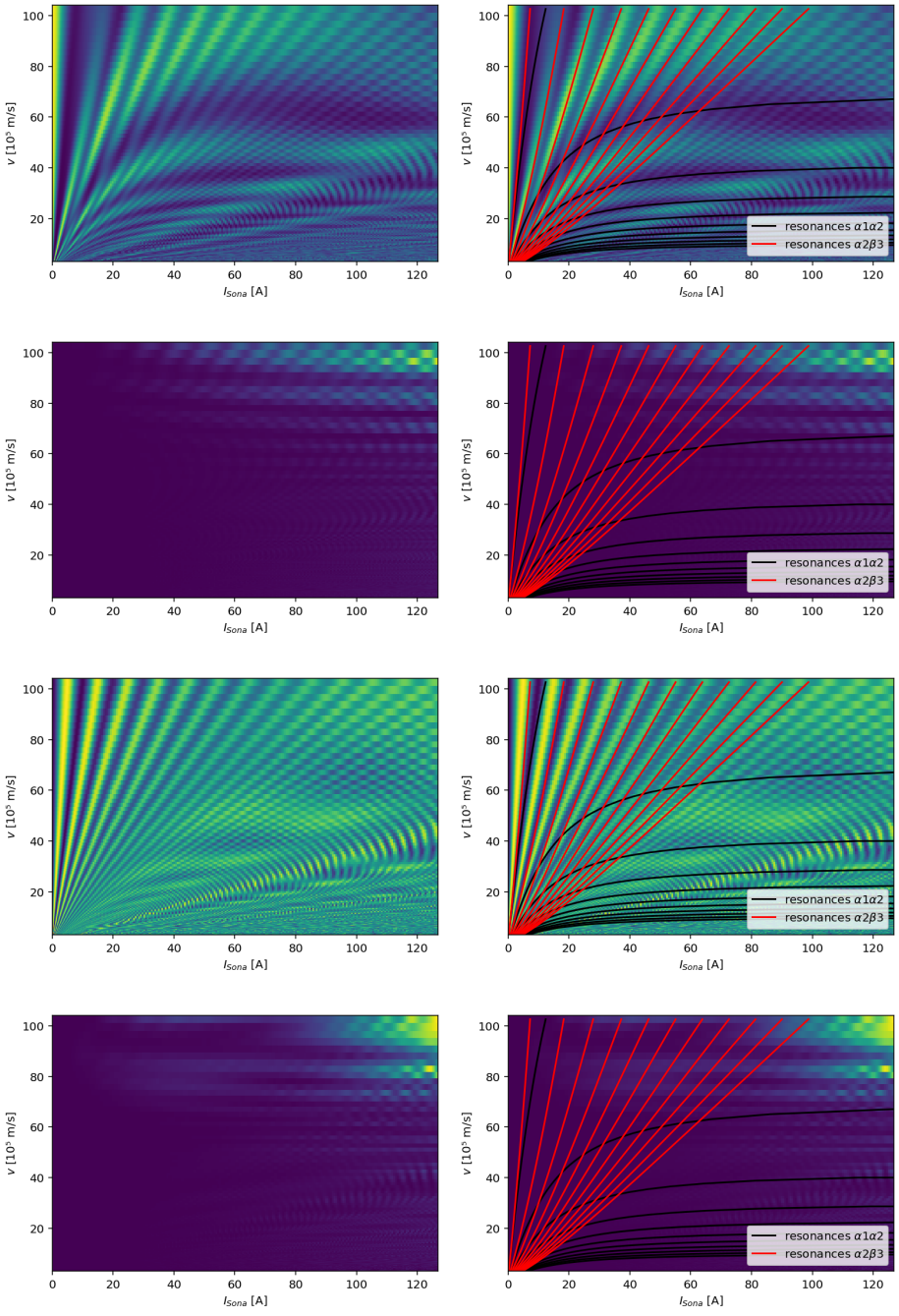

Figure 84: Extended simulations with $\alpha 1\beta 3$-, $\alpha 1\beta 4$-, $\alpha 2\beta 3$- and $\alpha 2\beta 4$-settings (top to bottom) for various E_{kin}, including the resonances for manually fitted κ and λ (right), displayed as a function of the velocity. The color gradient does not match in between the images. The by magnitudes smaller intensity of the $\beta 4$-state is therefore not reflected by the colors.

References

[1] PG Sona. "A new method proposed to increase polarization in polarized ion sources of H^- and D^-". In: *Energia nucleare* 14 (1967), p. 295.

[2] R. D. Hight and R. T. Robiscoe. "Nonadiabatic transition in $n = 2$ atomic hydrogen". In: *Phys. Rev. A* 17 (2 Feb. 1978), pp. 561–565. DOI: 10.1103/PhysRevA.17.561. URL: https://link.aps.org/doi/10.1103/PhysRevA.17.561.

[3] A. Kponou et al. "Sona Transition Studies in the RHIC OPPIS". In: American Institute of Physics Conference Series 980 (Feb. 2008). Ed. by Ahovi Kponou, Yousef Makdisi, and Anatoli Zelenski, pp. 241–247. DOI: 10.1063/1.2888092.

[4] Ralf Engels et al. "Direct observation of transitions between quantum states with energy differences below 10 neV employing a Sona unit". In: *The European physical journal / D* 75.9 (2021), p. 257. ISSN: 1434-6079. DOI: 10.1140/epjd/s10053-021-00268-4. URL: //juser.fz-juelich.de/record/897325.

[5] V. V. Okorokov. "Coherent Excitation of Optical Spectra of Atoms Passing Through a Crystal". In: *Soviet Journal of Experimental and Theoretical Physics Letters* 2 (Aug. 1965), p. 111.

[6] V. V. Okorokov. "On the Coherent Excitation of Nuclei Moving Through Cristals". In: *Yadern. Fiz.* Vol: 2 (Dec. 1965). URL: https://www.osti.gov/biblio/4569676.

[7] Nicolas Faatz et al. "Hyperfine-spectroscopy measurement of metastable hydrogen atoms with a Sona-transition unit". In: *PoS* PSTP2022 (2023), p. 006. DOI: 10.22323/1.433.0006.

[8] Fritz Gassmann. "Quantentheorie – Einblick in die fremde Welt des Lichts und der Atome". In: Jan. 2016.

[9] Ralf Engels. "Entwicklung eines universellen Lambshift-Polarimeters für polarisierte Atomstrahl-Targets wie an ANKE/COSY". PhD thesis. Universität zu Köln, 2002.

[10] Nicolas Faatz. "Simulation of the occupation numbers of hyperfine substates passing external fields". Master's Thesis. RWTH Aachen University, Mar. 2023.

[11] Jan Steinhage. "Development of a quantium transition-unit with oscillating treansversal magnetic fields". Bachelor's Thesis. FH Aachen - University of Applied Sciences, Mar. 2024.

[12] Sahil Vijaykumar Aswani. “Optimization of the magnetic field configuration of a Sona transition unit”. Bachelor’s Thesis. FH Aachen - University of Applied Sciences, Aug. 2022.

[13] Christoph Schoberer. “Design and First Test of an Apparatus to Determine the Magnetic Field Inside a Lamb-Shift Polarimeter”. Bachelor’s Thesis. FH Aachen - University of Applied Sciences, July 2024.